

TARGET LOCALIZATION METHODS FOR FREQUENCY-ONLY MIMO RADAR

A THESIS SUBMITTED TO
THE GRADUATE SCHOOL OF NATURAL AND APPLIED SCIENCE
OF
MIDDLE EAST TECHNICAL UNIVERSITY

BY

YILMAZ KALKAN

IN PARTIAL FULFILLMENT OF THE REQUIREMENTS
FOR
THE DEGREE OF DOCTOR OF PHILOSOPHY
IN
ELECTRICAL AND ELECTRONICS ENGINEERING

SEPTEMBER 2012

Approval of the thesis:

TARGET LOCALIZATION METHODS FOR FREQUENCY-ONLY MIMO RADAR

submitted by **YILMAZ KALKAN** in partial fulfillment of the requirements for the degree of
**Doctor of Philosophy in Electrical and Electronics Engineering Department, Middle
East Technical University** by,

Prof. Dr. Canan Özgen
Dean, Graduate School of **Natural and Applied Sciences**

Prof. Dr. İsmet Erkmén
Head of Department, **Electrical and Electronics Engineering**

Prof. Dr. Buyurman Baykal
Supervisor, **Electrical and Electronics Engineering Dept., METU**

Examining Committee Members:

Prof. Dr. Yalçın Tanık
Electrical and Electronics Engineering Dept., METU

Prof. Dr. Buyurman Baykal
Electrical and Electronics Engineering Dept., METU

Prof. Dr. Orhan Arıkan
Electrical and Electronics Engineering Dept., Bilkent University

Prof. Dr. Temel Engin Tuncer
Electrical and Electronics Engineering Dept., METU

Assoc. Prof. Dr. Çağatay Candan
Electrical and Electronics Engineering Dept., METU

Date:

I hereby declare that all information in this document has been obtained and presented in accordance with academic rules and ethical conduct. I also declare that, as required by these rules and conduct, I have fully cited and referenced all material and results that are not original to this work.

Name, Last Name: YILMAZ KALKAN

Signature :

ABSTRACT

TARGET LOCALIZATION METHODS FOR FREQUENCY-ONLY MIMO RADAR

Kalkan, Yılmaz

Ph.D., Department of Electrical and Electronics Engineering

Supervisor : Prof. Dr. Buyurman Baykal

September 2012, 121 pages

This dissertation is focused on developing the new target localization and the target velocity estimation methods for frequency-only multi-input, multi-output (MIMO) radar systems with widely separated antennas. If the frequency resolutions of the transmitted signals are enough, only the received frequencies and the Doppler shifts can be used to find the position of the target.

In order to estimate the position and the velocity of the target, most multistatic radars or radar networks use multiple independent measurements from the target such as time-of-arrival (TOA), angle-of-arrival (AOA) and frequency-of-arrival (FOA). Although, frequency based systems have many advantages, frequency based target localization methods are very limited in literature because of the fact that highly non-linear equations are involved in solutions. In this thesis, alternative target localization and the target velocity estimation methods are proposed for frequency-only systems with low complexity.

One of the proposed methods is able to estimate the target position and the target velocity based on the measurements of the Doppler frequencies. Moreover, the target movement direction can be estimated efficiently. This method is referred to as "Target Localization via Doppler Frequencies - **TLDF**" and it can be used for not only radar but also all frequency-

based localization systems such as Sonar or Wireless Sensor Networks.

Besides the TLDF method, two alternative target position estimation methods are proposed as well. These methods are based on the Doppler frequencies, but they require the target velocity vector to be known. These methods are referred to as "Target Localization via Doppler Frequencies and Target Velocity - **TLD&V** methods" and can be divided into two sub-methods. One of them is based on the derivatives of the Doppler Frequencies and hence it is called as "Derivated Doppler - **TLD&V-DD** method". The second method uses the Maximum Likelihood (ML) principle with grid search, hence it is referred to as "Sub-ML, **TLD&V-subML** method".

The more realistic signal model for ground based, widely separated MIMO radar is formed as including Swerling target fluctuations and the Doppler frequencies. The Cramer-Rao Bounds (CRB) are derived for the target position and the target velocity estimations for this signal model. After the received signal is constructed, the Doppler frequencies are estimated by using the DFT based periodogram spectral estimator. Then, the estimated Doppler frequencies are collected in a fusion center to localize the target.

Finally, the multiple targets localization problem is investigated for frequency-only MIMO radar and a new data association method is proposed. By using the TLDF method, the validity of the method is simulated not only for the targets which are moving linearly but also for the maneuvering targets.

The proposed methods can localize the target and estimate the velocity of the target with less error according to the traditional isodoppler based method. Moreover, these methods are superior than the traditional method with respect to the computational complexity. By using the simulations with *MATLAB*[®], the superiorities of the proposed methods to the traditional method are shown.

Keywords: MIMO Radar, Doppler shift, target localization, velocity estimation, Cramer-Rao Bound

ÖZ

SADECE FREKANS BİLGİSİ KULLANAN MIMO RADAR İÇİN HEDEF KONUMLAMA YÖNTEMLERİ

Kalkan, Yılmaz

Doktora, Elektrik ve Elektronik Mühendisliği Bölümü

Tez Yöneticisi : Prof. Dr. Buyurman Baykal

Eylül 2012, 121 sayfa

Bu tezde, sadece frekans bilgisi kullanan, antenleri geniş alana yayılmış, çoklu-giriş, çoklu-çıkış (ÇGÇÇ) radar sistemleri için yeni hedef konumlama ve hız kestirim yöntemlerinin geliştirilmesi üzerinde durulmuştur. Eğer yayımlanan sinyallerin frekans çözünürlüğü yeteri kadar iyi ise, hedefin konumunu bulabilmek için sadece alınan frekanslar ve Doppler kayması kullanılabilir.

Hedefin konumunun ve hızının kestirilebilmesi için birçok çoklstatik radar veya radar ağları, hedeften gelen, varış-zamanı, varış-açısı ve varış-frekansı gibi çoklu, bağımsız ölçümleri kullanırlar. Frekans temelli sistemlerin bir çok avantajına rağmen, frekans temelli hedef konumlama yöntemlerinin, çözümlerinde hayli doğrusal olmayan denklemler içermelerinden dolayı literatürdeki uygulamaları oldukça kısıtlıdır. Bu tezde, sadece-frekans bilgisi kullanan sistemler için, daha az karmaşık, alternatif hedef konumlama ve hız kestirim yöntemleri önerilmiştir.

Önerilen yöntemlerden biri, hedefin konumunu ve hedefin hızını Doppler frekansları temeline dayanan ölçümlerden kestirebilmektedir. Bunun yanında, hedefin hareket yönü de etkin bir şekilde kestirilebilmektedir. Bu yöntem "Doppler Frekansları yoluyla Hedef Konumlama - DFHK" olarak isimlendirilmiştir ve sadece radarlarda değil, sonar ve kablosuz sensör ağları

gibi frekans temelli tüm hedef konumlama sistemlerinde de kullanılabilir.

DFHK yönteminin yanında, alternatif iki yöntem daha önerilmiştir. Bu yöntemler de Doppler frekansı temelinde çalışır ancak hedefin hız vektörüne de ihtiyaç duyarlar. Bu yöntemler, "Doppler Frekansları ve Hedef Hızı yoluyla Hedef Konumlama - **D&HHK**" yöntemleri olarak isimlendirilmiştir ve iki alt gruba ayrılabilir. Bunlardan birincisi Doppler frekansının türevine dayandığı için "Türevlenmiş Doppler, **D&HHK-TD** yöntemi" olarak isimlendirilir. İkinci yöntem ise en yüksek olabilirlik ilkesi ve ızgara arama yöntemine dayandığı için "**D&HHK-subML** yöntemi" olarak isimlendirilmiştir.

Yerde konuşlu ve geniş olarak dağıtılmış ÇGÇÇ radarlar için, Swerling hedef dalgalanmalarını ve Doppler frekanslarını da içeren daha gerçekçi bir sinyal modeli yapılandırıldı. Bu sinyal modeli için, hedef hız ve hedef konum kestirimi Cramer-Rao Sınırları (CRS) türetildi. Alınan sinyal yapılandırıldıktan sonra, Doppler frekansları DFT temelli periodogram frekans kestirimci ile kestirildi. Daha sonra, kestirilen Doppler frekansları hedefi konumlayabilmek için bir merkezi birleştirme biriminde toplandı.

Son olarak, sadece frekans bilgisini kullanan ÇGÇÇ radar için çoklu hedef konumlama problemi ele alındı ve yeni bir veri ilişkilendirme yöntemi önerildi. DFHK yöntemi kullanılarak, önerilen yöntemin geçerliliği sadece doğrusal hareket eden hedef için değil, aynı zamanda manevra yapan hedef için de gösterildi.

Önerilen yöntemler, eş-Doppler eğrilerinin kullanıldığı geleneksel yönteme göre daha az hatayla hedef konumlayabilmekte ve hedefin hızını kestirebilmektedir. Ayrıca bu yöntemler hesaplama karmaşıklığı olarak da geleneksel yöntemden daha üstündür. *MATLAB*[®] programı kullanılarak yapılan benzetimlerle, önerilen yöntemlerin geleneksel yönteme göre üstünlüğü gösterildi.

Anahtar Kelimeler: ÇGÇÇ Radar, Doppler kayması, hedef konumlama, hız kestirimi, Cramer-Rao Sınırı

*To my lovely wife Nurcan,
my son Hüseyin Toprak, my daughter Hayat Güneş
and
to my parents.*

ACKNOWLEDGMENTS

I am heartily thankful to my supervisor, Prof. Dr. Buyurman Baykal, whose encouragement, guidance and support from the initial to the final level enabled me to present this thesis. He showed me different ways to approach a research problem and the need to be persistent to accomplish any goal. He taught me that, how I can broaden my horizon while trying to find a way for any problem.

I would like to thank Prof. Dr. Yalçın Tanık and Prof. Dr. Orhan Arıkan for their valuable suggestions during the whole period and for their time during the Progress Committee meetings. They showed me how a good academician being with their endless knowledge and patience.

I am also would like to thank to my dear friends Dr. Tansu Filik, Dr. Evren Ekmekçi, Dr. A.Hayrettin Yüzer, Barış Özyer, Umut Tilki, Dr. Sebahattin Topal, Dr. Oğuzhan Erdem, Akif Durdu, Atilla Dönük, Dr. Feza Carlak, Dr. Naci Genç, Ahmet M. Elbir and all other ÖYP assistants in METU EEE department for their support and friendship from the beginning of this long way in METU to the end.

I would like to thank my former roommates; T.Kaya Yaşar, Erhan Örümlü, Dr. Fatih Bayramoğlu, Dr. Serkan Karakütük and M.Onur Özeç for their friendship and company who made my times in the department enjoyable and worthy.

I am also very grateful to my parents for their sincere love and endless support during my life and my thesis.

Finally, I want to thank to the one special in my life, my lovely wife Nurcan Kalkan, for her support, patience and love that keep me eager and hopeful to accomplish this thesis. I could not have completed my thesis without her unlimited support and patience.

TABLE OF CONTENTS

ABSTRACT	iv
ÖZ	vi
ACKNOWLEDGMENTS	ix
TABLE OF CONTENTS	x
LIST OF TABLES	xiii
LIST OF FIGURES	xiv
CHAPTERS	
1 INTRODUCTION	1
1.1 Introduction and Motivation	1
1.2 Objectives and Contributions	2
1.2.1 Objectives	2
1.2.2 Contributions	3
1.3 Organization of the Thesis	4
2 BACKGROUND	6
2.1 Historical Overview	6
2.2 MIMO Radar	8
2.2.1 MIMO Radar with Colocated Antennas	9
2.2.2 MIMO Radar with Widely Separated Antennas	11
2.3 Target Localization by Using Doppler Shift	12
2.3.1 Basic Principles of Doppler-Only Radars	13
2.3.2 Localization by using Doppler Shift	16
2.4 Literature Overview	18
3 SIGNAL MODEL and THE CRAMER-RAO BOUND FOR FREQUENCY- ONLY MIMO RADAR	20

3.1	Signal and Noise Model	21
3.2	Properties of the Target Fluctuations	25
3.3	Target Model	29
3.4	Cramer-Rao Bound for Target Localization and Velocity Estimation .	32
4	TARGET LOCALIZATION METHODS FOR FREQUENCY-ONLY MIMO RADAR	44
4.1	Target Localization via Doppler Frequencies - TLDF	48
4.1.1	2x2 MIMO Radar Case	49
4.1.2	2x3 MIMO Radar Case	50
4.1.3	General Case	51
4.2	Target Localization via Doppler Frequencies and Target Velocity - TLD&V	57
4.2.1	First Method : Differentiated Doppler - TLD&V-DD . . .	57
4.2.2	Second Method : Sub-ML Estimator - TLD&V-subML .	65
5	SIMULATION RESULTS	70
5.1	Frequency Estimation	71
5.2	Grid Search	75
5.3	Target Localization and Velocity Estimation Simulations	76
5.4	Complexity Analysis	83
5.5	Comparison with Pulsed Radar	84
5.6	Why Pulse Compression?	86
5.6.1	Pulse Compression	87
6	TARGET LOCALIZATION FOR MULTIPLE TARGETS	90
6.1	Doppler and Velocity Resolutions	90
6.2	Data Association	92
6.2.1	Choosing Correct Association	96
6.3	Simulations	97
7	CONCLUSION	105
	REFERENCES	110
A	Radar Frequency Bands and General Usage	114
B	Derivation of the Fisher Information Matrix	115

C	Signal-to-Noise-Ratio (SNR)	118
	CURRICULUM VITAE	120

LIST OF TABLES

TABLES

Table 3.1	Swerling Target Models	26
Table 5.1	3x3 MIMO Radar Simulation Parameters and Assumptions	77
Table 5.2	Computation times for 10 trials (second)	83
Table 6.1	Doppler frequencies for both target	93
Table 6.2	Possible Doppler frequencies for two targets and 2x2 MIMO radar	94
Table 6.3	Data association results for 3 targets and for different cases.	103
Table A.1	Radar Frequency Bands and General Usage	114

LIST OF FIGURES

FIGURES

Figure 2.1	Patent document of Hülsmeier's telemobiloskop (1)	7
Figure 2.2	Patent document of Hülsmeier's telemobiloskop (2)	7
Figure 2.3	MIMO radar (a) versus Phased Array(b) (figure from [5])	10
Figure 2.4	Radar backscatterer as function of azimuth (figure from [6])	11
Figure 2.5	Monostatic and bistatic radars.	14
Figure 2.6	Equi-TOA positions (ellipses) in a bistatic radar	16
Figure 2.7	Cassini ovals	17
Figure 2.8	Different Cassini ovals	17
Figure 3.1	The MIMO radar geometry. a) for N_T transmitters and N_R receivers, b) for single transmitter-receiver.	21
Figure 3.2	a) Block diagram of the whole system. b) Demodulator filterbanks. c) Doppler filterbanks.	24
Figure 3.3	100-bin histogram of a unit mean exponential sample sequence generated in MATLAB using equation (3.16)	27
Figure 3.4	100-bin histogram of a unit mean 4^{th} – degree chi square sample sequence generated in MATLAB using equation (3.18)	28
Figure 3.5	100-bin histogram of a unit mean Rayleigh sample sequence generated in MATLAB using equation (3.20)	29
Figure 3.6	Target model	30
Figure 3.7	Dividing the observation time in blocks.	31
Figure 3.8	System geometry used for the CRB simulations.	38
Figure 3.9	CRBs for target position estimation when target at position1.	40

Figure 3.10 CRBs for target velocity estimation when target at position1.	40
Figure 3.11 CRBs for target position estimation when target at position2.	41
Figure 3.12 CRBs for target velocity estimation when target at position2.	41
Figure 3.13 The CRBs for target position estimation when target at position 2. Target direction is swept from 0 to 2π	42
Figure 3.14 The CRBs for target velocity estimation when target at position 2. Target direction is swept from 0 to 2π	42
Figure 3.15 CRBs for target position estimation when target at position 3. Target direc- tion is swept from 0 to 2π	43
Figure 3.16 CRBs for target velocity estimation when target at position 3. Target direc- tion is swept from 0 to 2π	43
Figure 4.1 MIMO radar geometry. a) for N_T transmitters and N_R receivers, b) for single transmitter-receiver pair.	46
Figure 4.2 Simulation geometries	47
Figure 4.3 Cost functions and contour plots for the TLDF method at low SNR (SNR = -10 dB) for different geometries.	54
Figure 4.4 Cost functions and contour plots for the TLDF method at high SNR (SNR = 30 dB) for different geometries.	55
Figure 4.5 Cost function and contour plot for the TLDF method when 5 Hz carrier frequency offset exists. (SNR = 30 dB, target at case 2.)	56
Figure 4.6 Cost functions and contour plots for the TLD&V-DD method at low SNR (SNR = -10 dB) for different geometries.	60
Figure 4.7 Cost functions and contour plots for the TLD&V-DD method at high SNR (SNR = 30 dB) for different geometries.	61
Figure 4.8 MIMO radar simulation geometry for TLD&V-DD method.	62
Figure 4.9 Target localization for 2x2 MIMO radar. Grid size = 1000m.	63
Figure 4.10 Target localization for 2x2 MIMO radar. Grid size = 250m.	63
Figure 4.11 Target localization for 250m grid size. a) 2x2 MIMO radar, b) 2x3 MIMO radar, c) 3x3 MIMO radar	64
Figure 4.12 Target localization for different 3x3 MIMO radar geometries.	65

Figure 4.13 Cost functions and contour plots for the TLD&V-subML method at low SNR (SNR = -10 dB) for different geometries.	68
Figure 4.14 Cost functions and contour plots for the TLD&V-subML method at high SNR (SNR = 30 dB) for different geometries.	69
Figure 5.1 Frequency estimations for a target at case1, position2. No target fluctuation and the DFT size is 2^{16}	72
Figure 5.2 Frequency estimations for a target at case2 and for different target fluctuations. The DFT size is 2^N	72
Figure 5.3 Frequency estimations for a target at case3 with Swerling-0 type target fluctuations. The DFT size is 2^N	73
Figure 5.4 Frequency estimations for a target at case2. No target fluctuations exist and the DFT size is 2^{18} . Target is moving.	74
Figure 5.5 Frequency estimations for a target at case1, position2. No target fluctuations exist and the DFT size is 2^{18} . Target is moving.	74
Figure 5.6 Grid search in (x, y) coordinates.	75
Figure 5.7 The target position and the target velocity estimation performances of the TLDF and the traditional FOA methods for a target in different positions (case 1).	78
Figure 5.8 The target position and the target velocity estimation performances of the TLDF and the traditional FOA methods for a target in different positions (case 2 and case 3).	79
Figure 5.9 Target direction estimation performances of the TLDF method for different target cases.	79
Figure 5.10 The target position estimation performances of the TLDF methods for a target in different positions (after velocity updates).	81
Figure 5.11 The target position estimation performances of the TLD&V and the traditional FOA methods for a target in different positions.	82
Figure 5.12 Range measurement by using pulses (from [59]).	84
Figure 5.13 Signal powers with and without pulse compression.	86

Figure 5.14 Resolving targets in range (I) two resolved targets by short-pulse (II) two unresolved targets by long-pulse (III) two resolved targets by using pulse compression with long-pulse (figure from [59])	88
Figure 5.15 Comparison of the TLDF method localization performance with pulsed radar RMS range errors with pulse compression (pulse comparison ratio=1e+4). . .	89
Figure 6.1 Position ambiguities in observation time for different target velocities. . . .	91
Figure 6.2 Doppler and velocity resolutions with respect to the observation time. . . .	92
Figure 6.3 The sytem geometry for multitarget case.	93
Figure 6.4 Motion of the target 1.	97
Figure 6.5 All possible groups for data association problem, 2 targets, Case1.	98
Figure 6.6 All possible groups for data association problem, 2 targets, Case2.	99
Figure 6.7 All possible groups for data association problem, 2 targets, Case3.	100
Figure 6.8 All possible groups for data association problem, 2 targets, Case4.	101
Figure 6.9 Target motion scenarios for data association problem for 3 targets.	102

CHAPTER 1

INTRODUCTION

This thesis is on MIMO radar systems localizing the moving target by using only the received frequencies and hence the Doppler shift informations. In this introductory chapter, short introduction and motivation of the thesis is given in Section 1.1. Objectives and the contributions of this work are summarized in Section 1.2. Finally, in Section 1.3, the organization of the remaining parts of the thesis is presented.

1.1 Introduction and Motivation

The acronym for **RA**dio **D**etection **A**nd **R**anging gives the well-known word **"RADAR"** and today is a common term in the world. All early radars used radio waves, but some modern radar systems use optical waves and lasers. Basically, a radar system transmits an electromagnetic (EM) wave via its transmitter and collects the backscattered waves from the target to detect or ranging it. Although the most important and brilliant developments were presented with the military requirements, today radars are used in the many areas from weather prediction to speed measurement of the vehicles in traffic.

In recent years, radar terminology has gained a new term called as MIMO radar. It refers to a radar network which employs multiple, spatially distributed or colocated transmitters and receivers. Actually, MIMO radar can be viewed as a type of radar network and the term "MIMO" was borrowed from the wireless communications. Because of the similarities between the radar and the communication systems in which they both includes antennas to receive and transmit signals, this close relationship is not suprising. Although some, insists that MIMO Radar is not a new one, MIMO radar term has been commonly used in the last

decade. Moreover, the subclasses of MIMO radar, which are MIMO radars with colocated antennas and with widely separated antennas, are started to use depending upon the physical locations of the transmit and the receive units.

The MIMO radar works are commonly focused on the target detection and the waveform design problems. The use of the MIMO radar for target localization and target tracking is very limited. On the other hand, though, inexpensive and simple structure of the continuous wave (CW) radars, Doppler-only radar systems cover the very small area in the whole radar systems especially for target localization. Moreover, CW radars can measure Doppler shift precisely and they have low probability of intercept (LPI) characteristic because of their low transmit peak power with respect to the pulsed radars. These advantages of MIMO radars (having the widely separated transmit/receive sites, hence the angular spread) and the CW radars (precise Doppler measurement) can be used for target localization efficiently. In the case of the time resolution of the received signal is not enough, this Doppler only systems can be vital. In such a case, the time information will be faithless and if the frequency resolution of the system is enough, the received frequencies and the Doppler shift are able to be used for different aims such as the target localization or target tracking.

1.2 Objectives and Contributions

1.2.1 Objectives

The first objective of this thesis is to investigate the target localization performance of the frequency-only MIMO radar. Especially, when the received signal's time resolution is not good or not enough, using the frequency information is more reliable than using the time information. For this purpose, continuous wave (CW) radar is used for its high frequency resolution. The next objective of this thesis is to develop more general signal model for the MIMO radar. In MIMO radar works, target fluctuations are generally ignored or simple models are preferred. In this thesis, the Doppler shift and the target fluctuations are covered in the signal model. Moreover, the multiple targets localization for frequency-only MIMO radar is another objective. Finally, the derivation of the Cramer Rao Bounds for target localization and velocity estimation for the frequency-only MIMO radar is the last aim of the thesis.

1.2.2 Contributions

The main contributions of the thesis can be summarized as follows

- Alternative target localization methods for frequency/doppler-only systems are proposed. These new methods are applied to the frequency based MIMO radar and the localization performances of them are investigated. Actually, these proposed methods are system independent, meaning that, these methods can be applied to the different systems such as sonar or wireless sensor networks. Only requirement is having the estimation of the frequencies (and hence the Doppler frequencies) of the received signals. After getting the received frequencies and the Doppler shifts, then these datas can be used for all frequency based systems for target localization or another aims such as target tracking.
- In general, the Doppler based systems require the angle-of-arrival information besides of the Doppler shifts to localize or track the target. On the other hand, one of the proposed methods (Target Localization via Doppler Frequencies (TLDF) method), does not require extra information and works only using the estimated frequencies of the received signals. TLDF method can estimate the target position and target velocity with target direction directly using the estimated frequencies.
- Other two proposed methods (Target Localization via Doppler Frequencies and Target Velocity (TLD&V) methods) require the target velocity to be known besides of the Doppler frequencies to estimate the target position. The target velocity and direction can be estimated accurately using the TLDF method, then the TLD&V methods can be used to estimate the target position efficiently. Using the simulations, the target position estimation performances of the proposed methods are compared to the traditional iso-Doppler curves based target localization method and the superiorities of them are shown.
- The multiple targets localization performances of the proposed methods are investigated using the maneuvering and non-maneuvering targets. Hence, the validity of the proposed method is shown for multiple targets and for maneuvering targets. Data association for frequency-only MIMO radar is achieved.

- The signal model is expanded as including the Doppler shifts and the target fluctuations. On the contrary of point scatterer model, the target is modelled as composed of many small scatterers. Swerling target fluctuation models are used to model these target fluctuations. Hence, more realistic signal model is proposed.
- The Cramer Rao Bounds are calculated for the target localization of proposed target and signal model for widely separated MIMO radar. Cramer Rao Bound is derived for the target position and the target velocity estimations.

1.3 Organization of the Thesis

The thesis is organized as follows

Chapter 2 gives the brief historical development of radars and basic principles. Moreover, the general principles and knowledges in the scope of this thesis are summarized. After general radar information, MIMO radar and the Doppler-only systems are discussed. With a literature survey on MIMO radar and the target localization problem, this chapter is ended.

Chapter 3 starts with the signal model for frequency-only MIMO radar. This model includes Doppler shifts and the amplitude fluctuations because of the target motion. After modeling the received signal, the CRB is derived for the defined target and the signal model. The target localization problem using the frequency or Doppler shift informations is a nonlinear estimation problem, hence the CRB must be calculated carefully. By using the Swerling target fluctuation models, and the Fisher Information Matrix (FIM), CRBs are obtained for the target position and the target velocity estimations in two dimensional space.

Chapter 4 analyses the target localization methods for frequency-only (or Doppler-only) MIMO radars in detail. In this chapter, three target localization methods are presented for frequency-only MIMO radar. The first method is totally new method and it is based on the received frequencies only. This method can estimate the target velocity and the direction of the target as well. The second method is an expansion of a passive target localization method proposed for a sonar system. This method is expanded to the active MIMO radar case. The third method uses the Maximum-Likelihood (ML) method together with the grid search.

Chapter 5 includes the simulation results by using *MATLAB*[®]. Performances of the proposed

three target localization methods are presented and compared with the traditional isodoppler based method and the CRBs. Similarly, the target velocity estimation performance of the proposed method is compared with the CRB. The simulations are obtained for different number of transmitters and the receivers and for different target positions. Moreover, the complexity analysis of the proposed methods can be found in this chapter.

Chapter 6 deals with the target localization problem for multiple targets. The Doppler and velocity resolutions for Doppler-only systems are explained in this chapter. Then, the data association problem is investigated. For different system geometries and different targets the target localization performances are simulated. In simulations, maneuvering targets are studied as well and the validity of the proposed methods for maneuvering target case is shown.

And finally the chapter 7 is conclusion chapter and presents the short summary of all thesis and states the possible research areas for the future.

CHAPTER 2

BACKGROUND

2.1 Historical Overview

The word **RADAR** comes from the acronym for **RA**dio **D**etection **A**nd **R**anging. As it can be seen from this acronym, a radar has two main functions : Detection of a target and after detection, range of this target must be found. The earliest roots of radar can be associated with the theoretical work of famous Scottish physicist James Clark Maxwell (1831 - 1879) who predicted the propagation of electromagnetic waves and the experimental work of German physicist Heinrich Rudolf Hertz (1857 - 1894) that confirmed Maxwell's theory. The experimental works showed that the electromagnetic waves could be reflected and returned back by the objects. If one collects this returning waves, it can be possible to make a decision on a target is present or not. This is the first and the most important task of a radar system which is known as the "target detection" or only the "detection" in radar terminology. After deciding a target is present, some informations about the target such as range or velocity of the target can be obtained. This second task is known as the "measuring the range of a target" or shortly "ranging" in radar terminology and it may be very critical for some radar systems.

Early forms of radar devices were developed at the beginning of the 20th century that were also able to measure the distance of the target besides detecting it. The idea of a radar device was around for a long time, but the technology wasn't available to make it work. In 1904, Christian Hülsmeyer, who is a German high frequency technician, invented a device which is known as the "**Telemobiloscop**" to control the traffic on the water. This telemobiloscop was able to measure the time of the electromagnetic waves reflected and returned back from a metal object and hence the distance was able to found. This can be seen as the first practical

radar, and for this first radar, Hülsmeyer applied to the patent and this patent document can be seen in Figure 2.1 and Figure 2.2.



Figure 2.1: Patent document of Hülsmeyer's telemobiloskop (1)



Figure 2.2: Patent document of Hülsmeyer's telemobiloskop (2)

In 1922, A.H. Taylor and L.C. Young got ahead to sense a wooden ship from long distance for the first time and in 1930, L.A. Hyland perceived a plane from long distance. One of the biggest advances came as the result of the efforts of Robert Watson-Watt, a British scientist. Robert Watson-Watt detected an aircraft by observing the beats between the echo signal and

directly the received signal. The equipment employed would now known an passive, continuous wave (CW), bistatic radar using the short-range BBC broadcast signal as the transmitter and a non-collocated receiver. Great Britian made a big effort to develop radar before World War II. They built a network of early warning radar stations called "Chain Home" around the country to warn people of enemy attacks. During World War II, development of the radar systems was accelerated around the world because of the such military requirements. From 1936, after the invention of the duplexer by the Naval Research Laboratory of US meaning of using a common antenna for the transmitting and the receiving signals, the pulsed monostatic systems gain popularity.

At the beginnig of the radar history, radar worked with only one transmitter and one receiver. This transmitter-receiver pair could be in the same location by using the same antenna (monostatic radar), or they could have distinct transmitter-receiver units at different positions (bistatic radar). With the development of the radar technology, the multistatic radars (more than one reveivers and/or transmitters) are started to being used. One promising way is to move from the individual radar with a single transmitting station and a single receiving station (usually colocated) to the multisite radar sytems (MSRS) which includes several spatially separated transmitting and receiving stations (or monostatic radars) coupled together for coopereative target observation [1].

There can be many classifications on radars other than physical locations of the transmitting and the receiving units. Depending upon the transmitted waveform, radars can be divided by two. If a radar system works with continuous waves (usually with constant amplitude), it is named as continuous wave (CW) radar. When the transmitted waves are pulses, these radars are called as pulsed radars. Moreover, active and passive radars are the types with and without transmitters, respectively. The book of Victor S. Chernyak [2] is the first and the most detailed book on the multisite radar systems. The detailed information about the classification of radar systems can be found therein.

2.2 MIMO Radar

Radar systems, which include more than one spatially separated transmitter and/or receiver stations are used widely in last decades. These radar systems are called multistatic radars,

multisite radar systems, netted radars and finally multi-input, multi-output (MIMO) radars. In [2], multisite radar systems (MSRS) is defined as "A radar system including several spatially separated transmitting, receiving and (or) transmitting-receiving facilities where information of each target from all sensors are fused and jointly processed". Similarly in [3], the MIMO radar is defined as; "radar system employing multiple transmit waveforms and having the ability to jointly process signals received at multiple receive antennas". As seen from these definitions; MIMO radar is the sub-class of MSRS. Actually, using the spatially separated multiple stations is not a new idea with MIMO radar, maybe using the uncorrelated, if possible orthogonal, signals from each transmitter can be thought as a new idea with MIMO radars.

MIMO radar system refers to a radar network which employs multiple, spatially distributed transmitters and the receivers. While in a general sense, MIMO radar can be viewed as a type of multistatic radars, the separate nomenclature suggests unique features that set MIMO radar apart from the multistatic radar literature and that have a close relation to the MIMO communications[4]. Unlike the standart phased-array radar which transmits scaled version of a single waveform from its antennas, MIMO radar system can transmit, via its antennas, multiple signals which can be correlated or uncorrelated to each other[5]. A simple figure comparing both systems can be seen in Figure 2.3 [5].

MIMO radar systems can be divided in two main branches with respect to the distance between antennas. In the first case; transmitting and receiving antennas are widely separated to capture the spatial diversity of the target's radar cross section (RCS). In the second case; waveform diversity allowed by transmit and receive antenna arrays containing elements that are colocated. Some works on both "widely separated antennas" and "colocated antennas" cases are summarized at the review articles given in [4] and [5].

2.2.1 MIMO Radar with Colocated Antennas

As it is showed in [5], the waveform diversity enables the MIMO radar superiority in several fundamental aspects, including:

- Improved parameter identifiability,
- Direct application of adaptive arrays for the parameter estimation and target detection,

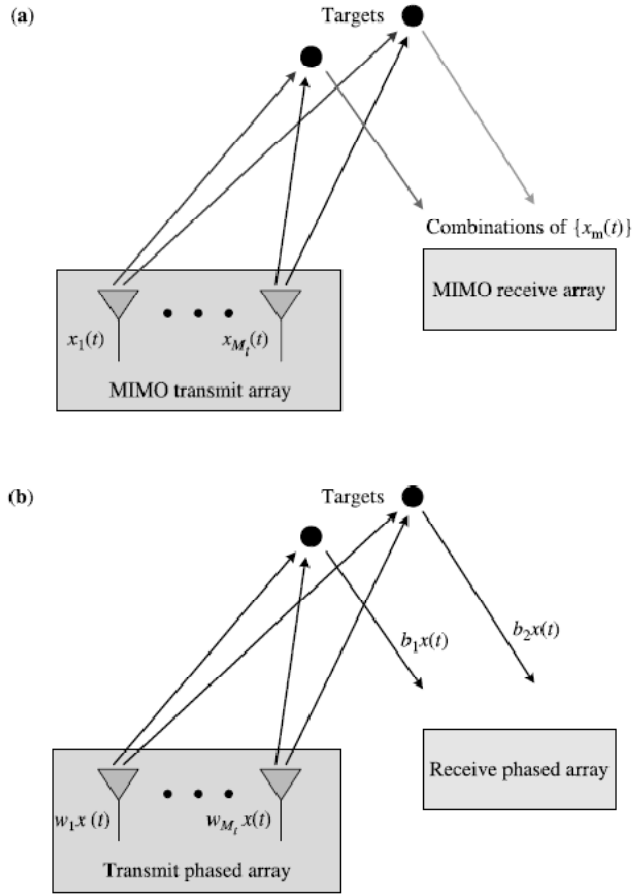


Figure 2.3: MIMO radar (a) versus Phased Array(b) (figure from [5])

- Enhancement of flexible transmit beampattern design.

Specifically, it is shown that:

- The maximum number of the targets which can be uniquely identified by the MIMO radar is up to N_T times that of its phased-array counterpart, where N_T is the number of the transmit antennas,
- The echoes due to targets at different locations can be linearly independent of each other, which allows the direct application of many adaptive techniques to achieve high resolution and excellent interference rejection capability,
- The probing signals transmitted via its antennas can be optimized to obtain several transmit beampattern designs with superior performance.

2.2.2 MIMO Radar with Widely Separated Antennas

From a model point of view, widely separated antennas take the advantage of the spatial properties of the extended targets, while with co-located antennas, the target is modeled as a point with no spatial properties. Each configuration and model has its strengths and challenges[4].

For quite some time, it has been understood that radar targets provide a rich scattering environment yielding 5-20 dB target RCS fluctuations, as illustrated in Figure 2.4 (figure from [6]). Such targets display essentially independent scattering returns when illuminated from sufficiently different directions. The premise of MIMO radar with widely separated antennas is that angular spread (RCS variations as a function of aspect) can be exploited to improve radar performance in a variety of ways.

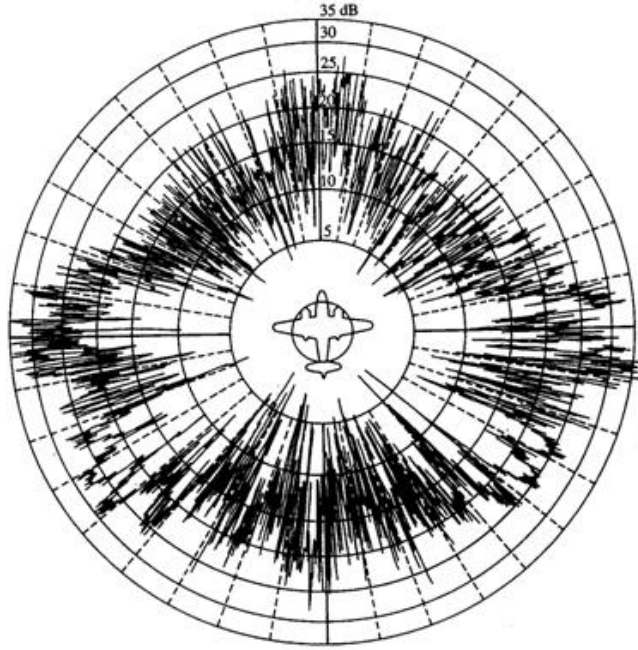


Figure 2.4: Radar backscatterer as function of azimuth (figure from [6])

In radar, the idea is that any individual look at the target might have a small amplitude return with a significant probability, but by increasing the number of looks, the probability that all the looks have same amplitude returns can be made arbitrarily small [4]. In MIMO radar, a multidimensional signal space is created when the returns from multiple scatterers or targets combine to generate a rich target backscatterer. With suitable design, from the transmitter to

the target and from target to the receiver paths can be separated and this separation can be used to exploit for improving the radar performance.

2.3 Target Localization by Using Doppler Shift

The primitive task of a radar was the target detection and that is to say that whether a target exists or not. With the time, the expectations from the radars have being increased. Today, besides the target detection, many parameters like velocity, position and the classification of targets, about the many kind of the targets can be estimated with modern radar units. With the technological developments of the electronic systems and the signal processors, returned signals from the target can be analyzed with high precision. Hence, the returned signal is more valuable and more meaningful with respect to the early days of the radar systems. In general, the used informations on the signal returned back from the target can be given as;

- Time-of-Arrival (TOA)
- Angle-of-Arrival (AOA),
- Frequency-of-Arrival (FOA).

TOA gives the arriving time of the transmitted signal's from the transmitter to the receiver after reflected by the target. AOA includes the angle information of the returned signal from the target. Similarly, FOA includes the frequency information of the backscattered signal.

In general, TOA is used for determining the range of the target, whereas FOA is used for the velocity estimation of the moving target and they can be used in cooperation to localize a target together with AOA. The detailed analysis of the target positioning by using TOA and/or AOA can be found in [2, 6].

Although many radar units have been developed so far, the number of the radars which operate only with the received frequency information (and hence with the doppler frequency) to localize a moving target is very low. The main aim of this thesis is to investigate the target localization algorithms for MIMO radars by using only the received frequencies or specifically the doppler shift informations.

The FOA information is commonly used for target localization when radar units are passive meaning that, there is no transmitter. In [7], Chan and Jardine proposed a method to estimate the target state by using only the doppler shifted frequencies for a sonar system. Actually, radar and sonar are very close applications, only difference is the transmission medium and the used signal type. In the same paper, it is shown that, a non-maneuvering target can be localized from the Doppler-shift measurements by using multi sensor architecture. In here, there are N passive sensors, and they try to localize a moving source which is non-maneuvering and radiates a constant frequency tone signal. Similar methods and some modifications can be seen in [8, 9, 10].

2.3.1 Basic Principles of Doppler-Only Radars

In 1842, Christian Andreas Doppler, an Austrian scientist, suggested a hypothesis which is now known as the "Doppler effect". According to Doppler, wavelength and the frequency of any physical quantity which shows wave property, is sensed in differently from an observer at different times and different places. This phenomenon was proved by Dutch physicist Christophorus Ballot using the sound waves in 1845. He showed that, the frequency of sound increases as closing to the source and decreases as retreating.

In radar systems, the doppler effect is used for moving target detection [6]. When a radar signal is scattered from a moving target, the frequency of the returned signal is shifted by the Doppler frequency. This Doppler shift is related with the carrier frequency of the transmitted signal and the velocity of the target. Similarly, for a passive radar, doppler shift exists because of the target motion. But if there is no target or platform motion, there is no doppler shift on the received frequencies. As shown in [7], a non-maneuvering target can be localized from Doppler-shift measurements by using multi sensor architecture. Here, there are N passive sensors, and they try to localize a moving source which is non-maneuvering and radiates a constant frequency tone signal. This radiated signal is received with different doppler-shifted versions by each receiver because of the motion of the target and the locations of the receivers.

In Figure 2.5, the geometry of a bistatic radar is shown. As explained before, bistatic radar includes one transmitter and one receiver which are physically separated from each others. On the other hand, monostatic radars include the transmitter and the receiver antennas collocated.

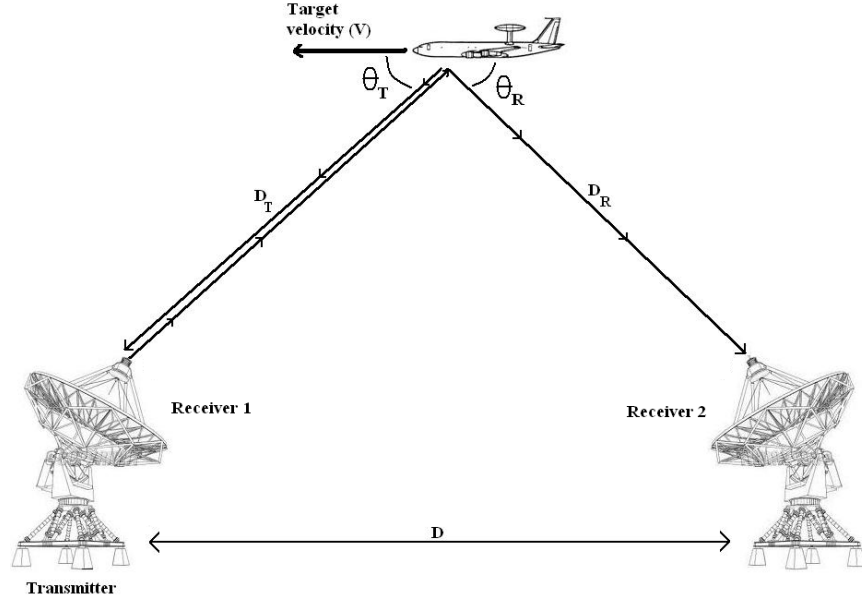


Figure 2.5: Monostatic and bistatic radars.

For example, in Figure 2.5, if transmitter receives the returned signal, this structure is called as monostatic radar (Trasmitter and Receiver 1 pair). If the trasnmitted signal is received from the distinct receiver, this time, the radar becomes bistatic (Trasmitter and Receiver 2 pair). The doppler frequencies can be written as[6];

$$f_{d_{monostatic}} = \frac{2f_c V}{c} \cos \theta_T \quad (2.1)$$

$$f_{d_{bistatic}} = \frac{f_c V}{c} (\cos \theta_T + \cos \theta_R) \quad (2.2)$$

where $f_{d_{monostatic}}$ is the doppler frequency of the monostatic radar, $f_{d_{bistatic}}$ is the doppler frequency of the bistatic radar, c is the speed of the light, f_c is the carrier frequency of the transmitted signal, θ_T and θ_R are the angles between the transmitter and the target movement direction and the Receiver 2 and the target movement direction respectively.

If the time-of-arrival (TOA) information exists, say t_{TOA} , then a monostatic radar is able to calculate the range of the target as;

$$D_T = \frac{c \times t_{TOA}}{2} \quad (2.3)$$

For monostatic radar, as the transmitter and the receiver are in the same location, the half of the signal flying time gives the distance of the target directly. But for bistatic radar, finding the range from the TOA information is more complex than monostatic range equation. In bistatic radar, if t_{TOA} is known, then the total flying time of the signal from transmitter to the target and from target to the receiver is known. If this total distance is called as $L = D_T + D_R$, by using the angle-of-arrival (AOA) informations, the distance from the receiver to the target can be found as;

$$D_R = \frac{L^2 - D^2}{2(L - D \cos \theta_R)} \quad (2.4)$$

By using the many estimation methods like beamforming etc, the AOA informations can be estimated. If D, L and θ_R are all known, then D_T can be calculated by using the D_R found in (2.4) as;

$$D_T^2 = D^2 + D_R^2 - 2DD_R \cos(\theta_R) \quad (2.5)$$

As it can be seen from the equations (2.1) and (2.2), Doppler shift of the received signal is determined by the carrier frequency of the transmitted signal, the target velocity and the system geometry or locations of the radar units. Especially for monostatic radar, when the path of the moving target is orthogonal to the radar's aspect angle, returned signal includes zero doppler. This phenomenon is known as blind speed of the target. In such a case, although the target is moving, doppler shift is zero and the target seems as if steady and non-moving. The same situation appears for the bistatic radar when the target is moving perpendicularly both to the transmitter and to the receiver's baseline (or direct path). But this has very low probability than the monostatic case.

Using more than one transmitter and/or receiver units overcome the problems of blind speeds. When a multistatic or MIMO radar is used, some receivers may be faced with blind speeds but the other receivers, which are physically at different locations, measure the doppler shifts different from zero. And these measured doppler shifts can be very different from the each others because of the system geometry. This is the one advantage of the multistatic or MIMO radars with widely separated antennas.

2.3.2 Localization by using Doppler Shift

The main problem in bistatic radar is the synchronization of the transmitter and the receiver units which is a prerequisite to find the target position by using time of arrival (TOA) information. Usually, if the angles between the transmitter and the target and the receiver and the target and TOA are known, then an ellipsoid (isorange curve) which the target is on can be drawn as in Figure 2.6 [11]. If the system includes more than one bistatic radar, by using their ellipsoids, the position of the target can be found from their intersection. This process requires at least three bistatic radar units for localizing the target unambiguously [6].

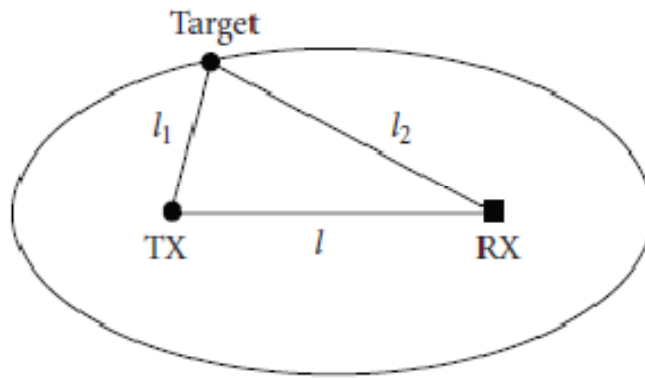


Figure 2.6: Equi-TOA positions (ellipses) in a bistatic radar

Another important curves for the bistatic radar is known as the Cassini ovals or Cassini ellipses shown as Figure 2.7 [12].

In 1680, famous astronomer Cassini investigated Cassini ovals when he was studying on the relative motions of the Earth and the Sun. For two fixed points, with a distance $l = 2A$, a point which is apart from these fixed points with distance of l_1 and l_2 gives the cassini ovals with fixed $l_1 \times l_2 = B^2$. The shape of the curves depends on B/A , hence three case can be defined as;

- If $A < B$, then this produces a single loop with an oval (leftmost figure) or a dog bone shape (the second plot in Figure 2.8),
- If $A = B$, then the shape is a lemniscate (the third plot in Figure 2.8),
- If $A > B$, then the shape consists of two loops (rightmost plot in Figure 2.8).

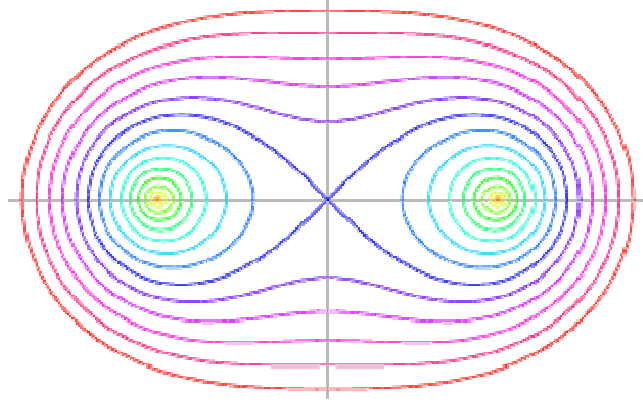


Figure 2.7: Cassini ovals

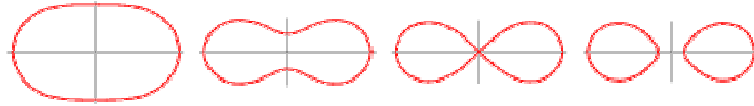


Figure 2.8: Different Cassini ovals

From the bistatic radar point of view, if the curve of constant received power is drawn according to receiver side, these points produce a cassini oval with foci in the transmitter and the receiver. Many of these ellipses can be used to target positioning.

In similar manner, the received frequencies can be used for the target localization. Frequency of arrival (FOA) or Frequency difference of arrival (FDOA) methods are generally used for estimating the transmitter location in a passive radar/sonar system. This method is based on the measurement of the frequency of the received signal at two spatially separated moving receivers. FDOA method was originally developed by radio astronomers and they called this method as the very long baseline interferometer (VLBI). The similar concept is named as differential doppler, frequency difference of arrival (FDOA), inregrated doppler [13].

The method is similar to the isorange curves based TOA method. After obtained the received frequencies from the backscattered signals, because of the doppler effect, the received frequencies will be related to the target position. When the received frequencies and the transmitted frequencies are known, doppler shift is also known and hence the locus of points for that doppler shift gives a curve which is called as isodoppler curve or shortly as isodop. If

more than one isodops can be obtained, then the intersection of all isodops gives the target location.

2.4 Literature Overview

MIMO radar is highly popular research area since 2004. There are many works in the literature on MIMO radar for both colocated and widely separated cases. The starting point of the MIMO radar with widely separated case can be shown as the works of Fishler et al. [14, 15, 16]. In [14], the impact of transmit diversity on the error of Direction Finding (DF) techniques is shown based on the average Cramer Rao Bound (CRB). In [15], improvements in detection performance with MIMO radar are investigated for widely separated case. In [16], the work in [14] is expanded for outage CRB case and addressed for the correlated target aspects.

There are many works in literature on target localization for MIMO radar both widely separated and colocated antennas cases [3, 17, 18, 19]. In [3] and [17] the high resolution target localization is investigated for MIMO radar with widely separated antennas whereas in [18] and [19] localization algorithms are proposed for MIMO radar with colocated antennas case.

In [3], target localization methods for MIMO radar is summarized, and Cramer Rao Lower Bound (CRLB) is derived. In the same paper, target localization is performed by using Time Difference of Arrival (TDOA) information. After the derivation of CRLB, two estimators are proposed; the maximum likelihood estimator (MLE) and the best linear unbiased estimator (BLUE). But these estimators and CRB calculation do not include doppler information. Here, the CRLB is derived when localization is performed for both coherent and non-coherent cases and in [20], CRB is derived when there is a phase error on coherent processing. Similarly, in [21], CRB is studied for MIMO radar with widely separated antennas case when modeling error exists on angle of arrival information.

In [22], the detailed analysis of attainable gain on MIMO radar-based systems for target localization procedure is given. CRB is derived for coherent and non-coherent processing for widely separated case. TDOA and AOA informations are used for target localization.

In [23], target tracking is considered for a network of Doppler radars. These radars work only

monostatic configuration and Cramer-Rao bound on motion parameter uncertainty is obtained for phase and frequency based estimation strategies.

In [24], CRB is derived for moving target localization in a doppler frequency-only radar system, which includes 2 transmitters and one receiver. In here, observations are assumed as the received frequencies and the CRB is derived when frequency measurement error is white and gaussian.

In [25], a method for the target tracking for MIMO radar is proposed. The proposed method is the amplitude-comparison monopulse MIMO radar, and it uses directed beam for target tracking. As shown in [7], a non-maneuvering target can be localized from Doppler-shift measurements by using multi sensor architecture. In here, there are N passive sensors, and they try to localize a moving source which is non-maneuvering and radiates a constant frequency tone signal.

In [26], the target detection problem with MIMO radar is investigated when the clutter is non-gaussian and heterogeneous.

Waveform design is another popular research area for MIMO radar. There are many works on MIMO radar waveform design optimization for target detection or target localization [27, 28, 29, 30].

The major tool for analyzing the radar signals is the ambiguity functions. In [31], the classical ambiguity function is expanded to the MIMO radar case. And in [32], properties of MIMO radar ambiguity functions are investigated.

Besides the target detection, the target localization and the waveform design/optimization for MIMO radars, there are many new areas which can be exemplified as; compressed sensing for MIMO radar [33] and beamforming for MIMO radars [34].

MIMO or multistatic concept (having more than one transmitter and receiver units) is today used in many areas. The narrowband tomography approach proposed by Wicks and others [35, 36] and sensing cardiopulmonary activity [37] can be shown as examples of these areas. On the other hand, the geolocation of a stationary emitter by using delay and doppler informations is still popular research areas [38, 39].

CHAPTER 3

SIGNAL MODEL and THE CRAMER-RAO BOUND FOR FREQUENCY-ONLY MIMO RADAR

In this dissertation, the target localization and the target velocity estimation methods for the frequency-only MIMO radar are proposed. Actually, these methods are applicable for all the frequency based systems, for instance sonar or wireless sensor networks. The distinctions between these systems are the transmission medium and the properties of the radiated signals. Therefore, to analyze the performances of the proposed target localization methods, suitable signal model must be constructed and then, the physical bounds must be defined for the target localization and the target velocity estimation problem.

In this chapter, firstly the signal model for frequency-only MIMO radar is given. This model includes the Doppler shift and the target fluctuations. These amplitude and phase variations are modelled using the Swerling target fluctuation models.

Surely, each bound depends on the signal model and the probability density functions of the random variables. Hence, before detailed analysis of the CRB, the signal model must be given. Then, the Cramer Rao Bounds (CRB) for the target localization and the target velocity estimation problems are investigated using defined signal and the target models.

3.1 Signal and Noise Model

The MIMO radar includes N_T transmitters and N_R receivers which are widely separated, ground based and stationary. The whole radar pairs are working in bistatic manner meaning that, the transmitters do not receive any returned signals. Hence, the total number of $N = N_T \times N_R$ bistatic radar pairs exist. They are located in two dimensional plane as in Figure 3.1.

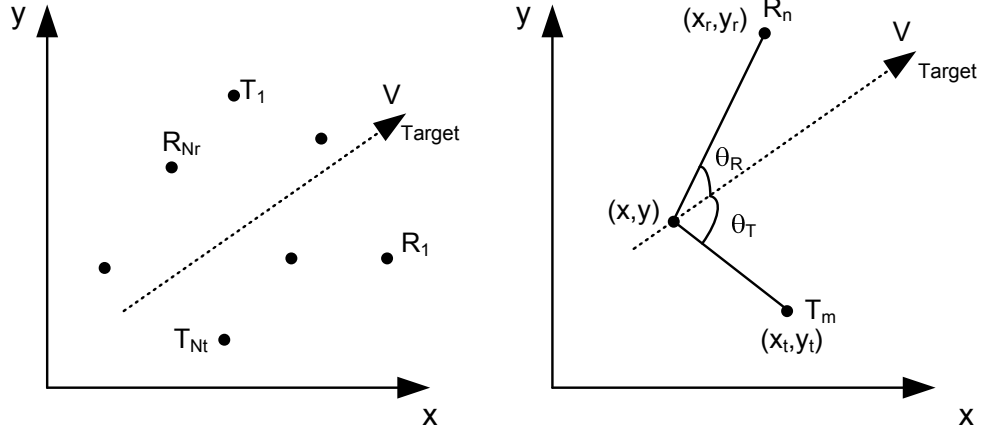


Figure 3.1: The MIMO radar geometry. a) for N_T transmitters and N_R receivers, b) for single transmitter-receiver.

N_T transmitters radiate unmodulated, continuous wave (CW) tone signals with distinct frequencies which are f_1, f_2, \dots, f_{N_T} . N_R receivers intercept these signals as attenuated and time delayed with Doppler-shifted frequencies because of the target motion. Each receiver can measure N_T radiated frequencies and each transmitted signal can be separated in the receiver sites. The frequency separations of the transmitters are tuned carefully to satisfy the following condition

$$f_{j-1} < f_j \mp f_{d_{max}} < f_{j+1} \quad ; \quad \text{for all } j \quad (3.1)$$

where $f_{d_{max}}$ is the maximum Doppler frequency of the whole system, and the transmitted frequencies are assumed as

$$f_1 < f_2 < \dots < f_{N_T} \quad (3.2)$$

Let N_T transmitters be arbitrary located at $T_j = (x_{T_j}, y_{T_j})$, $j = 1, 2, \dots, N_T$. The signals that are scattered by the target at (x, y) are collected using N_R receivers placed at arbitrary

coordinates $R_i = (x_{R_i}, y_{R_i})$, $i = 1, 2, \dots, N_R$. The set of transmitted waveforms in lowpass equivalent form is $\sqrt{E_e} s_k(t)$, $k = 1, 2, \dots, N_T$ where $\int_0^T |s_k(t)|^2 dt = 1$, $E_e = E/N_T$ is the normalized transmitted energy while E is the total transmitted energy, and T is the total observation time [40].

Consider the baseband representation of the signal observed at the l^{th} receiver due to the transmissions from all N_T transmitters. The received signal of the l^{th} receiver can be written as

$$r_l(t) = \sqrt{E_e} \sum_{k=1}^{N_T} \Psi s_k(t - \tau_{lk}) \exp(-j2\pi f_k \tau_{lk}) + w_l(t) \quad (3.3)$$

where Ψ is the spatially homogeneous, possibly complex reflectivity of the target, f_k is the carrier frequency of the k^{th} transmitter, $w_l(t)$ is the spatially and temporally white circularly symmetric zero mean gaussian noise with autocorrelation function $\sigma_w^2 \delta(\tau)$ and τ_{lk} is the time delay which is the sum of the time delays from the k^{th} transmitter to the target and from the target to the l^{th} receiver which defined as

$$\tau_{lk} = \frac{1}{C} (L_{T_k} + L_{R_l}) \quad (3.4)$$

where C is the speed of the light, L_{T_k} and L_{R_l} represent the distances between the target and the k^{th} transmitter and the target and the l^{th} receiver respectively. These distances can be defined as follows

$$L_{T_k} = \sqrt{(x - x_{T_k})^2 + (y - y_{T_k})^2}, \quad k = 1, 2, \dots, N_T \quad (3.5)$$

$$L_{R_l} = \sqrt{(x - x_{R_l})^2 + (y - y_{R_l})^2}, \quad l = 1, 2, \dots, N_R \quad (3.6)$$

The model given in equation (3.3) is the model used in [40]. This signal model is widely used in the literature for MIMO radar, but as can be seen, this model does not include the Doppler shift. To get the signal model for the frequency-only MIMO radar, the Doppler frequency shift has to be included. If this is the case, the signal model becomes

$$r_l(t) = \sqrt{E_e} \sum_{k=1}^{N_T} \Psi s_k(t - \tau_{lk}) \exp(-j2\pi(f_k + f_{d_{lk}})(t - \tau_{lk})) + w_l(t) \quad (3.7)$$

where $f_{d_{lk}}$ is the Doppler frequency of the k^{th} transmitted frequency at the l^{th} receiver and it is given by

$$f_{d_{lk}} = -\frac{f_k}{C} \left(\frac{(x - x_{T_k})V_x + (y - y_{T_k})V_y}{\sqrt{(x - x_{T_k})^2 + (y - y_{T_k})^2}} + \frac{(x - x_{R_l})V_x + (y - y_{R_l})V_y}{\sqrt{(x - x_{R_l})^2 + (y - y_{R_l})^2}} \right) \quad (3.8)$$

Finally, the target fluctuations should be modelled more generally to obtain more realistic model. Let $A_{lk}(t)$ be the complex target fluctuations. The statistical properties of the $A_{lk}(t)$ will be given in the next section. For this case, the signal model becomes

$$r_l(t) = \sqrt{E_e} \sum_{k=1}^{N_T} A_{lk}(t) s_k(t - \tau_{lk}) \exp(-j2\pi(f_k + f_{d_{lk}})(t - \tau_{lk})) + w_l(t) \quad (3.9)$$

As the transmitted signals are narrow band (NB) then, $s_k(t - \tau_{lk}) \approx s_k(t)$. There is nearly no change of the signal envelope for the time delay [41, 42]. Then, the received signal of the l^{th} receiver can be written as

$$r_l(t) = \sqrt{E_e} \sum_{k=1}^{N_T} A_{lk}(t) s_k(t) \exp(-j2\pi(f_k + f_{d_{lk}})(t - \tau_{lk})) + w_l(t) ; \quad 0 \leq t \leq T \quad (3.10)$$

After sampling with period T_s , the signal samples are given by

$$r_l[n] = r_l(nT_s) \quad ; \quad n = 1, 2, \dots, N \quad (3.11)$$

and

$$\mathbf{r}_l = [r_l[1], r_l[2], \dots, r_l[N]]^T \quad ; \quad l = 1, 2, \dots, N_R \quad (3.12)$$

The exact received signal is the combination of all the received frequencies as follows

$$\mathbf{r} = [r_1 \quad r_2 \quad \dots \quad r_{N_R}]^T \quad (3.13)$$

The block diagram of the whole system can be seen in Figure 3.2 in the next page. Each receiver receives N_T signals with N_T distinct frequencies. These received signals downconverted to the baseband using N_T demodulator filterbanks (Figure 3.2.b) using Low Pass Filters with $W = W_{d_{max}}$ where $W_{d_{max}}$ is the maximum Doppler frequency of the system in radian per second. Then downconverted signal is transferred to the Doppler filterbanks to limit the signal bandwidth to $B = 1/T$ where T is the total observation time. Finally the Doppler frequencies are estimated and sent to the fusion center to find the target position.

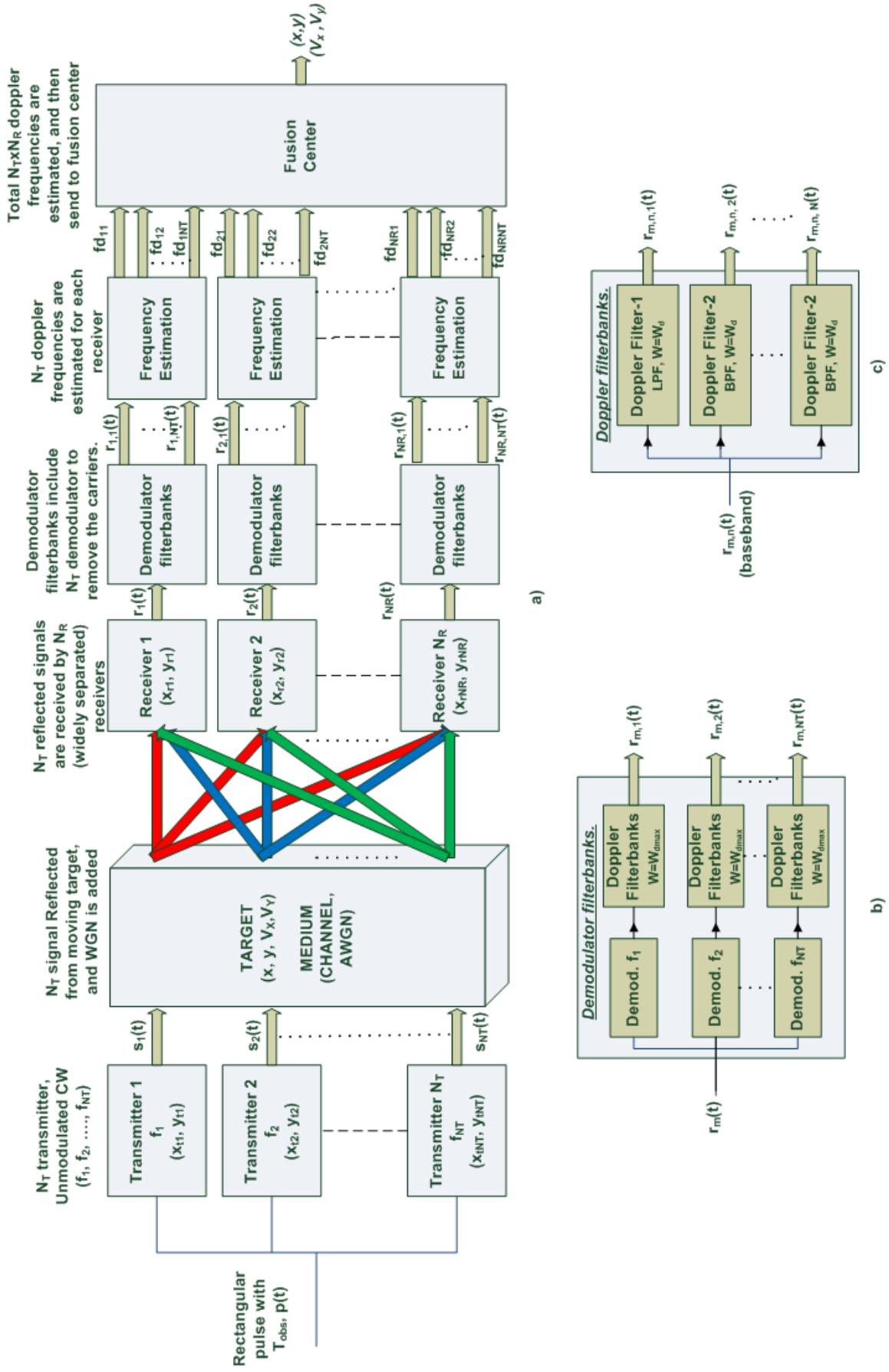


Figure 3.2: a) Block diagram of the whole system. b) Demodulator filterbanks. c) Doppler filterbanks.

3.2 Properties of the Target Fluctuations

The magnitude of the backscattered signal from the target depends on the property of the scattering object. This property is known as the radar cross section (RCS) of the scattering object and defined as [6]

$$P_r = \frac{P_t G}{4\pi R^2} \cdot \frac{\sigma}{4\pi R^2} \quad (3.14)$$

where P_r is the reradiated power density back at the radar, P_t is the transmitted power, G is the gain of the antenna, R is the distance of the target to the radar and σ is the RCS of the target.

The radar cross sections of the complex targets such as the missiles, aircrafts, ships and ground vehicles can vary depending on the aspect angle and the carrier frequency. The complex objects are constituted from many individual scatterers, hence each individual scatterer produces an echo signal which is characterized by an amplitude and phase. These echoes are summed up at the receiver to form a resultant signal.

A small change in aspect angle of a radar target may result big changes in the RCS. This situation can be seen in famous figure from Skolnik in Figure 2.4. If the aspect angle of the target changes relative to the radar, there will be changes in the distances to the scatterers. This cause the changes in the relative phases of the echo signal from the different scatterers. A relative phase is greater than 2π radians can yield a significant change in the resultant phase and amplitude of the composite echo signal, that results in target cross section fluctuations or fading.

A popular method for representing the target fluctuations are described by Peter Swerling [43]. Swerling models are the models of the probability density function (pdf) and time correlation properties of the radar backscatter from a complex target [44]. Developed in the early days of the radar, Swerling models apply to finite group of pulses. They were developed with the model of a rotating surveillance radar in mind. As the radar beam sweeps past a target (a single scan), it collects echoes from that target in the appropriate range bin for several pulses. Once the beam moves past the target, no more echoes are received until the next scan (in pulsed radar case), when the beam has swung back around the the target position again, another group of several pulses is then received. Detection is assumed to be attempted using all of the pulses from a single scan. Thus, the joint statistics of a group of target echo samples

from contiguous pulses of a single scan are of interest.

Swerling models are formed from the four combinations of two probability density functions (pdf's) for the individual echo powers and two assumptions regarding the decorrelation time, or independence, of pulses within a single scan according to the Table 3.1 [44]

Table 3.1: Swerling Target Models

probability density function of power	decorrelation	
	scan-to-scan	pulse-to-pulse
exponential	1	2
chi-square, degree 4	3	4

The individual echo powers (proportional to radar cross section) are assumed to exhibit either an exponential pdf (Swerling 1 and 2) or a 4th-degree chi-square pdf (Swerling 3 and 4). The corresponding voltage distributions (square root of power) are the Rayleigh and the 4th-degree chi distributions. The exponential probability density function of mean μ is given by [45]

$$p_x(x) = \begin{cases} \frac{1}{\mu} e^{-\frac{x}{\mu}} & ; \quad x \geq 0 \\ 0 & ; \quad x < 0 \end{cases} \quad (3.15)$$

The standart deviation of this exponential random variable is μ^2 . To generate the exponential random variable x , a simple way can be used by the following transformation [46]

$$x = -\mu \ln(u) \quad (3.16)$$

where u is a random variable which is uniform with (0, 1]. In Figure 3.3 the exponential pdf can be seen generated in this way using matlab.

Similarly, the 4th – degree chi-square probability density function of mean μ is given by [45]

$$p_x(x) = \begin{cases} \frac{4x}{\mu^2} e^{-\frac{2x}{\mu}} & ; \quad x \geq 0 \\ 0 & ; \quad x < 0 \end{cases} \quad (3.17)$$

The variance(σ^2) of this random variable is $\mu^2/2$. To generate 4th – degree chi-square random variable x , a simple way is to use [46]

$$x = -\frac{\mu}{2} \ln(u_1.u_2) \quad (3.18)$$

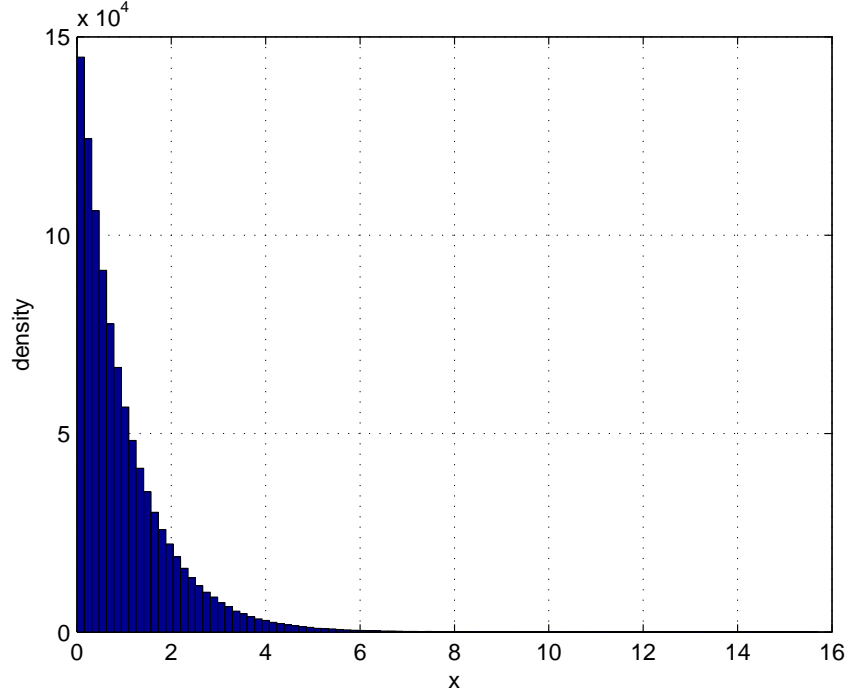


Figure 3.3: 100-bin histogram of a unit mean exponential sample sequence generated in MATLAB using equation (3.16)

where u_1 and u_2 are independent uniform $(0, 1]$ random variables. In Figure 3.4 the 4th – degree chi-square pdf can be seen generated in this way using matlab.

The Rayleigh voltage/exponential power pdf, which is obtained from law of large number argument, is appropriate for a target composed of a large number of approximately equal-strength scatterers, with no one scatterer dominant. It is often applied to large (with respect to wavelength), complex targets especially when viewed over changing aspect angles.

The Rayleigh probability density function of mean μ is given by [45]

$$p_x(x) = \begin{cases} \frac{\pi x}{2\mu^2} e^{-\frac{\pi x^2}{4\mu^2}} & ; \quad x \geq 0 \\ 0 & ; \quad x < 0 \end{cases} \quad (3.19)$$

The standart deviation of this Rayleigh random variable is $\mu \sqrt{(4 - \pi)/\pi} = 0.5227\mu$. A simple way to generate Rayleigh random variable x , is to use [46]

$$x = \sqrt{-\frac{4\mu^2}{\pi} \ln(u)} \quad (3.20)$$

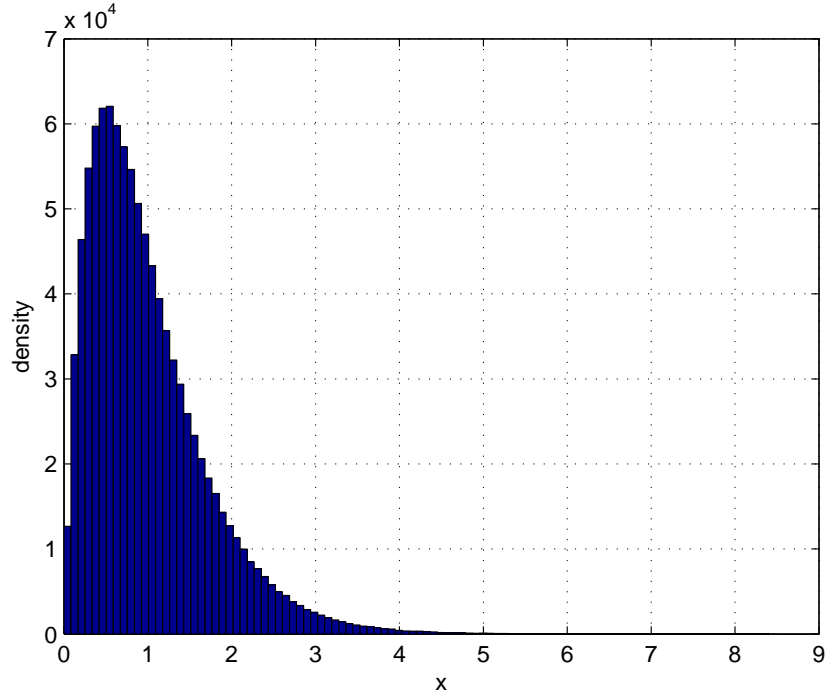


Figure 3.4: 100-bin histogram of a unit mean 4^{th} – degree chi square sample sequence generated in MATLAB using equation (3.18)

where u is uniform $(0, 1]$ random variable. In Figure 3.5 the Rayleigh pdf can be seen generated in this way using Matlab.

The 4^{th} -degree chi voltage/ 4^{th} -degree chi-square power pdf is an approximation to the pdf obtained in the case of a large number of equal strength scatterers plus a single, steady dominant scatterer, with the power of the dominant scatterer equal to $(1 + \sqrt{2})$ times the total power of all the small scatterers. This particular dominant/small scatterer ratio of $(1 + \sqrt{2})$ is the ratio that causes the first two moments of the Rice distribution to match the chi-square distribution. The exact distribution for this case is the Rice or Rician distribution, which can model any ratio of the dominant to lesser scatterers. However, the Swerling approximation is well-entrenched, partly because it is more analytically tractable.

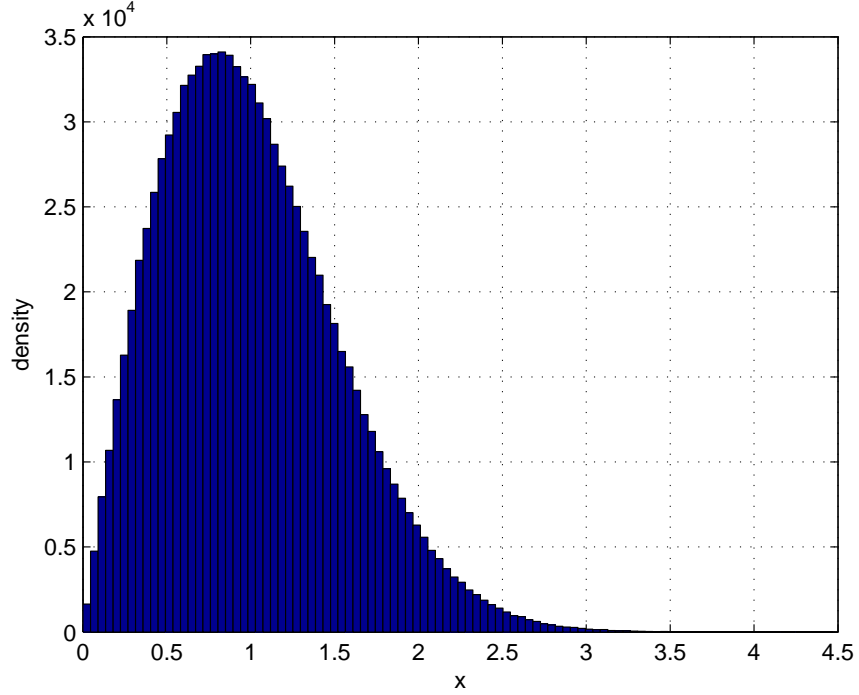


Figure 3.5: 100-bin histogram of a unit mean Rayleigh sample sequence generated in MATLAB using equation (3.20)

3.3 Target Model

All radars are ground based, stationary and the target is an aircraft, hence it can be modeled as a complex target. Moreover there is no clutter or multipath effect and there is only one target to be localized. If this is the case, the target consists of many small scatterers, and Swerling target models can be used safely to represent the target fluctuations. To choose the proper Swerling fluctuation model, the decorrelation time of the used signals must be calculated, and then the used probability density function must be defined.

The radars are operated in X-band because of the small sizes of the X-band radars, and the cost of them. These radars operate on a frequency of $8-12GHz$ and a wavelength of $2.5-4cm$. X-band radars are more sensitive than low-frequency radars and can detect smaller particles because of the smaller wavelength. Also, due to the small size of the radar, it can therefore be portable like the Doppler on Wheels (DOW). Most major airplanes are equipped with an X band radar to pick up turbulence and other weather phenomenon [47]. The other frequencies used for the radar applications can be seen in the Table A.1 [48] in Appendix A.

The geometry of the target and the radars is shown in Figure 3.6.

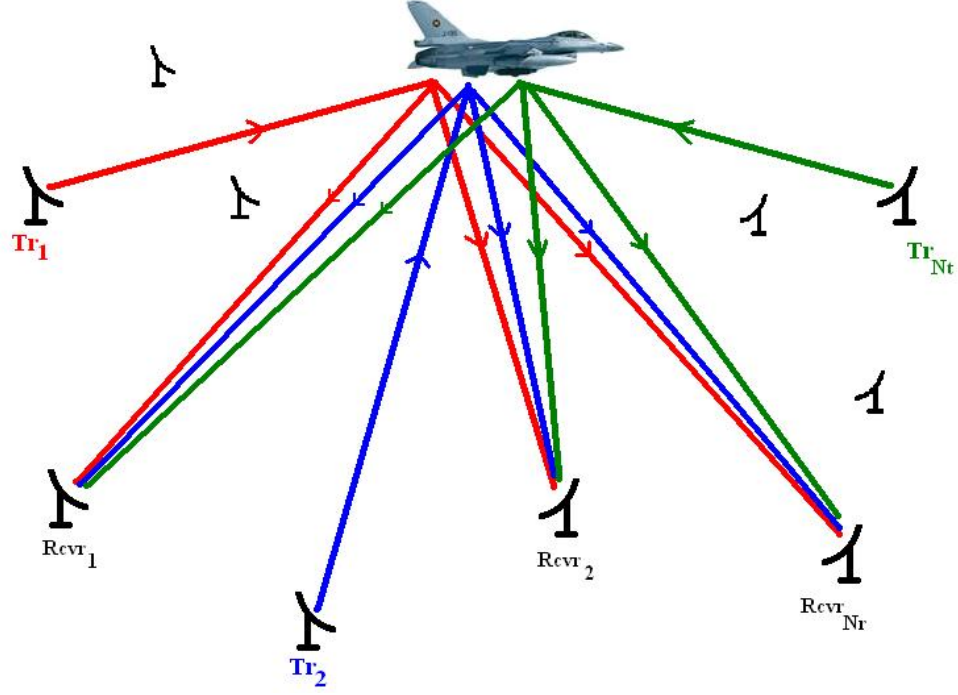


Figure 3.6: Target model

The maximum velocity of the target is chosen as $V_{max} = 900 \text{ kmph} = 250 \text{ m/sec}$ and the maximum carrier frequency is $f_{max} = 10.5 \text{ GHz}$. For these settings, the maximum Doppler frequency can be calculated as

$$\begin{aligned}
 f_{d_{max}} &= 2 \frac{V_{max}}{c} f_{max} \\
 &= 2 \frac{250}{3 \times 10^8} 10.5 \times 10^9 \\
 &= 17.5 \text{ kHz}
 \end{aligned} \tag{3.21}$$

By using the maximum Doppler frequency, the coherence time (T_c) can be calculated as

$$\begin{aligned}
 T_c &= \frac{1}{f_{d_{max}}} \\
 &= \frac{1}{17500} \\
 &= 57.143 \text{ } \mu\text{s}
 \end{aligned} \tag{3.22}$$

The coherence time is defined as the time duration over which the channel impulse response is essentially invariant in wireless communication. The coherence time implies that two signals arriving with a time separation greater than T_c are affected by the channel differently.

Therefore, this quantity can be used to find the decorrelation time of the received signals in MIMO radar. The samples in T_c time are faced with the same channel, hence the all samples in T_c will be affected same. On the other hand, two samples with distinction of T_c seconds will be uncorrelated to each other.

The observation time of the received signal is chosen as $T_{obs} = 10$ msec. The observation time is divided by 200 equi-length blocks which are $50 \mu sec$ as in Figure 3.7. Each block can be assumed as decorrelated to each other. These indicates that Swerling 2 or Swerling 4 type target fluctuations can be used. The selection of Swerling case depends on the type of the used pdf and actually it depends on the whether target includes a dominant scatterer or not. If target is composed of many small equi-size scatterers, then exponential pdf is used and this is Swerling 2 type target model. If target includes one dominant scatterer besides the small many ones, then the pdf is 4^{th} – degree chi-square pdf and it represents Swerling 4 type target model. In simulations, both cases are simulated together with non-fluctuating case (Swerling 0 or Swerling 5).

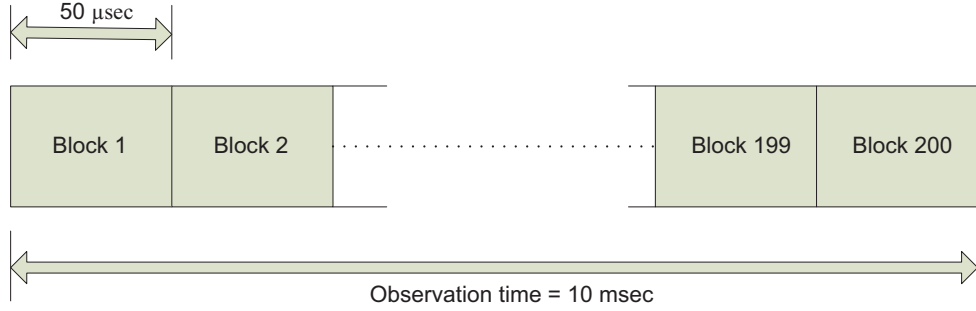


Figure 3.7: Dividing the observation time in blocks.

3.4 Cramer-Rao Bound for Target Localization and Velocity Estimation

Being able to place a lower bound on the variance of any unbiased estimator proves to be extremely useful in practice [49]. At worst, it provides a benchmark against which we can compare the performance of any unbiased estimator. Furthermore, it alerts us to the physical impossibility of finding an unbiased estimator whose variance is less than the bound. Although many such variance bounds exist, the Cramer-Rao lower bound (CRB) is by far the easiest to determine. Also, the theory allows us to determine if an estimator exists that attains the bound.

The CRB provides a lower bound for the mean square error (MSE) of any unbiased estimator for unknown parameters [40]. Given a vector parameter $\boldsymbol{\theta} = [\theta_1, \theta_2, \dots, \theta_m]^T$, assume that the estimator is unbiased. Then, the vector parameter CRB allow us to place a lower bound on the variance of each element. The CRB is defined as the $[i, i]$ element of the inverse of a matrix or [49]

$$\text{var}(\widehat{\theta}_i) \geq [\mathbf{J}^{-1}(\boldsymbol{\theta})]_{i,i} \quad (3.23)$$

where $\mathbf{J}(\boldsymbol{\theta})$ is the $m \times m$ Fisher Information matrix (FIM) and the elements of FIM are given by

$$[\mathbf{J}(\boldsymbol{\theta})]_{i,j} = -E \left[\frac{\partial^2 \ln p(\boldsymbol{\eta}; \boldsymbol{\theta})}{\partial \theta_i \partial \theta_j} \right] \quad (3.24)$$

for $i = 1, 2, \dots, m$; $j = 1, 2, \dots, m$ and where $p(\boldsymbol{\eta}; \boldsymbol{\theta})$ is the joint probability density function (pdf) of $\boldsymbol{\eta}$ and $\boldsymbol{\theta}$. And finally the CRB matrix can be found as

$$\mathbf{C}_{\text{CRB}} = [\mathbf{J}^{-1}(\boldsymbol{\theta})] \quad (3.25)$$

In the case of Gaussian observations, the CRB can be derived as shown in [49]. Assume that a random variable $\boldsymbol{\eta}$ has a Gaussian pdf as $\boldsymbol{\eta} \sim N(\boldsymbol{\mu}(\boldsymbol{\theta}), \mathbf{C}(\boldsymbol{\theta}))$, where $\boldsymbol{\mu}(\boldsymbol{\theta})$ is the $m \times 1$ mean vector and $\mathbf{C}(\boldsymbol{\theta})$ is the $m \times m$ covariance matrix both of which depend on $\boldsymbol{\theta}$. Then, the FIM is given by

$$[\mathbf{J}(\boldsymbol{\theta})]_{i,j} = 2\text{Re} \left[\left[\frac{\partial \boldsymbol{\mu}(\boldsymbol{\theta})}{\partial \theta_i} \right]^H \mathbf{C}^{-1}(\boldsymbol{\theta}) \left[\frac{\partial \boldsymbol{\mu}(\boldsymbol{\theta})}{\partial \theta_j} \right] \right] + \text{tr} \left[\mathbf{C}^{-1}(\boldsymbol{\theta}) \frac{\partial \mathbf{C}(\boldsymbol{\theta})}{\partial \theta_i} \mathbf{C}^{-1}(\boldsymbol{\theta}) \frac{\partial \mathbf{C}(\boldsymbol{\theta})}{\partial \theta_j} \right] \quad (3.26)$$

for $i = 1, 2, \dots, m$; $j = 1, 2, \dots, m$ and where $\frac{\partial \mathbf{C}(\boldsymbol{\theta})}{\partial \theta_k}$ is the $m \times m$ matrix with $[i, j]$ element $\frac{\partial [\mathbf{C}(\boldsymbol{\theta})]_{ij}}{\partial \theta_k}$.

For the target localization problem in two dimensional space, the vector of unknowns is defined as

$$\boldsymbol{\theta} \triangleq [x, y, V_x, V_y]^T \quad (3.27)$$

and for these unknowns, the Fisher Information Matrix can be formed as follows

$$\mathbf{J}(\boldsymbol{\theta}) = \begin{bmatrix} J_{xx} & J_{xy} & J_{xV_x} & J_{xV_y} \\ J_{yx} & J_{yy} & J_{yV_x} & J_{yV_y} \\ J_{V_x x} & J_{V_x y} & J_{V_x V_x} & J_{V_x V_y} \\ J_{V_y x} & J_{V_y y} & J_{V_y V_x} & J_{V_y V_y} \end{bmatrix}$$

For the problem given here, the received signal of the l^{th} receiver can be written as

$$r_l(t) = \sqrt{E_e} \sum_{k=1}^{N_T} A_{lk}(t) s_k(t) \exp(-j2\pi(f_k + f_{d_{lk}})(t - \tau_{lk})) + w_l(t) \quad (3.28)$$

$$= s_l(t, \boldsymbol{\theta}) + w_l(t) \quad ; \quad 0 \leq t \leq T \quad ; \quad l = 1, 2, \dots, N_R \quad (3.29)$$

where T is the total observation time and N_R is the total number of receivers. After sampling with period T_s , the signal samples are given by

$$r_l[n] = r_l(nT_s) \quad ; \quad n = 1, 2, \dots, N \quad (3.30)$$

$$r_l[n] = s_l[n, \boldsymbol{\theta}] + w_l[n] \quad ; \quad n = 1, 2, \dots, N \quad (3.31)$$

and

$$\mathbf{r}_l = [r_l[1], r_l[2], \dots, r_l[N]] \quad ; \quad l = 1, 2, \dots, N_R \quad (3.32)$$

$$\mathbf{s}_l(\boldsymbol{\theta}) = [s_l[1, \boldsymbol{\theta}], s_l[2, \boldsymbol{\theta}], \dots, s_l[N, \boldsymbol{\theta}]] \quad ; \quad l = 1, 2, \dots, N_R \quad (3.33)$$

The exact received signal is the combination of all the received frequencies as follows

$$\mathbf{r} = [\mathbf{r}_1, \mathbf{r}_2, \dots, \mathbf{r}_{N_R}]^T \quad (3.34)$$

and similarly

$$\mathbf{s}(\boldsymbol{\theta}) = [\mathbf{s}_1(\boldsymbol{\theta}), \mathbf{s}_2(\boldsymbol{\theta}), \dots, \mathbf{s}_{N_R}(\boldsymbol{\theta})]^T \quad (3.35)$$

Hence, $p(\mathbf{r}|\boldsymbol{\theta}) \sim N(\boldsymbol{\mu}(\boldsymbol{\theta}), \sigma^2)$, where $\boldsymbol{\theta} = [x, y, V_x, V_y]$ and $\mathbf{C}(\boldsymbol{\theta}) = \sigma^2 \mathbf{I}_{N_R \times N_R}$, therefore the second term in equation (3.26) is zero. In this case, the elements of the FIM can be written as

$$[J(\boldsymbol{\theta})]_{ij} = 2Re \left\{ \left[\frac{\partial \mathbf{s}(\boldsymbol{\theta})}{\partial \theta_i} \right]^H \mathbf{C}^{-1}(\boldsymbol{\theta}) \left[\frac{\partial \mathbf{s}(\boldsymbol{\theta})}{\partial \theta_j} \right] \right\} \quad (3.36)$$

$$= \frac{2}{\sigma^2} Re \left\{ \left[\frac{\partial \mathbf{s}(\boldsymbol{\theta})}{\partial \theta_i} \right]^H \left[\frac{\partial \mathbf{s}(\boldsymbol{\theta})}{\partial \theta_j} \right] \right\} \quad ; \quad i = 1, 2, 3, 4; \quad j = 1, 2, 3, 4 \quad (3.37)$$

where $(\theta_i, \theta_j) \in (x, y, V_x, V_y)$. This is given for the deterministic case. For the case given here, the signal model includes random target fluctuations, hence the FIM should be modified as

$$[J(\theta)]_{ij} = \frac{2}{\sigma^2} \text{Re} \left\{ E \left[\left[\frac{\partial \mathbf{s}(\theta)}{\partial \theta_i} \right]^H \left[\frac{\partial \mathbf{s}(\theta)}{\partial \theta_j} \right] \right] \right\} \quad (3.38)$$

where $E[.]$ shows the expected value operation and

$$\mathbf{s}(\theta) = \begin{bmatrix} \mathbf{s}_1(\theta) \\ \mathbf{s}_2(\theta) \\ \dots \\ \mathbf{s}_{N_R}(\theta) \end{bmatrix}, \quad \frac{\partial \mathbf{s}(\theta)}{\partial \theta_i} = \begin{bmatrix} \frac{\partial \mathbf{s}_1(\theta)}{\partial \theta_i} \\ \frac{\partial \mathbf{s}_2(\theta)}{\partial \theta_i} \\ \dots \\ \frac{\partial \mathbf{s}_{N_R}(\theta)}{\partial \theta_i} \end{bmatrix}$$

$$\frac{\partial \mathbf{s}(\theta)}{\partial \theta} = \begin{bmatrix} \frac{\partial \mathbf{s}_1(\theta)}{\partial x} & \frac{\partial \mathbf{s}_1(\theta)}{\partial y} & \frac{\partial \mathbf{s}_1(\theta)}{\partial V_x} & \frac{\partial \mathbf{s}_1(\theta)}{\partial V_y} \\ \frac{\partial \mathbf{s}_2(\theta)}{\partial x} & \frac{\partial \mathbf{s}_2(\theta)}{\partial y} & \frac{\partial \mathbf{s}_2(\theta)}{\partial V_x} & \frac{\partial \mathbf{s}_2(\theta)}{\partial V_y} \\ \dots & \dots & \dots & \dots \\ \frac{\partial \mathbf{s}_{N_R}(\theta)}{\partial x} & \frac{\partial \mathbf{s}_{N_R}(\theta)}{\partial y} & \frac{\partial \mathbf{s}_{N_R}(\theta)}{\partial V_x} & \frac{\partial \mathbf{s}_{N_R}(\theta)}{\partial V_y} \end{bmatrix}$$

It is required to calculate the differentials of $\mathbf{s}(\theta)$ with respect to the $\theta = [x, y, V_x, V_y]$ which are

$$\frac{\partial \mathbf{s}_l(\theta)}{\partial x}, \frac{\partial \mathbf{s}_l(\theta)}{\partial y}, \frac{\partial \mathbf{s}_l(\theta)}{\partial V_x} \text{ and } \frac{\partial \mathbf{s}_l(\theta)}{\partial V_y} ; \quad l = 1, 2, \dots, N_R \quad (3.39)$$

and

$$\frac{\partial \mathbf{s}_l(\theta)}{\partial \theta_i} = \left[\frac{ds_l[1, \theta]}{d\theta_i}, \frac{ds_l[2, \theta]}{d\theta_i}, \dots, \frac{ds_l[N, \theta]}{d\theta_i} \right] ; \quad l = 1, 2, \dots, N_R \quad (3.40)$$

hence, the required calculations are

$$\frac{ds_l[n, \theta]}{dx}, \frac{ds_l[n, \theta]}{dy}, \frac{ds_l[n, \theta]}{dV_x} \text{ and } \frac{ds_l[n, \theta]}{dV_y} ; \quad n = 1, 2, \dots, N \quad (3.41)$$

In baseband and after sampling with period T_s , the received signal of the l^{th} receiver can be written as

$$r_l[n] = \sqrt{E_e} \sum_{k=1}^{N_T} A_{lk}[n] s_k[n] \exp(-j2\pi f_{d_{lk}} T_s (n - \frac{\tau_{lk}}{T_s}) + j2\pi f_k \tau_{lk}) + w_l[n] \quad (3.42)$$

$$= s_l[n, \theta] + w_l[n] ; \quad n = 1, 2, \dots, N \quad (3.43)$$

where

$$s_l[n, \theta] = \sqrt{E_e} \sum_{k=1}^{N_T} A_{lk}[n] s_k[n] \exp(-j2\pi f_{d_{lk}} T_s (n - \frac{\tau_{lk}}{T_s}) + j2\pi f_k \tau_{lk}) ; \quad n = 1, 2, \dots, N \quad (3.44)$$

and

$$\frac{ds_l[n, \theta]}{dx} = -j2\pi T_s \sqrt{E_e} \sum_{k=1}^{N_T} A_{lk}[n] s_k[n] \exp(-j2\pi T_s \alpha_{l,k}(\theta)) \left(\frac{d\alpha_{l,k}(\theta)}{dx} \right) \quad (3.45)$$

$$\frac{ds_l[n, \theta]}{dy} = -j2\pi T_s \sqrt{E_e} \sum_{k=1}^{N_T} A_{lk}[n] s_k[n] \exp(-j2\pi T_s \alpha_{l,k}(\theta)) \left(\frac{d\alpha_{l,k}(\theta)}{dy} \right) \quad (3.46)$$

$$\frac{ds_l[n, \theta]}{dV_x} = -j2\pi T_s \sqrt{E_e} \sum_{k=1}^{N_T} A_{lk}[n] s_k[n] \exp(-j2\pi T_s \alpha_{l,k}(\theta)) \left(\frac{d\alpha_{l,k}(\theta)}{dV_x} \right) \quad (3.47)$$

$$\frac{ds_l[n, \theta]}{dV_y} = -j2\pi T_s \sqrt{E_e} \sum_{k=1}^{N_T} A_{lk}[n] s_k[n] \exp(-j2\pi T_s \alpha_{l,k}(\theta)) \left(\frac{d\alpha_{l,k}(\theta)}{dV_y} \right) \quad (3.48)$$

where

$$\alpha_{l,k}(\theta) = f_{d_{lk}} (n - \frac{\tau_{lk}}{T_s}) - \frac{1}{T_s} f_k \tau_{lk} \quad (3.49)$$

where $f_{d_{lk}}$ is the Doppler shift of the k^{th} transmitted frequency at the l^{th} receiver and it is given by

$$f_{d_{lk}} = -\frac{f_k}{C} \left(\frac{(x - x_{T_k})V_x + (y - y_{T_k})V_y}{\sqrt{(x - x_{T_k})^2 + (y - y_{T_k})^2}} + \frac{(x - x_{R_l})V_x + (y - y_{R_l})V_y}{\sqrt{(x - x_{R_l})^2 + (y - y_{R_l})^2}} \right) \quad (3.50)$$

Similarly, τ_{lk} is the time delay of the k^{th} transmitted signal at the l^{th} receiver and it is written as

$$\tau_{lk} = \frac{1}{C} \left(\sqrt{(x - x_{T_k})^2 + (y - y_{T_k})^2} + \sqrt{(x - x_{R_l})^2 + (y - y_{R_l})^2} \right) \quad (3.51)$$

From these equations, the elements of the FIM can be calculated as follows (see Appendix B);

$$J_{xx} = \frac{8E_e(\pi T_s)^2 R_A(0)}{\sigma_n^2} \sum_{l=1}^{N_R} \sum_{k=1}^{N_T} \sum_{n=1}^N |s_k[n]|^2 \left(\frac{d\alpha_{l,k}(\theta)}{dx} \right)^2 + \beta_{x,x} \quad (3.52)$$

$$J_{yy} = \frac{8E_e(\pi T_s)^2 R_A(0)}{\sigma_n^2} \sum_{l=1}^{N_R} \sum_{k=1}^{N_T} \sum_{n=1}^N |s_k[n]|^2 \left(\frac{d\alpha_{l,k}(\theta)}{dy} \right)^2 + \beta_{y,y} \quad (3.53)$$

$$J_{V_x V_x} = \frac{8E_e(\pi T_s)^2 R_A(0)}{\sigma_n^2} \sum_{l=1}^{N_R} \sum_{k=1}^{N_T} \sum_{n=1}^N |s_k[n]|^2 \left(\frac{d\alpha_{l,k}(\theta)}{dV_x} \right)^2 + \beta_{V_x, V_x} \quad (3.54)$$

$$J_{V_y V_y} = \frac{8E_e(\pi T_s)^2 R_A(0)}{\sigma_n^2} \sum_{l=1}^{N_R} \sum_{k=1}^{N_T} \sum_{n=1}^N |s_k[n]|^2 \left(\frac{d\alpha_{l,k}(\theta)}{dV_y} \right)^2 + \beta_{V_y, V_y} \quad (3.55)$$

$$J_{xy} = J_{yx} = \frac{8E_e(\pi T_s)^2 R_A(0)}{\sigma_n^2} \sum_{l=1}^{N_R} \sum_{k=1}^{N_T} \sum_{n=1}^N |s_k[n]|^2 \left(\frac{d\alpha_{l,k}(\boldsymbol{\theta})}{dx} \right) \left(\frac{d\alpha_{l,k}(\boldsymbol{\theta})}{dy} \right) + \beta_{x,y} \quad (3.56)$$

$$J_{xV_x} = J_{V_x x} = \frac{8E_e(\pi T_s)^2 R_A(0)}{\sigma_n^2} \sum_{l=1}^{N_R} \sum_{k=1}^{N_T} \sum_{n=1}^N |s_k[n]|^2 \left(\frac{d\alpha_{l,k}(\boldsymbol{\theta})}{dx} \right) \left(\frac{d\alpha_{l,k}(\boldsymbol{\theta})}{dV_x} \right) + \beta_{x,V_x} \quad (3.57)$$

$$J_{xV_y} = J_{V_y x} = \frac{8E_e(\pi T_s)^2 R_A(0)}{\sigma_n^2} \sum_{l=1}^{N_R} \sum_{k=1}^{N_T} \sum_{n=1}^N |s_k[n]|^2 \left(\frac{d\alpha_{l,k}(\boldsymbol{\theta})}{dx} \right) \left(\frac{d\alpha_{l,k}(\boldsymbol{\theta})}{dV_y} \right) + \beta_{x,V_y} \quad (3.58)$$

$$J_{yV_x} = J_{V_x y} = \frac{8E_e(\pi T_s)^2 R_A(0)}{\sigma_n^2} \sum_{l=1}^{N_R} \sum_{k=1}^{N_T} \sum_{n=1}^N |s_k[n]|^2 \left(\frac{d\alpha_{l,k}(\boldsymbol{\theta})}{dy} \right) \left(\frac{d\alpha_{l,k}(\boldsymbol{\theta})}{dV_x} \right) + \beta_{y,V_x} \quad (3.59)$$

$$J_{yV_y} = J_{V_y y} = \frac{8E_e(\pi T_s)^2 R_A(0)}{\sigma_n^2} \sum_{l=1}^{N_R} \sum_{k=1}^{N_T} \sum_{n=1}^N |s_k[n]|^2 \left(\frac{d\alpha_{l,k}(\boldsymbol{\theta})}{dy} \right) \left(\frac{d\alpha_{l,k}(\boldsymbol{\theta})}{dV_y} \right) + \beta_{y,V_y} \quad (3.60)$$

$$J_{V_x V_y} = J_{V_y V_x} = \frac{8E_e(\pi T_s)^2 R_A(0)}{\sigma_n^2} \sum_{l=1}^{N_R} \sum_{k=1}^{N_T} \sum_{n=1}^N |s_k[n]|^2 \left(\frac{d\alpha_{l,k}(\boldsymbol{\theta})}{dV_x} \right) \left(\frac{d\alpha_{l,k}(\boldsymbol{\theta})}{dV_y} \right) + \beta_{V_x, V_y} \quad (3.61)$$

where

$$\beta_{i,j} = \frac{8E_e(\pi T_s)^2}{\sigma_n^2} \sum_{l=1}^{N_R} \sum_{n=1}^N \sum_{k=1}^{N_T} \sum_{\substack{m=1 \\ m \neq k}}^{N_T} s_k^*[n] s_m[n] \cos(2\pi T_s(\alpha_{l,m}(\boldsymbol{\theta}) - \alpha_{l,k}(\boldsymbol{\theta}))) \left(\frac{d\alpha_{l,k}(\boldsymbol{\theta})}{d\theta_i} \right) \left(\frac{d\alpha_{l,m}(\boldsymbol{\theta})}{d\theta_j} \right)$$

The required differentials can be calculated as

$$\frac{d\alpha_{l,k}(\boldsymbol{\theta})}{dx} = \left(n - \frac{\tau_{lk}}{T_s} \right) \frac{df_{d_{l,k}}}{dx} - \frac{f_k + f_{d_{l,k}}}{T_s} \frac{d\tau_{l,k}}{dx} \quad (3.62)$$

$$\frac{d\alpha_{l,k}(\boldsymbol{\theta})}{dy} = \left(n - \frac{\tau_{lk}}{T_s} \right) \frac{df_{d_{l,k}}}{dy} - \frac{f_k + f_{d_{l,k}}}{T_s} \frac{d\tau_{l,k}}{dy} \quad (3.63)$$

$$\frac{d\alpha_{l,k}(\boldsymbol{\theta})}{dV_x} = \left(n - \frac{\tau_{lk}}{T_s} \right) \frac{df_{d_{l,k}}}{dV_x} \quad (3.64)$$

$$\frac{d\alpha_{l,k}(\boldsymbol{\theta})}{dV_y} = \left(n - \frac{\tau_{lk}}{T_s} \right) \frac{df_{d_{l,k}}}{dV_y} \quad (3.65)$$

and

$$\frac{df_{d_{l,k}}}{dx} = -\frac{f_k}{c} \left(V_x \left(\frac{1}{L_{T_k}} + \frac{1}{L_{R_l}} \right) - \frac{(x - x_{T_k})K_{T_k}}{L_{T_k}^3} - \frac{(x - x_{R_l})K_{R_l}}{L_{R_l}^3} \right) \quad (3.66)$$

$$\frac{df_{d_{l,k}}}{dy} = -\frac{f_k}{c} \left(V_y \left(\frac{1}{L_{T_k}} + \frac{1}{L_{R_l}} \right) - \frac{(y - y_{T_k})K_{T_k}}{L_{T_k}^3} - \frac{(y - y_{R_l})K_{R_l}}{L_{R_l}^3} \right) \quad (3.67)$$

$$\frac{df_{d_{l,k}}}{dV_x} = -\frac{f_k}{c} \left(\frac{x - x_{T_k}}{L_{T_k}} + \frac{x - x_{R_l}}{L_{R_l}} \right) \quad (3.68)$$

$$\frac{df_{d_{l,k}}}{dV_y} = -\frac{f_k}{c} \left(\frac{y - y_{T_k}}{L_{T_k}} + \frac{y - y_{R_l}}{L_{R_l}} \right) \quad (3.69)$$

and

$$\frac{d\tau_{lk}}{dx} = \frac{1}{c} \left(\frac{x - x_{T_k}}{L_{T_k}} + \frac{x - x_{R_l}}{L_{R_l}} \right) \quad (3.70)$$

$$\frac{d\tau_{lk}}{dy} = \frac{1}{c} \left(\frac{y - y_{T_k}}{L_{T_k}} + \frac{y - y_{R_l}}{L_{R_l}} \right) \quad (3.71)$$

where

$$L_{T_k} = \sqrt{(x - x_{T_k})^2 + (y - y_{T_k})^2} \quad , k = 1, 2, \dots, N_T \quad (3.72)$$

$$L_{R_l} = \sqrt{(x - x_{R_l})^2 + (y - y_{R_l})^2} \quad , l = 1, 2, \dots, N_R \quad (3.73)$$

$$K_{T_k} = (x - x_{T_k})V_x + (y - y_{T_k})V_y \quad , k = 1, 2, \dots, N_T \quad (3.74)$$

$$K_{R_l} = (x - x_{R_l})V_x + (y - y_{R_l})V_y \quad , l = 1, 2, \dots, N_R \quad (3.75)$$

Using the above equations, the CRB matrix can be found as the inverse of the FIM as

$$\mathbf{C}_{\text{CRB}} = [\mathbf{J}^{-1}(\theta)] \quad (3.76)$$

The CRBs for the unknowns (x, y, V_x, V_y) are on the main diagonal of this matrix as

$$C_{CRB_x} = \mathbf{C}_{\text{CRB}}(1, 1) \quad (3.77)$$

$$C_{CRB_y} = \mathbf{C}_{\text{CRB}}(2, 2) \quad (3.78)$$

$$C_{CRB_{V_x}} = \mathbf{C}_{\text{CRB}}(3, 3) \quad (3.79)$$

$$C_{CRB_{V_y}} = \mathbf{C}_{\text{CRB}}(4, 4) \quad (3.80)$$

and the target position and velocity estimation bounds can be calculated as follows

$$CRB_{loc} = \sqrt{C_{CRB_x}^2 + C_{CRB_y}^2} \quad (3.81)$$

$$CRB_{vel} = \sqrt{C_{CRB_{V_x}}^2 + C_{CRB_{V_y}}^2} \quad (3.82)$$

Because of the complex calculations, the closed form expression for the CRB could not be found. Hence, the CRB is calculated numerically for the target position and the target velocity estimations. The CRBs for the target position and the target velocity estimations depend on the target position, velocity and the system geometry. Hence, to evaluate the performances, system geometry and the target position should be defined. In the following figure, simulation

geometry can be seen for the CRB results. The target is assumed at three different positions and directions with $V = 800$ kmph velocity. For 2×2 MIMO radar case, Tr1, Tr2, Rec1 and Rec2 are used as the transmitters and the receivers. For 2×3 MIMO radar case, Rec3 is included as the third receiver, and for 3×3 MIMO radar case, Tr3 is included being the third transmitter.

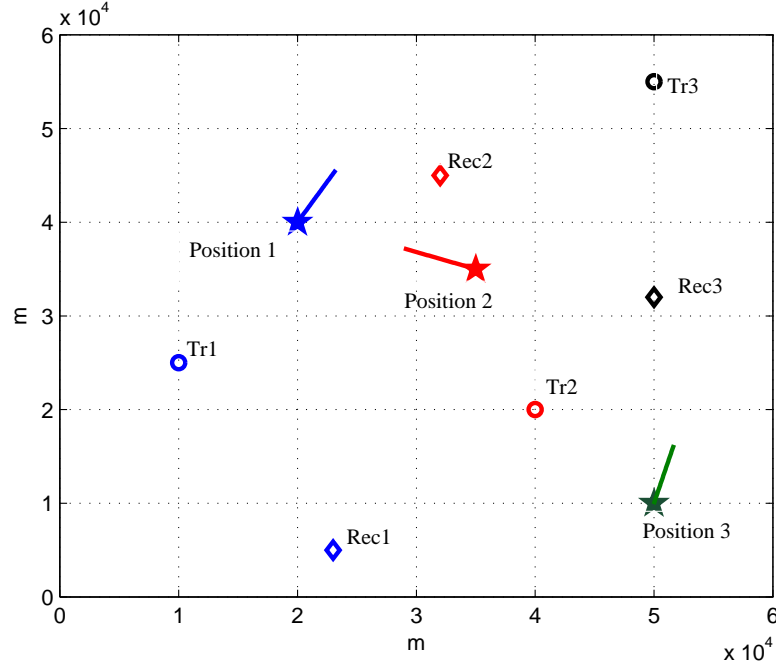


Figure 3.8: System geometry used for the CRB simulations.

In the following figures, the CRBs can be seen for the target position and the target velocity estimations for different number of transmitters and the receivers. For these simulations, the used transmitter frequencies are, 10, 10.3 and 10.5 GHz respectively. The observation time is used as $T = 1, 10, 100$ msec and the time delays (τ_{lk}) and the Doppler frequencies ($f_{d_{lk}}$) are assumed as totally known.

As the maximum Doppler frequency of the system is calculated as $f_{d_{max}} = 17.5$ KHz, to estimate the Doppler frequencies, a sampling frequency which is equivalent to the Nyquist sampling frequency is used ($f_s = 35$ KHz). For all three cases, including Swerling 2, Swerling 4 and no fluctuation cases, $R_A(0) = 1$. It turns out that, the CRB's are the same, because the CRB depends only on the value of $R_A(0)$.

The CRB's for different observation times can be seen for different target positions. As expected, when the observation time increases, the bound decreases because the extra information increases the estimation performance. Similarly, bound decreases when the number of transmit and receive sites increases.

For these simulations the target is assumed stationary on the observation time. The target's position and the velocity are constant and hence the time delays and the Doppler frequencies in the returned signals are all constant on the observation time frame. Hence, the CRB can go to zero theoretically by increasing the observation time. On the other hand, the target is moving on the observation time and the target motion produces position ambiguity. For example, if the target is moving with the velocity $V = 900 \text{ kmph} = 250 \text{ meter/second}$, this target changes its position 2.5 meter for 10 milisecond observation time. Similarly, if the observation time is 1 second, then the target moves 250 meter. Hence, the observation time is an important parameter for CRB as well. For the simulations given here, the observation times are chosen as distinct as possible to show the differences of the CRB curves easily. Finally, the Signal-to-Noise (power) ratio (SNR) is defined as $SNR = E_e/N_0$ (see Appendix C for SNR definition).

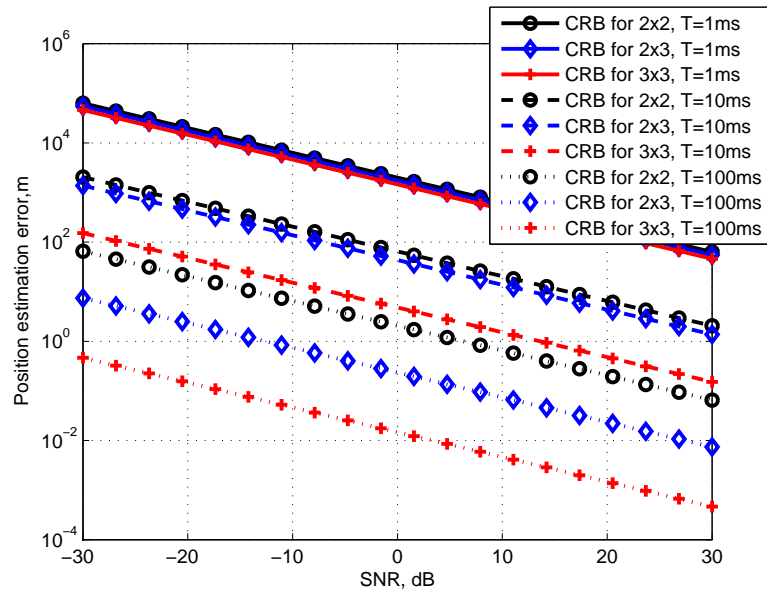


Figure 3.9: CRBs for target position estimation when target at position 1.

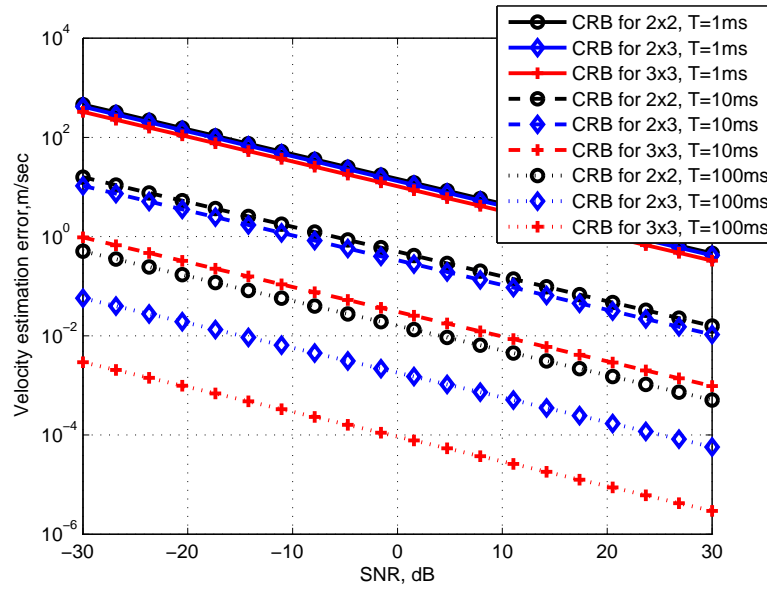


Figure 3.10: CRBs for target velocity estimation when target at position 1.

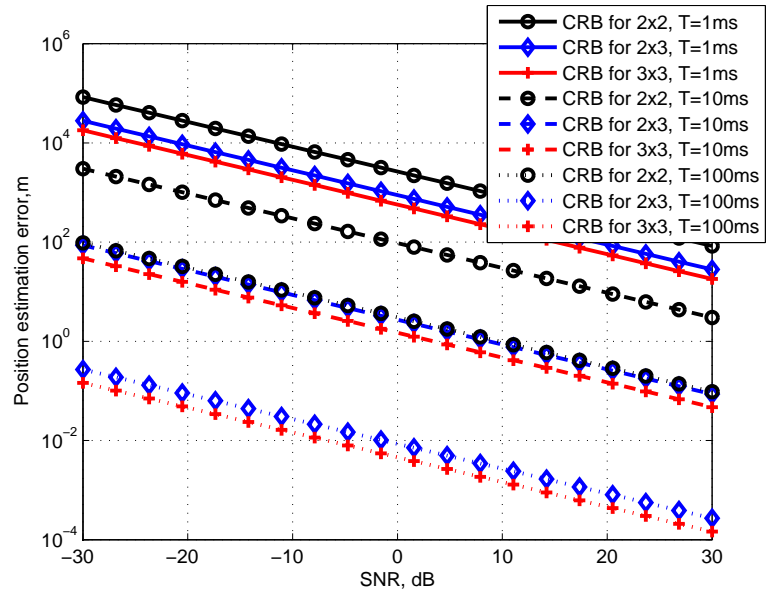


Figure 3.11: CRBs for target position estimation when target at position2.

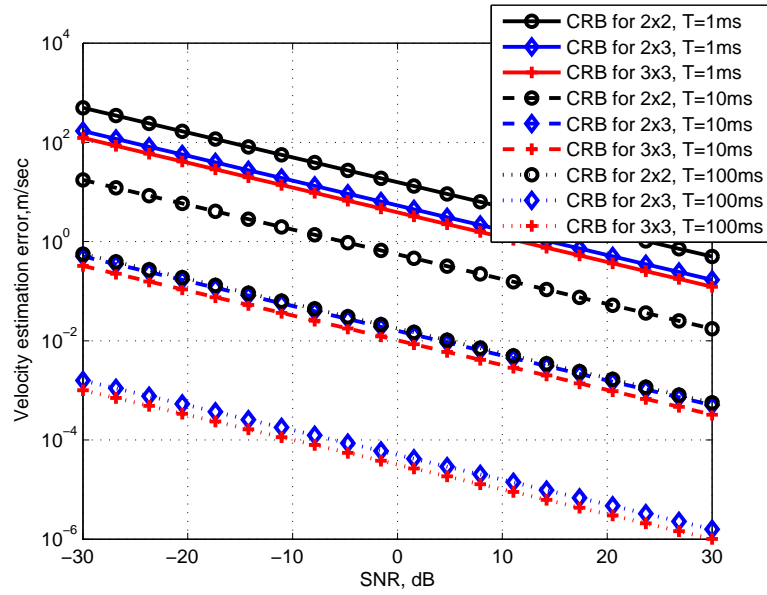


Figure 3.12: CRBs for target velocity estimation when target at position2.

In the following figures, the CRB's can be seen for targets at position 2 and positions 3 with different directions of motion. Targets are assumed moving with constant velocity of $V = 800$ kmph and the angle of the target direction is swept from 0 to 2π . For these simulations, the observation time and the SNR are chosen as 10 ms and 20 dB respectively.

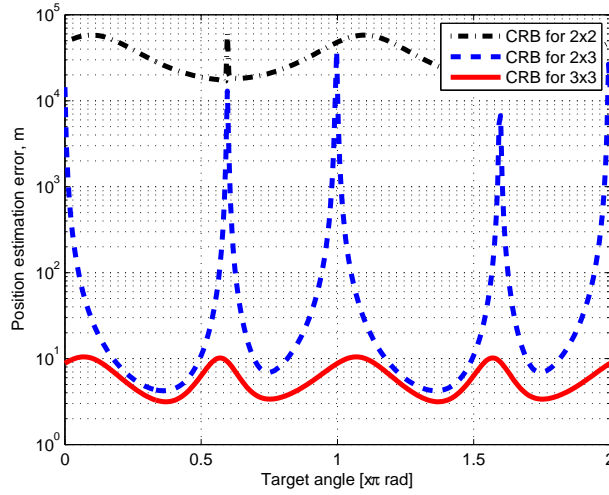


Figure 3.13: The CRBs for target position estimation when target at position 2. Target direction is swept from 0 to 2π .

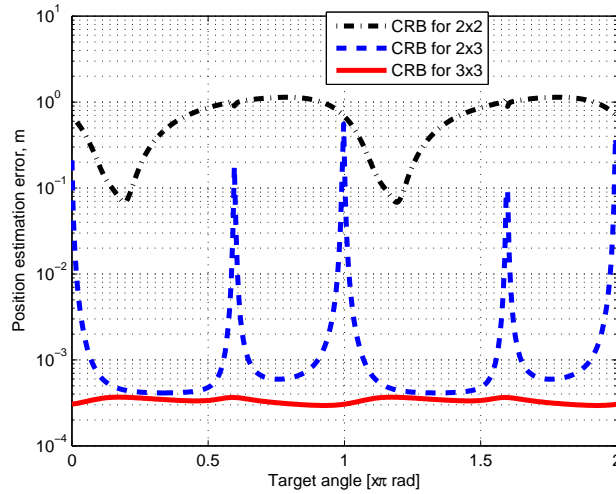


Figure 3.14: The CRBs for target velocity estimation when target at position 2. Target direction is swept from 0 to 2π .

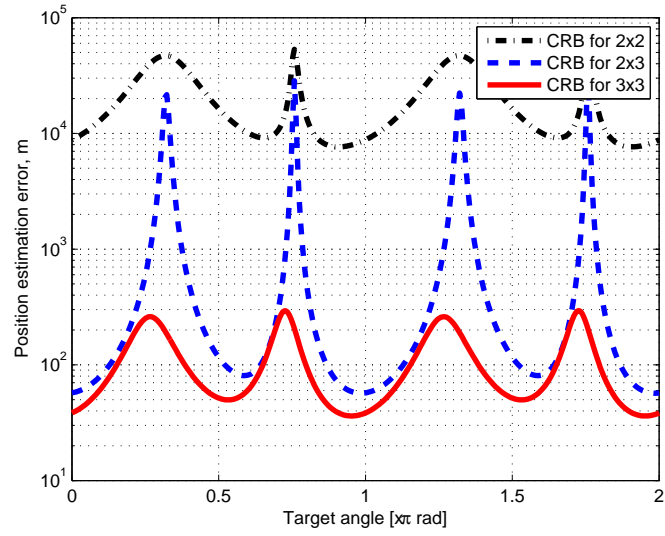


Figure 3.15: CRBs for target position estimation when target at position 3. Target direction is swept from 0 to 2π .

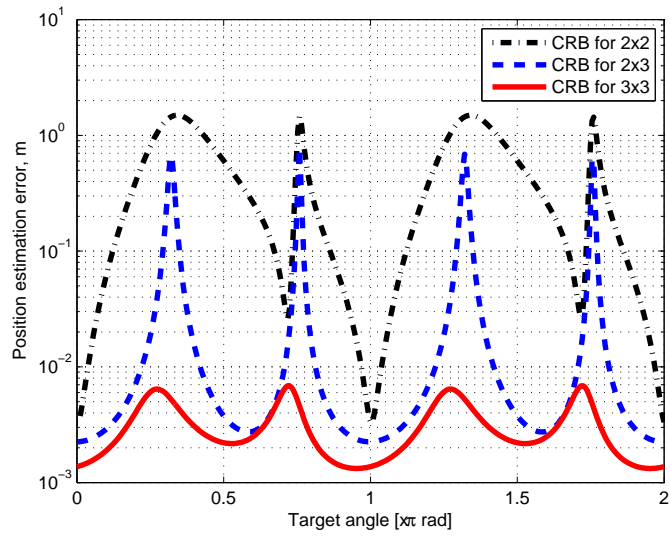


Figure 3.16: CRBs for target velocity estimation when target at position 3. Target direction is swept from 0 to 2π .

CHAPTER 4

TARGET LOCALIZATION METHODS FOR FREQUENCY-ONLY MIMO RADAR

The frequency-only methods for emitter localization has been discussed in the literature since World War II. The typical example to these methods is Differential Doppler (DD), also known as the frequency difference of arrival (FDOA) [50, 51]. FDOA, measures the differences of the received frequencies between the receivers, hence it eliminates the need to know the exact transmit frequency. If the transmit frequencies are all known, instead of using the difference of the frequencies, the received frequencies can be used directly. This method is known as the frequency of arrival (FOA) and it requires the transmit frequencies.

For the target localization problem, the frequency based methods can be used efficiently as the transmit frequencies are all known. By using narrowband signals and the Discrete Fourier Transform (DFT), the Doppler frequency can be estimated accurately using low complexity methods. Although, the frequency based systems have many advantages, frequency based target localization methods are very limited in the literature because of the fact that highly non-linear equations are involved in solutions.

In this chapter, a new target localization method is proposed for widely separated MIMO radars. The proposed method is able to estimate the target position and the target velocity based on the measurements of the Doppler frequencies. Moreover, the target direction can be estimated efficiently. Estimated Doppler frequencies are collected in a fusion center. Then, the target position and the velocity vector are estimated using the Doppler frequencies with grid search in the fusion center. This method is called as the "Target Localization via Doppler Frequencies - **TLDF** method".

The proposed method, TLDF can estimate the position, velocity and the direction of the target directly. Besides the TLDF method, two alternative target position estimation methods are proposed as well. These methods are based on the Doppler frequencies, but they also requires the target velocity vector to be known. Hence, after the target velocity is estimated by using the TLDF method, these alternative methods can be used for the target position estimation. These methods are called as the "Target Localization via Doppler Frequencies and Target Velocity - **TLD&V** methods".

The **TLDF** method is purely new method for target localization for the frequency-only MIMO radar. In this method, the estimated frequencies from the received signals are grouped with respect to the transmitters in a vector-matrix form. By using the all obtained matrix-vector equations, a cost function is defined. Then, the cost function is solved with grid search.

Two **TLD&V** methods use the estimated target velocity besides the Doppler frequencies. The first **TLD&V** method is an expansion of a passive localization method given in [7]. This idea is applied to the active MIMO radar case for the target localization. For MIMO radar, the application of the method is more complex than the passive radar case. The method is based on the differentials of the received frequencies, and hence it is called as the "Derivated Doppler" method (**TLD&V-DD** method) for target localization.

The second **TLD&V** method is called as the **TLD&V-subML**. This method uses the Maximum Likelihood (ML) principle for target localization. The obtained ML equation is solved using the grid search, hence it is sub-optimum. Therefore, this method becomes sub-ML solution of the problem. Or it can be called as the ML with grid search.

For all three methods, after defining the cost functions for target localization, grid search is used for minimizing these cost functions.

For the analysis, MIMO radar with N_T transmitters and N_R receivers which are widely separated from each other is used. Each transmitter-receiver pair works in bistatic manner and there is no monostatic radar configuration, i.e., transmitters do not receive any signal. Hence, using N_T transmitters and N_R receivers, the total number of N , ($N = N_T \times N_R$) bistatic radars is obtained, and hence the total number of N received signals is included.

Usually, if the angles between the transmitter and the target and the receiver and the target and the time of arrivals (TOA's) are all known, then an ellipsoid which the target is on can be

drawn. These kind of ellipsoids are called as isorange curves. If more than one bistatic radars exist, then by using their isorange curves, the position of the target can be determined using the intersection of the isorange curves. This process requires at least three bistatic radar units for unambiguous position information [6]. On the other hand, if the time of arrivals do not exist or do not estimated accurately, then the frequency of arrivals can be used to localize the target.

The geometry of the system being considered is shown in Figure 4.1. Figure 4.1.a shows the general geometry of N_T transmitters and N_R receivers whereas Figure 4.1.b shows the geometry for single transmitter-receiver pair.

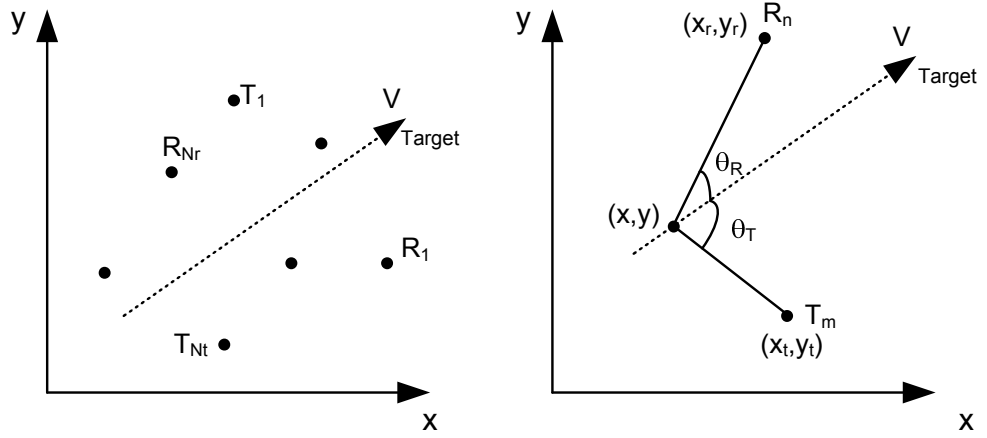


Figure 4.1: MIMO radar geometry. a) for N_T transmitters and N_R receivers, b) for single transmitter-receiver pair.

A target is moving on a constant speed (V). N_T transmitters radiate signals using distinct frequencies which are f_1, f_2, \dots, f_{N_T} . N_R receivers intercept the Doppler-shifted versions of these frequencies because of the target motion. Each receiver can measure N_T radiated frequencies and each transmitted frequency can be separated in the receivers. The i^{th} receiver intercepts a frequency which is radiated from the j^{th} transmitter as [6]

$$f_{j,i} = f_j \left(1 + \frac{V}{c} (\cos \theta_{T_j} + \cos \theta_{R_i}) \right) \quad (4.1)$$

$$= f_j + f_j \frac{V}{c} (\cos \theta_{T_j} + \cos \theta_{R_i}) \quad (4.2)$$

$$= f_j + f_{d_{j,i}} \quad (4.3)$$

where c is the speed of the light ($c \cong 3 \times 10^5$ kmph), $f_{j,i}$ is the received frequency of the j^{th}

transmitter at the i^{th} receiver, f_j is the carrier frequency of the transmitted signal from the j^{th} transmitter, θ_{T_j} and θ_{R_i} are the angles between the j^{th} transmitter and the target velocity path and the i^{th} receiver and the target velocity vector respectively. Here, $f_{d_{ji}}$ is the Doppler frequency between the transmitted and the received signals and it can be positive or negative depends on the target direction.

After having obtained the received frequencies, then the target localization should be realized by using these frequencies. For the analysis of the proposed methods, simulations should be done. The geometries used in simulation can be seen in the following figures.

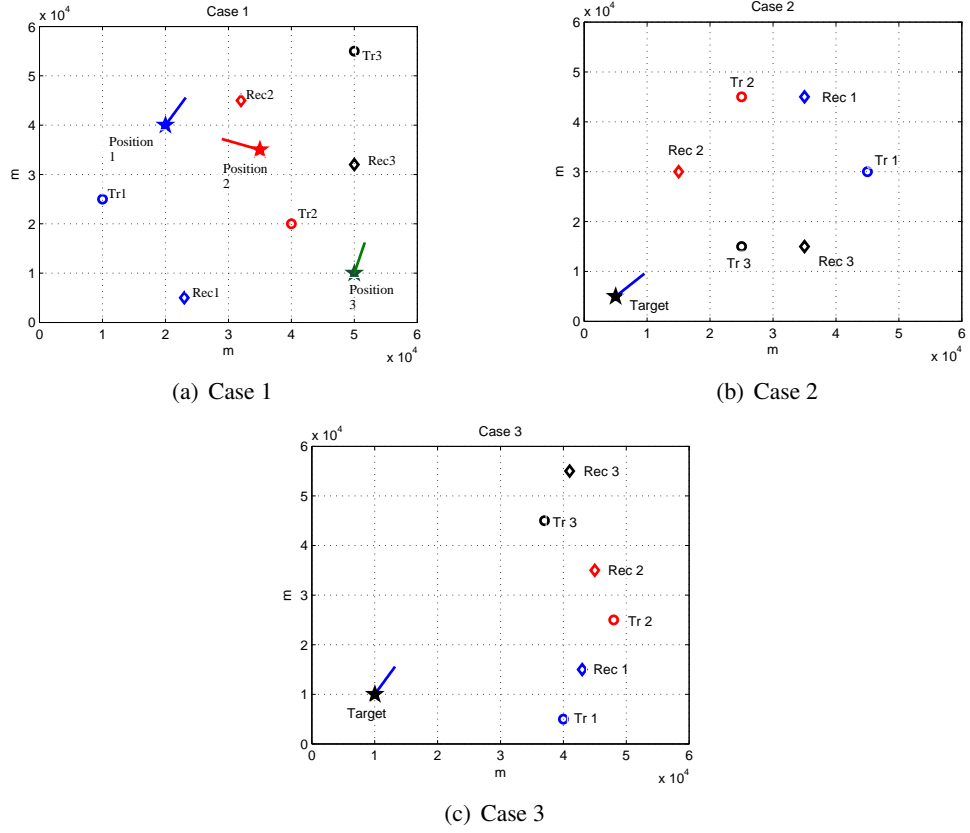


Figure 4.2: Simulation geometries

For the simulations, the locations of the transmitters, receivers and the target can be seen in Figure 4.2. The target velocities are assumed constant and $V = 800$ kmph for each configuration.

4.1 Target Localization via Doppler Frequencies - TLDF

The i^{th} receiver intercepts a frequency which is radiated from the j^{th} transmitter given in equation (4.3) as

$$f_{j,i} = f_j \left(1 + \frac{V}{c} (\cos \theta_{T_j} + \cos \theta_{R_i}) \right) \quad (4.4)$$

By using the cosine theorem, the cosinus of the angles in equation (4.4) can be written with respect to the target, the receiver, the transmitter locations and the target velocities on both directions as

$$\cos \theta_{T_j} = - \frac{(x - x_{T_j})V_x + (y - y_{T_j})V_y}{V \sqrt{(x - x_{T_j})^2 + (y - y_{T_j})^2}} \quad (4.5)$$

$$\cos \theta_{R_i} = - \frac{(x - x_{R_i})V_x + (y - y_{R_i})V_y}{V \sqrt{(x - x_{R_i})^2 + (y - y_{R_i})^2}} \quad (4.6)$$

Inserting the equations (4.5) and (4.6) into equation (4.4), the following equation can be obtained

$$f_{j,i} = f_j - \frac{f_j}{c} \left(\frac{(x - x_{T_j})V_x + (y - y_{T_j})V_y}{\sqrt{(x - x_{T_j})^2 + (y - y_{T_j})^2}} + \frac{(x - x_{R_i})V_x + (y - y_{R_i})V_y}{\sqrt{(x - x_{R_i})^2 + (y - y_{R_i})^2}} \right) \quad (4.7)$$

Rearranging the equation (4.7) gives,

$$\frac{f_{j,i} - f_j}{f_j} c = - \left(\frac{(x - x_{T_j})V_x + (y - y_{T_j})V_y}{\sqrt{(x - x_{T_j})^2 + (y - y_{T_j})^2}} + \frac{(x - x_{R_i})V_x + (y - y_{R_i})V_y}{\sqrt{(x - x_{R_i})^2 + (y - y_{R_i})^2}} \right) \quad (4.8)$$

For any MIMO radar structure, all the received frequencies radiated from the same transmitter can be grouped by using equation (4.8). Then, the obtained matrix equations can be solved for unknown target velocity. The target position can be determined by using the Least Squares (LS) criteria.

If frequency difference of arrival (FDOA) information is obtained, then the following equations can be written by using equation (4.7)

$$f_{j,i} - f_{j,k} = \frac{f_j}{c} \left(\frac{(x - x_{R_k})V_x + (y - y_{R_k})V_y}{\sqrt{(x - x_{R_k})^2 + (y - y_{R_k})^2}} - \frac{(x - x_{R_i})V_x + (y - y_{R_i})V_y}{\sqrt{(x - x_{R_i})^2 + (y - y_{R_i})^2}} \right) \quad (4.9)$$

by using the same transmitted signals for both received signals, and

$$f_{j,i} - f_{k,i} = f_j - f_k + \frac{K_{R_i}}{L_{R_i}} \left(\frac{f_k - f_j}{c} \right) + \frac{1}{c} \left(\frac{f_k K_{T_k}}{L_{T_k}} - \frac{f_k K_{T_j}}{L_{T_j}} \right) \quad (4.10)$$

by using the same receiver's signal for all transmitted signals. Here,

$$K_{T_j} = (x - x_{T_j})V_x + (y - y_{T_j})V_y \quad (4.11)$$

$$K_{R_i} = (x - x_{R_i})V_x + (y - y_{R_i})V_y \quad (4.12)$$

$$L_{T_j} = \sqrt{(x - x_{T_j})^2 + (y - y_{T_j})^2} \quad , j = 1, 2, \dots, N_T \quad (4.13)$$

$$L_{R_i} = \sqrt{(x - x_{R_i})^2 + (y - y_{R_i})^2} \quad , i = 1, 2, \dots, N_R \quad (4.14)$$

where (x, y) , (x_{T_j}, y_{T_j}) and (x_{R_i}, y_{R_i}) are the coordinates of the target, the j^{th} transmitter and the i^{th} receiver, respectively at that measurement time.

Using equation (4.8) directly instead of the FDOA information is simpler and less complex.

4.1.1 2x2 MIMO Radar Case

If the system includes 2 transmitters and 2 receivers, the total number of 4 radar units and hence 4 received frequencies which are $f_{1,1}$, $f_{1,2}$, $f_{2,1}$ and $f_{2,2}$ can be obtained. Using equation (4.8) and making group of the received frequencies with respect to the transmitter frequencies, then the following vector-matrix equations can be written

$$c\mathbf{b}_1 = -\mathbf{A}_1\mathbf{v} \quad \text{and} \quad c\mathbf{b}_2 = -\mathbf{A}_2\mathbf{v} \quad (4.15)$$

where c is the speed of light, \mathbf{b}_i is size 2x1 vector, \mathbf{A}_i ($i = 1, 2$) is size 2x2 matrix, \mathbf{v} is size 2x1 vector as

$$\mathbf{A}_i = \begin{bmatrix} \frac{x-x_{T_i}}{L_{T_i}} + \frac{x-x_{R_1}}{L_{R_1}} & \frac{y-y_{T_i}}{L_{T_i}} + \frac{y-y_{R_1}}{L_{R_1}} \\ \frac{x-x_{T_i}}{L_{T_i}} + \frac{x-x_{R_2}}{L_{R_2}} & \frac{y-y_{T_i}}{L_{T_i}} + \frac{y-y_{R_2}}{L_{R_2}} \end{bmatrix}$$

$$\mathbf{b}_i = \begin{bmatrix} \frac{f_{i,1}-f_i}{f_i} \\ \frac{f_{i,2}-f_i}{f_i} \end{bmatrix}, \quad \mathbf{v} = \begin{bmatrix} V_x \\ V_y \end{bmatrix}$$

where L_{T_i} and L_{R_j} are the distances between the target and the i^{th} transmitter and the j^{th} receiver respectively and they can be calculated as in equations (4.13) and (4.14).

As can be seen, \mathbf{A}_i 's depend only on the positions of the target, the receivers and the transmitters. The receivers and the transmitters are stationary and the locations of them are totally

known. \mathbf{b}_i 's include the transmitted and the received frequencies and all of them are also known (or estimated). Only unknowns are the target positions (x, y) and the target velocity vector \mathbf{v} . To find the target position, these non-linear vector-matrix equations must be solved. This problem is very complex. Hence, the grid search can be used to reduce the complexity of the problem. For the grid search, a new cost function must be defined and it must be independent from the target velocity, \mathbf{v} (or it must depend only on the target position). By using equation (4.15), the target velocity vector \mathbf{v} can be estimated as

$$\hat{\mathbf{v}} = -c\mathbf{A}_2^{-1}\mathbf{b}_2 \quad (4.16)$$

and inserting equation (4.16) into equation (4.15) gives

$$\hat{\mathbf{b}}_1 = \mathbf{A}_1\mathbf{A}_2^{-1}\mathbf{b}_2 \quad (4.17)$$

Finally, the new cost function is defined as

$$J = \|\mathbf{b}_1 - \mathbf{A}_1\mathbf{A}_2^{-1}\mathbf{b}_2\|_2 \quad (4.18)$$

In equation (4.18), \mathbf{b}_1 includes the estimated frequencies, $\mathbf{A}_1\mathbf{A}_2^{-1}\mathbf{b}_2$ is the estimation of \mathbf{b}_1 ($\hat{\mathbf{b}}_1 = \mathbf{A}_1\mathbf{A}_2^{-1}\mathbf{b}_2$) and it includes frequencies as well. Hence, the frequency estimation error can be defined as being $e = \mathbf{b}_1 - \mathbf{A}_1\mathbf{A}_2^{-1}\mathbf{b}_2$. From this point of view, actually the cost function given in equation (4.18) minimizes the frequency estimation error not the estimation error of the target positions. Actually, we try to find the closest Doppler frequency to the estimated Doppler frequency using the possible target positions. For the chosen target position in two dimensional space the Doppler frequency of the target is calculated, then the Doppler estimation error is calculated for predefined target position. Finally the target position which has the minimum frequency error is chosen being the target position. In simulations, the efficiency of this method is shown.

4.1.2 2x3 MIMO Radar Case

For the other MIMO radar structures different from 2x2 MIMO radar case, the similar vector-matrix equations can be written. For the simplification of the equations, the same transmitted frequencies should be grouped together. Therefore, the matrix equations as much as the number of the transmitters are obtained. Hence, the number of the equations changes with respect

to the number of the used transmitters. Because of this fact, 2x3 MIMO radar and 3x2 MIMO radar cases give different results. In this chapter, we will only deal with the 2x3 MIMO radar case which has 2 transmitters and 3 receivers.

For 2x3 MIMO radar case, the same matrix equations can be written as in equation (4.15). The only difference is size of the vectors and matrices because of the third receiver included in. These new vector and matrix become

$$\mathbf{A}_i = \begin{bmatrix} \frac{x-x_{T_i}}{L_{T_i}} + \frac{x-x_{R_1}}{L_{R_1}} & \frac{y-y_{T_i}}{L_{T_i}} + \frac{y-y_{R_1}}{L_{R_1}} \\ \frac{x-x_{T_i}}{L_{T_i}} + \frac{x-x_{R_2}}{L_{R_2}} & \frac{y-y_{T_i}}{L_{T_i}} + \frac{y-y_{R_2}}{L_{R_2}} \\ \frac{x-x_{T_i}}{L_{T_i}} + \frac{x-x_{R_3}}{L_{R_3}} & \frac{y-y_{T_i}}{L_{T_i}} + \frac{y-y_{R_3}}{L_{R_3}} \end{bmatrix}$$

$$\mathbf{b}_i = \begin{bmatrix} \frac{f_{i,1}-f_i}{f_i} \\ \frac{f_{i,2}-f_i}{f_i} \\ \frac{f_{i,3}-f_i}{f_i} \end{bmatrix}, \quad \mathbf{v} = \begin{bmatrix} V_x \\ V_y \end{bmatrix}$$

As the number of the transmitters are equal for 2x2 MIMO radar and 2x3 MIMO radar cases, after formed these matrices, the same cost function as in equation (4.18) can be used for the grid search and these cases can be generalized. If the system includes 2 transmitters and N_R receivers then, the similar matrices can be obtained with N_R rows. Then, equation (4.18) can be used as cost function for all 2x N_R MIMO structures. For this case, \mathbf{A}_i 's are size $N_R \times 2$ matrices and \mathbf{b}_i 's are size $N_R \times 1$ vectors.

4.1.3 General Case

As explained in the previous sections, the size of the vectors, matrices and the number of the matrix equations depend on the number of the receivers and the number of the transmitters respectively. Therefore, when the system has transmitters more than 2, say N_T , then the N_T matrix equations can be obtained as follows

$$c\mathbf{b}_i = -\mathbf{A}_i\mathbf{v} \quad ; \quad i = 1, 2, \dots, N_T \quad (4.19)$$

If the system includes total number of N_R receivers, then these matrix and the vectors can be

written as

$$\mathbf{A}_i = \begin{bmatrix} \frac{x-x_{T_i}}{L_{T_i}} + \frac{x-x_{R_1}}{L_{R_1}} & \frac{y-y_{T_i}}{L_{T_i}} + \frac{y-y_{R_1}}{L_{R_1}} \\ \frac{x-x_{T_i}}{L_{T_i}} + \frac{x-x_{R_2}}{L_{R_2}} & \frac{y-y_{T_i}}{L_{T_i}} + \frac{y-y_{R_2}}{L_{R_2}} \\ \dots & \dots \\ \frac{x-x_{T_i}}{L_{T_i}} + \frac{x-x_{R_{N_R}}}{L_{R_{N_R}}} & \frac{y-y_{T_i}}{L_{T_i}} + \frac{y-y_{R_{N_R}}}{L_{R_{N_R}}} \end{bmatrix}$$

$$\mathbf{b}_i = \begin{bmatrix} \frac{f_{i,1}-f_i}{f_i} \\ \frac{f_{i,2}-f_i}{f_i} \\ \dots \\ \frac{f_{i,N_R}-f_i}{f_i} \end{bmatrix}, \quad \mathbf{v} = \begin{bmatrix} V_x \\ V_y \end{bmatrix}$$

Here, \mathbf{A}_i 's are size $N_R \times 2$ matrices, \mathbf{b}_i 's are size $N_R \times 1$ vectors. The N_T matrix equations as given in equation (4.19) can be combined

$$c\mathbf{b} = -\mathbf{A}\mathbf{v} \quad (4.20)$$

where

$$\mathbf{A} = \begin{bmatrix} \mathbf{A}_1 \\ \mathbf{A}_2 \\ \dots \\ \mathbf{A}_{N_T} \end{bmatrix}, \quad \mathbf{b} = \begin{bmatrix} \mathbf{b}_1 \\ \mathbf{b}_2 \\ \dots \\ \mathbf{b}_{N_T} \end{bmatrix}$$

Then, the target velocity vector can be estimated as

$$\hat{\mathbf{v}} = -c\mathbf{A}^{-1}\mathbf{b} \quad (4.21)$$

After the target velocity ($\hat{\mathbf{v}}$) is estimated, N_T distinct cost functions can be found using equation (4.19) as

$$J_i = \| c\mathbf{b}_i + \mathbf{A}_i\hat{\mathbf{v}} \|_2 \quad ; \quad i = 1, 2, \dots, N_T \quad (4.22)$$

From the above equation, one can write

$$\begin{aligned} J_i &= \| c\mathbf{b}_i + \mathbf{A}_i\hat{\mathbf{v}} \|_2 \\ &= \| c\mathbf{b}_i - c\mathbf{A}_i\mathbf{A}^{-1}\mathbf{b} \|_2 \\ &= c \| \mathbf{b}_i - \mathbf{A}_i\mathbf{A}^{-1}\mathbf{b} \|_2 \end{aligned} \quad (4.23)$$

where C is the speed of light. Because C is constant, it can be safely dropped, and finally J_i can be written as

$$J_i = \| \mathbf{b}_i - \mathbf{A}_i \mathbf{A}^{-1} \mathbf{b} \|_2 \quad ; \quad i = 1, 2, \dots, N_T \quad (4.24)$$

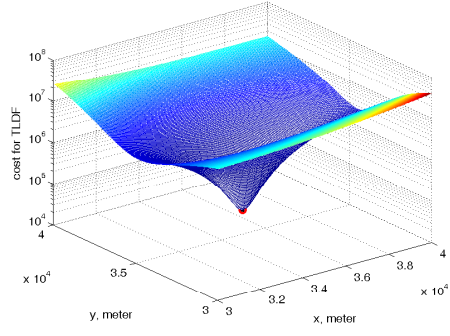
Finally, for general case, the cost function becomes

$$J = \frac{1}{N_T} \sqrt{\sum_{i=1}^{N_T} J_i^2} \quad (4.25)$$

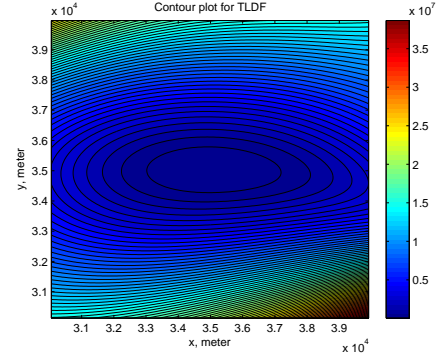
Note that; the matrix \mathbf{A} is square only if $N_R = 2$ and $N_T = 1$. In general, \mathbf{A} is not square and, if this is the case, the inverse of \mathbf{A} can be calculated via pseudo-inversion as, $\mathbf{A}^+ = (\mathbf{A}^H \mathbf{A})^{-1} \mathbf{A}^H$ [52]. Here \mathbf{A}^H denotes the hermitian (complex conjugate and transpose) of matrix \mathbf{A} .

This cost function can be seen in the following pages (Figures 4.3 and 4.3) for different geometries and target positions which are given in Figure 4.2. The contour plots for the same cost functions are given on the right hand side of each plot. To obtain these figures, $10 \times 10 \text{ km}^2$ area is searched grid by grid by using 100 meters apart grid points and the target is assumed exactly on the grid. The Doppler frequencies are estimated by using the periodogram spectral estimator. The DFT size is 2^{18} and there is no target fluctuation.

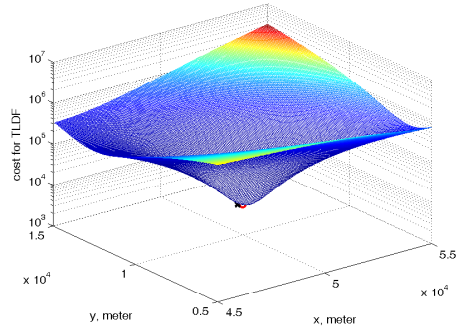
In these figures, red circle (●) shows the position which is the minimum of the cost function and black x (x) shows the exact target position. (This configuration is used for plotting the cost functions of other proposed methods.)



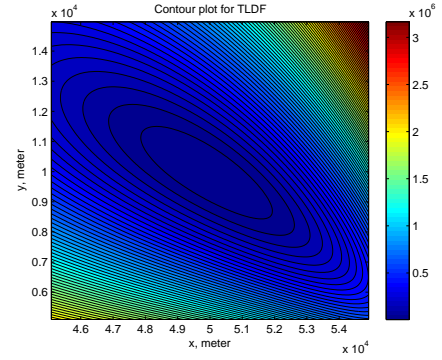
(a) Target at Case 1, Position 2



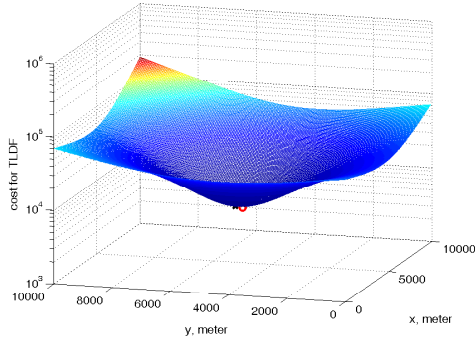
(b) Target at Case 1, Position 2



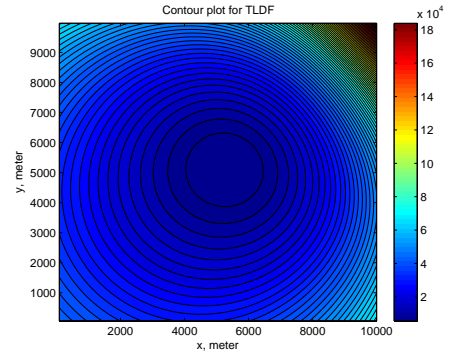
(c) Target at Case 1, Position 3



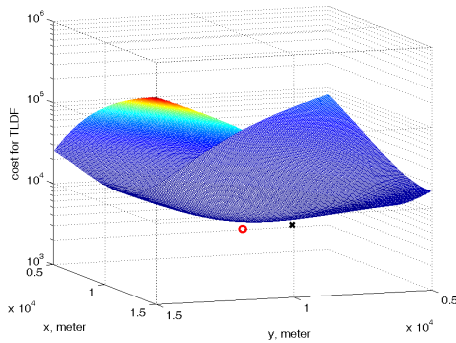
(d) Target at Case 1, Position 3



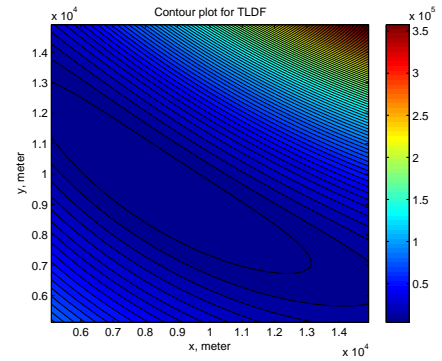
(e) Target at Case 2



(f) Target at Case 2

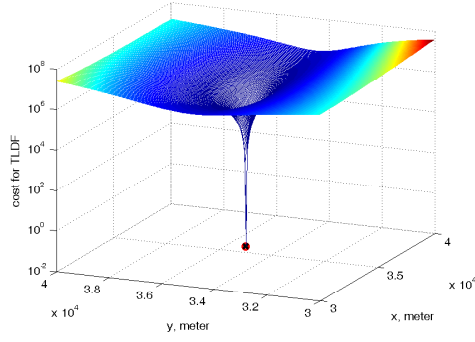


(g) Target at Case 3

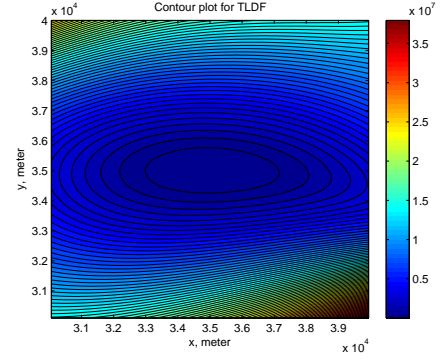


(h) Target at Case 3

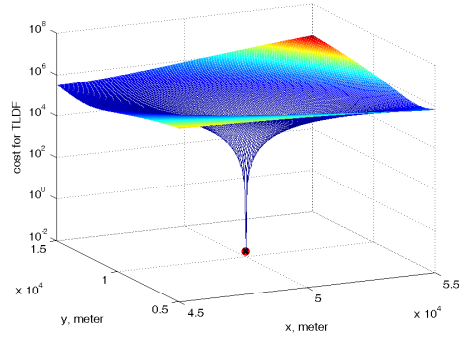
Figure 4.3: Cost functions and contour plots for the TLDF method at low SNR (SNR = -10 dB) for different geometries.



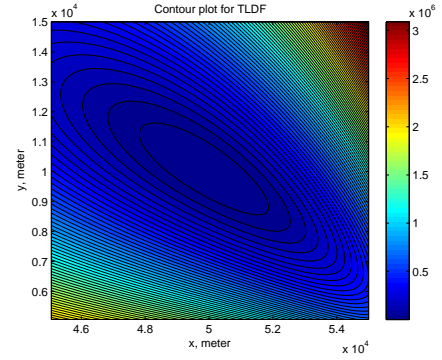
(a) Target at Case 1, Position 2



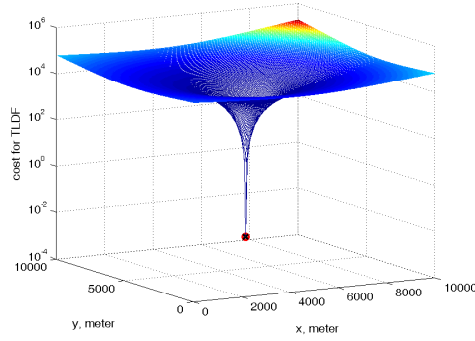
(b) Target at Case 1, Position 2



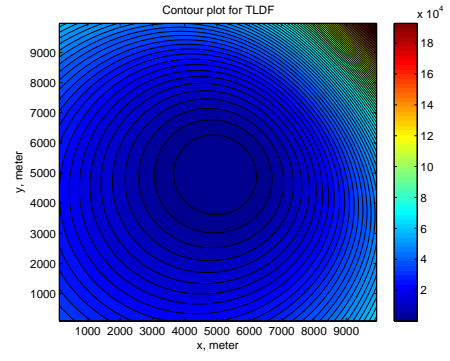
(c) Target at Case 1, Position 3



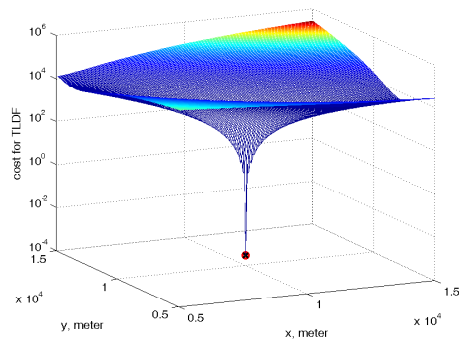
(d) Target at Case 1, Position 3



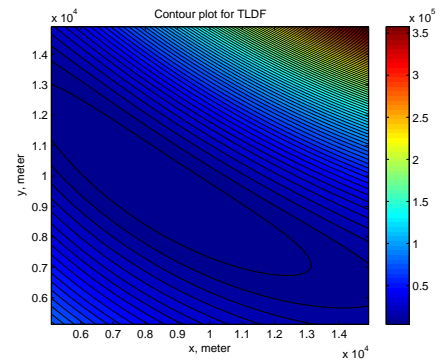
(e) Target at Case 2



(f) Target at Case 2



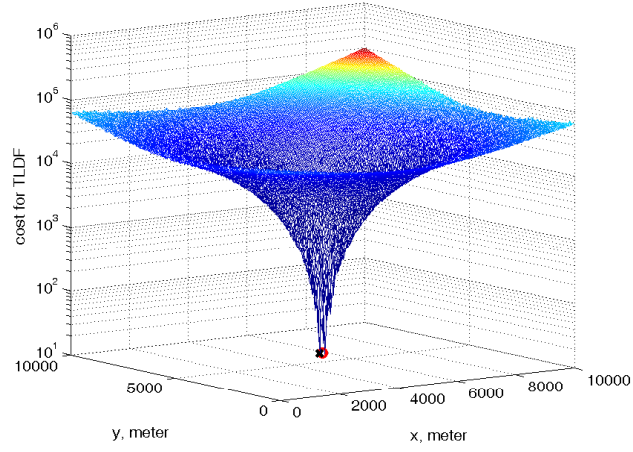
(g) Target at Case 3



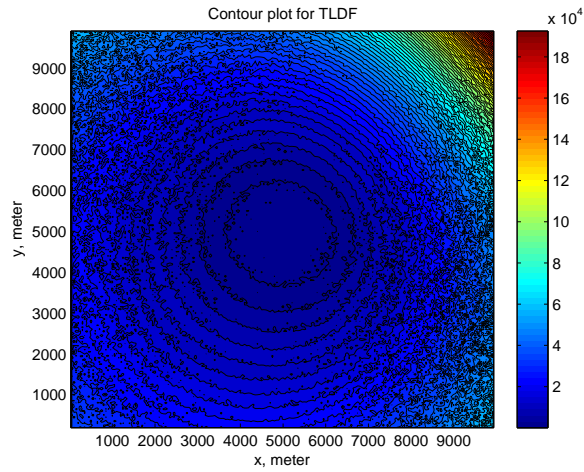
(h) Target at Case 3

Figure 4.4: Cost functions and contour plots for the TLDF method at high SNR (SNR = 30 dB) for different geometries.

To get these figures, carrier frequency offset is assumed as zero. Hence, the cost functions are very smooth. Actually, there is some carrier frequency offset and the smoothness of the cost function is being destroyed. When 5 Hz offset frequency is added to the carrier frequencies, the obtained cost function and the contour plots can be seen in Figure 4.5.



(a) Cost function



(b) Contour plot

Figure 4.5: Cost function and contour plot for the TLDF method when 5 Hz carrier frequency offset exists. (SNR = 30 dB, target at case 2.)

This method was presented in "IEEE 2010 European Radar Conference - EuRAD'10". The full work with simulation results can be found in [53].

4.2 Target Localization via Doppler Frequencies and Target Velocity - TLD&V

4.2.1 First Method : Differentiated Doppler - TLD&V-DD

As shown in [7], a non-maneuvering target can be localized using Doppler-shift measurements in a multi sensors architecture. In [7], there are total number of N sensors (as receivers), and they try to localize a moving source which is non-maneuvering and radiates tone signal with constant frequency. This source is an under-water vehicle, hence this is a passive sonar system. In this thesis, the method given in [7] is expanded to the active MIMO radar case. Instead of using a target which radiates a tone signal, an active MIMO radar configuration with widely separated N_T transmitters and N_R receivers is used to localize an aircraft.

In [7], it is shown that, measuring the transmitted frequencies and Doppler shifts using four passive sensors is enough to localize a radiated target. The Doppler shift information can be obtained using the sensor outputs for each measurement time with the help of the frequency difference between the transmitted and the received signals. The Doppler shift can also be found after two consecutive measurements from their difference.

The differential of equation (4.3) with respect to time is

$$\dot{f}_{j,i} = -f_j \frac{V}{c} (\dot{\theta}_{T_j} \sin \theta_{T_j} + \dot{\theta}_{R_i} \sin \theta_{R_i}) \quad (4.26)$$

The angular speeds can be written as [7]

$$\dot{\theta}_{T_j} = \frac{V \sin \theta_{T_j}}{L_{T_j}}, \quad \dot{\theta}_{R_i} = \frac{V \sin \theta_{R_i}}{L_{R_i}} \quad (4.27)$$

where L_{T_j} and L_{R_i} are the distances between the target and the j^{th} transmitter and the target and the i^{th} receiver respectively defined in equations (4.14, 4.13).

It follows that, inserting the equation (4.27) into the equation (4.26) gives

$$\dot{f}_{j,i} = -f_j \frac{V^2}{c} \left(\frac{\sin^2 \theta_{T_j}}{L_{T_j}} + \frac{\sin^2 \theta_{R_i}}{L_{R_i}} \right) \quad (4.28)$$

Rearranging the equation (4.28), we obtain

$$V^2 \left(\frac{\sin^2 \theta_{T_j}}{L_{T_j}} + \frac{\sin^2 \theta_{R_i}}{L_{R_i}} \right) = -c \frac{\dot{f}_{j,i}}{f_j} \quad (4.29)$$

Then, using

$$V^2 (\cos \theta_{T_j} + \cos \theta_{R_i})^2 = \frac{c^2 (f_{j,i} - f_j)^2}{f_j^2} \quad (4.30)$$

and then, summing equations (4.29) and (4.30), it is obtained that

$$V^2 \mu_{i,j} = G_{i,j} + H_{i,j} \quad (4.31)$$

where

$$\mu_{i,j} = \left(\cos \theta_{T_j} + \cos \theta_{R_i} \right)^2 + \frac{\sin^2 \theta_{T_j}}{L_{T_j}} + \frac{\sin^2 \theta_{R_i}}{L_{R_i}} \quad (4.32)$$

and

$$G_{i,j} = \frac{c^2 (f_{j,i} - f_j)^2}{f_j^2}, \quad H_{i,j} = -c \frac{\dot{f}_{j,i}}{f_j} \quad (4.33)$$

All receivers know the transmitted frequencies $(f_1, f_2 \dots f_{N_T})$ and hence, after each reception the transmitted frequency is determined accurately by the receiver. As the Doppler frequencies can be estimated, there are no unknowns in equation (4.33). Therefore, in equation (4.31), the unknowns are $V, \theta_{T_j}, \theta_{R_i}, L_{T_j}$ and L_{R_i} . Because the position of the transmitters and the receivers are known, only the coordinates of the target (x, y) are unknown in equations (4.13) and (4.14).

In [7], passive localization problem is investigated. System includes only one target which radiates a tone signal and multiple receivers. Hence, there is only one angle in equations (from the target to the receiver) and with some algebraic operations, these equations can be written in the angle independent form. But in active MIMO radar case, the system includes transmitters as well. Both θ_{T_j} and θ_{R_i} are included in the equations, hence the equations are angle dependent. If the θ_{T_j} , and θ_{R_i} are all known, then the only unknowns are the velocity of the target (V) and the target position in equation (4.31). The proposed solution of equation (4.31) in [7] is by grid searching in the variables x and y . There is no need to include V in the grid search, because V can be written as a function of $G_{i,j}, H_{i,j}, \mu_{i,j}$ and it constant for all i, j

$$V^2 = \frac{G_{i,j} + H_{i,j}}{\mu_{i,j}} \quad (4.34)$$

Then, the cost function for grid search can be defined as

$$J = \sum_{i=1}^{N_R} \sum_{j=1}^{N_T} \left(V^2 - \frac{G_{i,j} + H_{i,j}}{\mu_{i,j}} \right)^2 \quad (4.35)$$

To solve this cost function for unknown V^2 , J can be differantieted with respect to the V^2 which is then equalized to zero

$$V^2 = \frac{1}{N} \sum_{i=1}^{N_R} \sum_{j=1}^{N_T} \left(\frac{G_{i,j} + H_{i,j}}{\mu_{i,j}} \right) \quad (4.36)$$

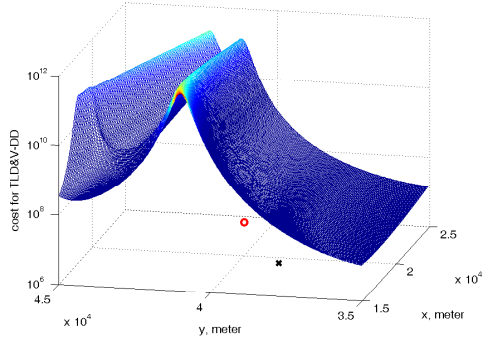
where, $N = N_T \times N_R$ is the total number of the bistatic radars. Inserting equation (4.36) into equation (4.35), the cost function for the derivated doppler method (J_1) can be obtained as

$$J_1 = \sum_{i=1}^{N_R} \sum_{j=1}^{N_T} \left(\frac{1}{N} \sum_{n=1}^{N_R} \sum_{m=1}^{N_T} \left(\frac{G_{n,m} + H_{n,m}}{\mu_{n,m}} \right) - \frac{G_{i,j} + H_{i,j}}{\mu_{i,j}} \right)^2 \quad (4.37)$$

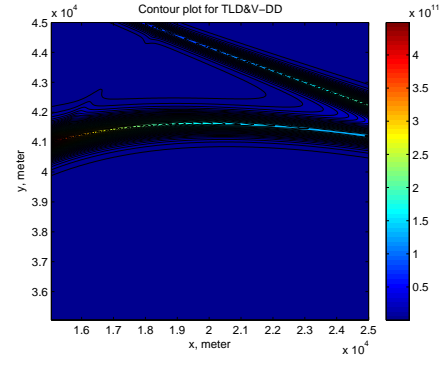
After normalizing the each term in equation (4.37), the cost function for the TLD&V-DD method is obtained as

$$J_1 = \sum_{i=1}^{N_R} \sum_{j=1}^{N_T} \left(1 - \frac{\frac{1}{N} \sum_{n=1}^{N_R} \sum_{m=1}^{N_T} \left(\frac{G_{n,m} + H_{n,m}}{\mu_{n,m}} \right)}{\frac{G_{i,j} + H_{i,j}}{\mu_{i,j}}} \right)^2 \quad (4.38)$$

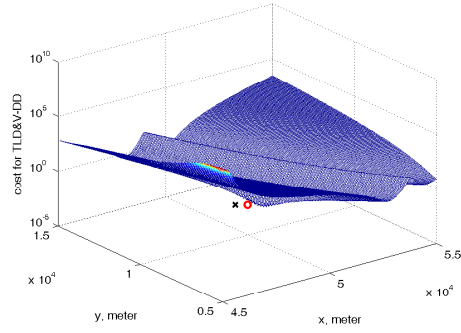
This cost function can be seen in the following pages for different geometries and target positions which are given in Figure 4.2.



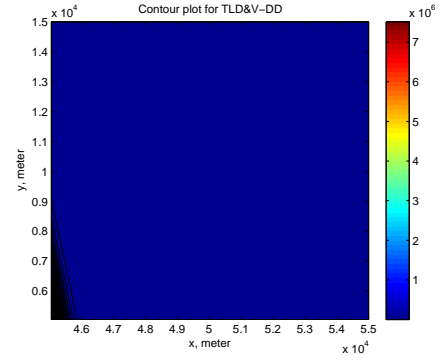
(a) Target at Case 1, Position 1



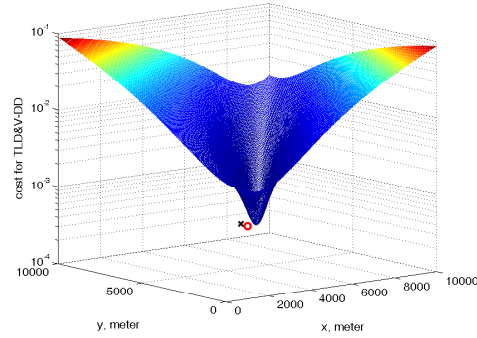
(b) Target at Case 1, Position 1



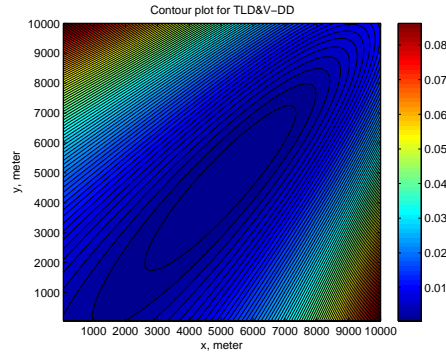
(c) Target at Case 1, Position 3



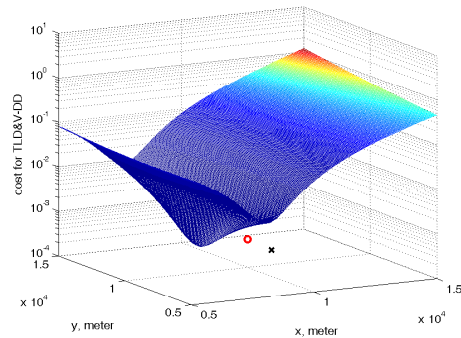
(d) Target at Case 1, Position 3



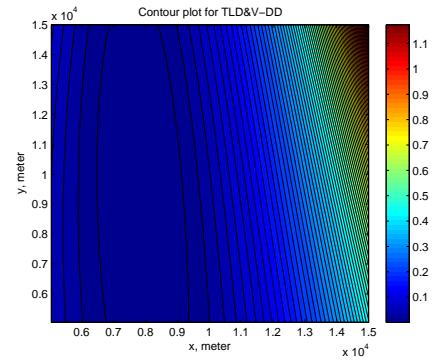
(e) Target at Case 2



(f) Target at Case 2

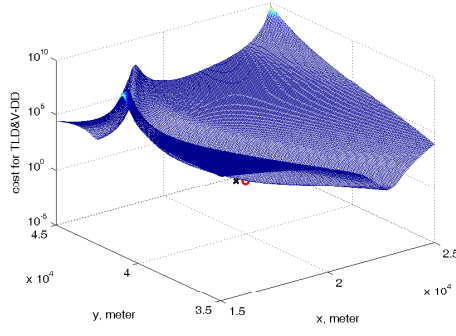


(g) Target at Case 3

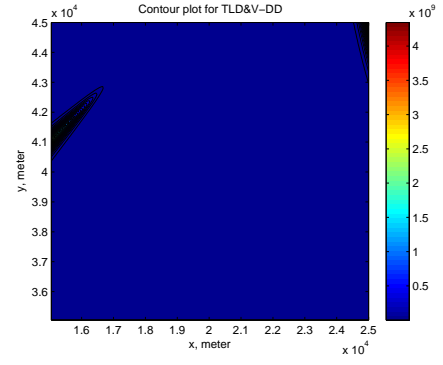


(h) Target at Case 3

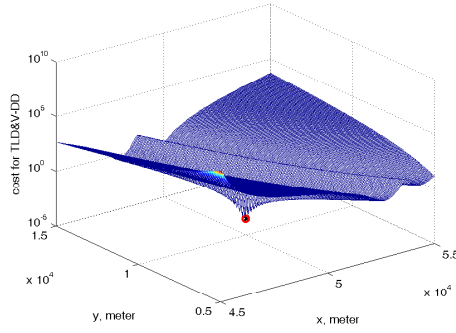
Figure 4.6: Cost functions and contour plots for the TLD&V-DD method at low SNR (SNR = -10 dB) for different geometries.



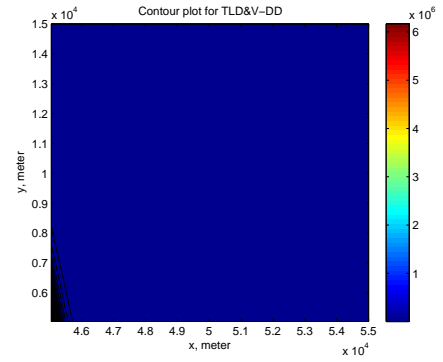
(a) Target at Case 1, Position 1



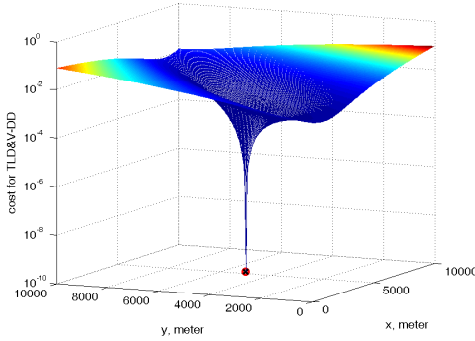
(b) Target at Case 1, Position 1



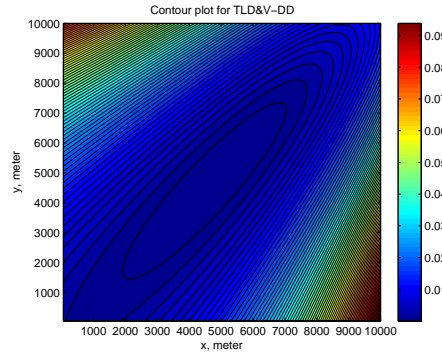
(c) Target at Case 1, Position 3



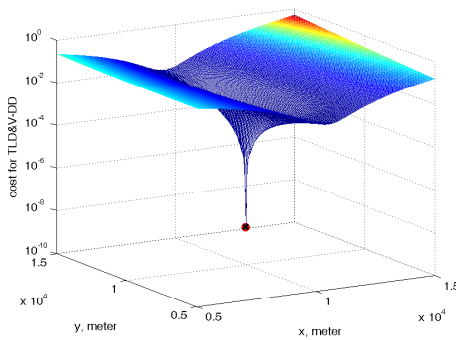
(d) Target at Case 1, Position 3



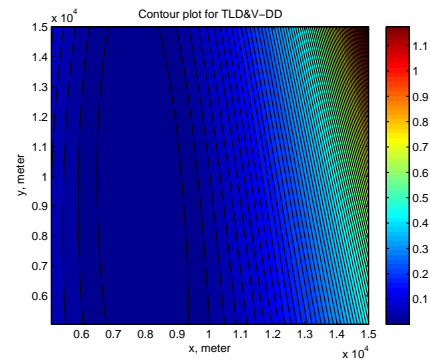
(e) Target at Case 2



(f) Target at Case 2



(g) Target at Case 3



(h) Target at Case 3

Figure 4.7: Cost functions and contour plots for the TLD&V-DD method at high SNR (SNR = 30 dB) for different geometries.

To evaluate the localization performances of the TLD&V-DD method, the simulation geometry given in Figure 4.8 is used.

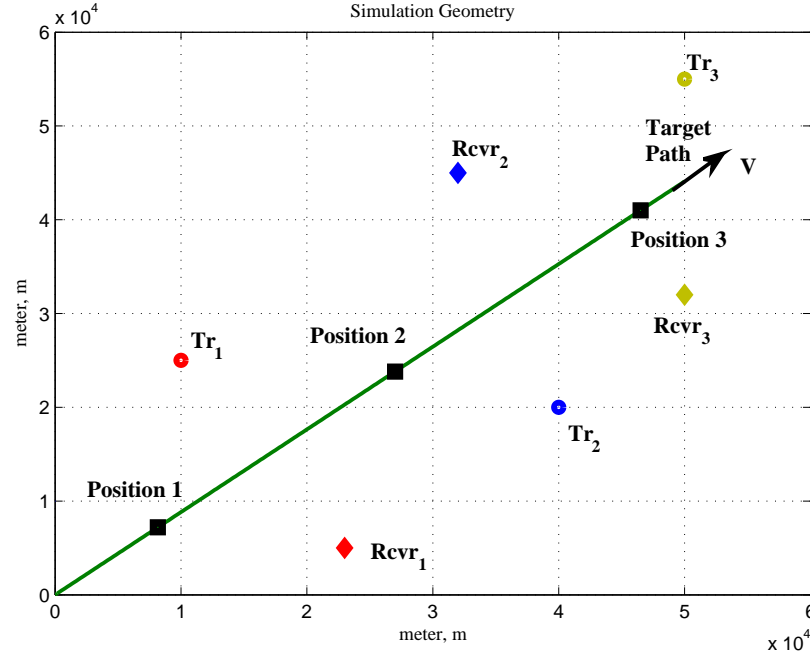


Figure 4.8: MIMO radar simulation geometry for TLD&V-DD method.

For 2×2 MIMO radar, Tr_1 and Tr_2 are used as the transmitters and $Rcvr_1$ and $Rcvr_2$ are used as the receivers. Similarly, $Rcvr_3$ is included for 2×3 MIMO radar case and Tr_3 is included for 3×3 MIMO radar as the third receiver and the third transmitter respectively. Each transmitter radiates a continuous wave (CW) tone signal which has distinct frequencies which are $f_1=200\text{MHz}$, $f_2=500\text{MHz}$ and $f_3=800\text{MHz}$ (for this method only). The target path is shown in Figure 4.8 as a solid line. For error calculations, the target is assumed in positions 1, 2 and 3 which can be seen in the same figure with ■ symbol. Total search area is $60 \times 60 \text{ km}^2$ and this area is searched grid by grid. Grid size is used as 250m and 1000m.

In figures below, the target path is evaluated at 29 consecutive points and estimated positions are plotted in the figures as "x". As can be seen from the Figure 4.9 and Figure 4.10, reducing the grid size also reduces the localization error. When the number of the transmitters and/or the receivers is increased, the target localization performance increases as well. This can be seen in Figure 4.11. For these simulations, there is no Doppler frequency error on the

estimated frequencies, and the exact Doppler frequencies are used.

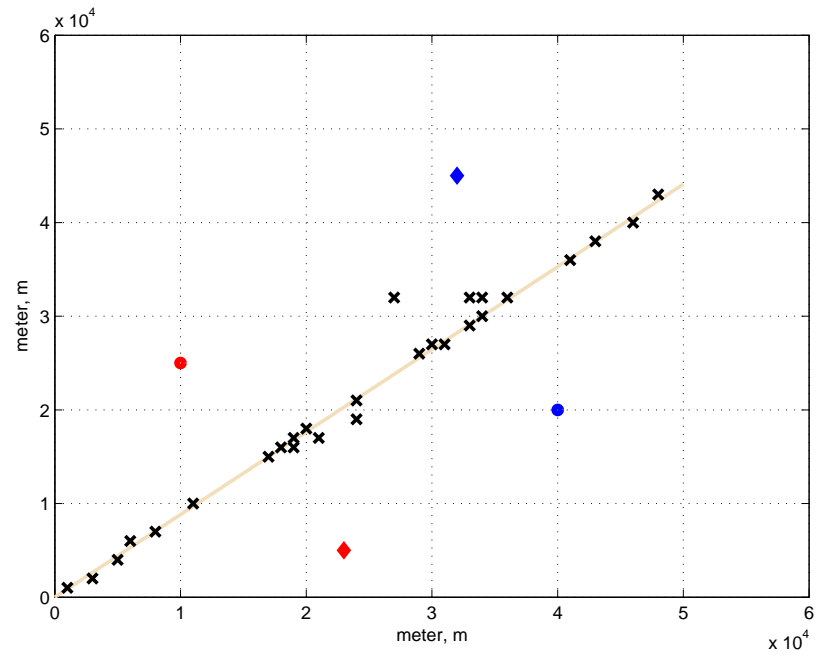


Figure 4.9: Target localization for 2x2 MIMO radar. Grid size = 1000m.

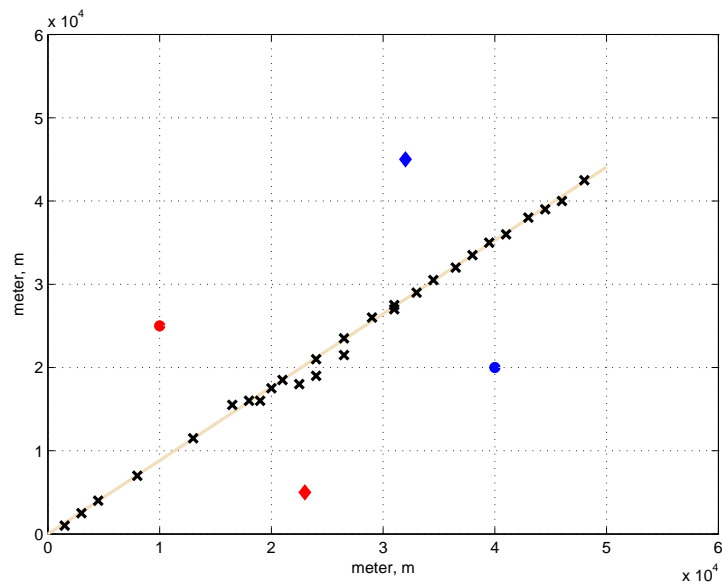


Figure 4.10: Target localization for 2x2 MIMO radar. Grid size = 250m.

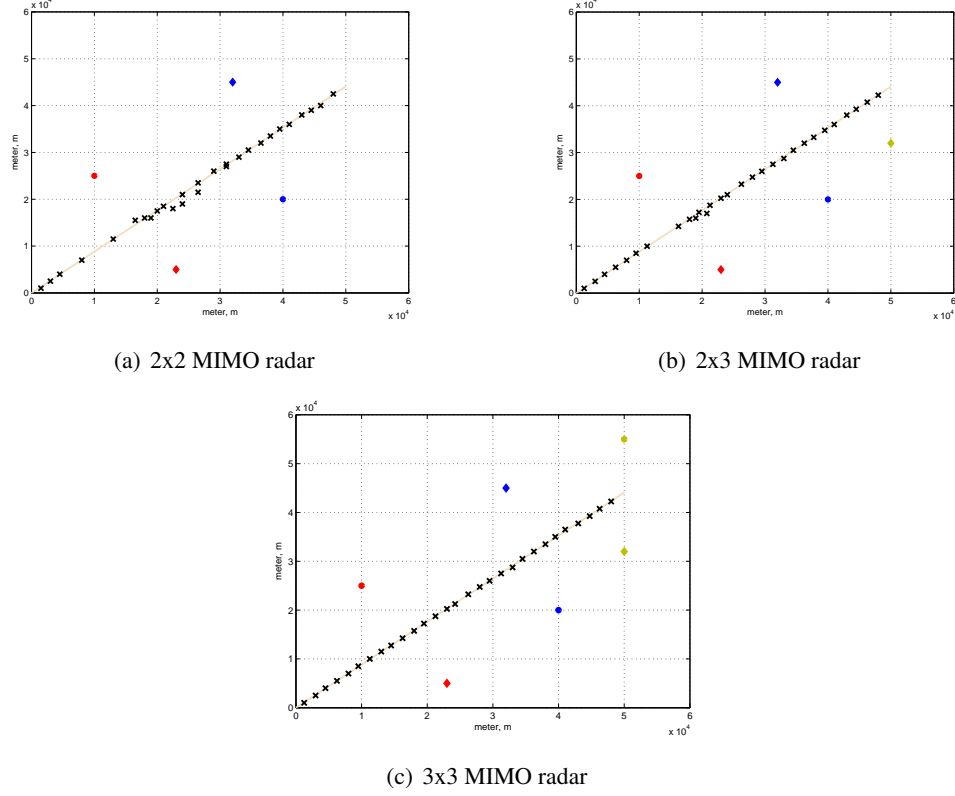


Figure 4.11: Target localization for 250m grid size. a) 2x2 MIMO radar, b) 2x3 MIMO radar, c) 3x3 MIMO radar

For the TLD&V-DD method, the target localization performances have also been studied using different MIMO radar geometries. 3×3 MIMO radar is used for these comparisons and the grid size is chosen as 1000m. In Figure 4.12, these geometries can be seen. In these figures, \bullet and \blacklozenge show the positions of the transmitters and the receivers respectively. Estimated target positions are plotted with "x".

These simulations show that, the target localization performance of the TLD&V-DD method highly depends on the system geometry. The distributed systems give better results because these systems increase the angular spread. Therefore, to obtain a better target localization performance, the number of the transmitters and/or the receivers should be increased and they should be widely separated.

Although this method can localize the target, it requires the target velocity vector to be known besides the Doppler frequencies. This is the disadvantage of the TLD&V-DD method.

This method is presented in "IEEE 2009 European Radar Conference - EuRAD'09". And the

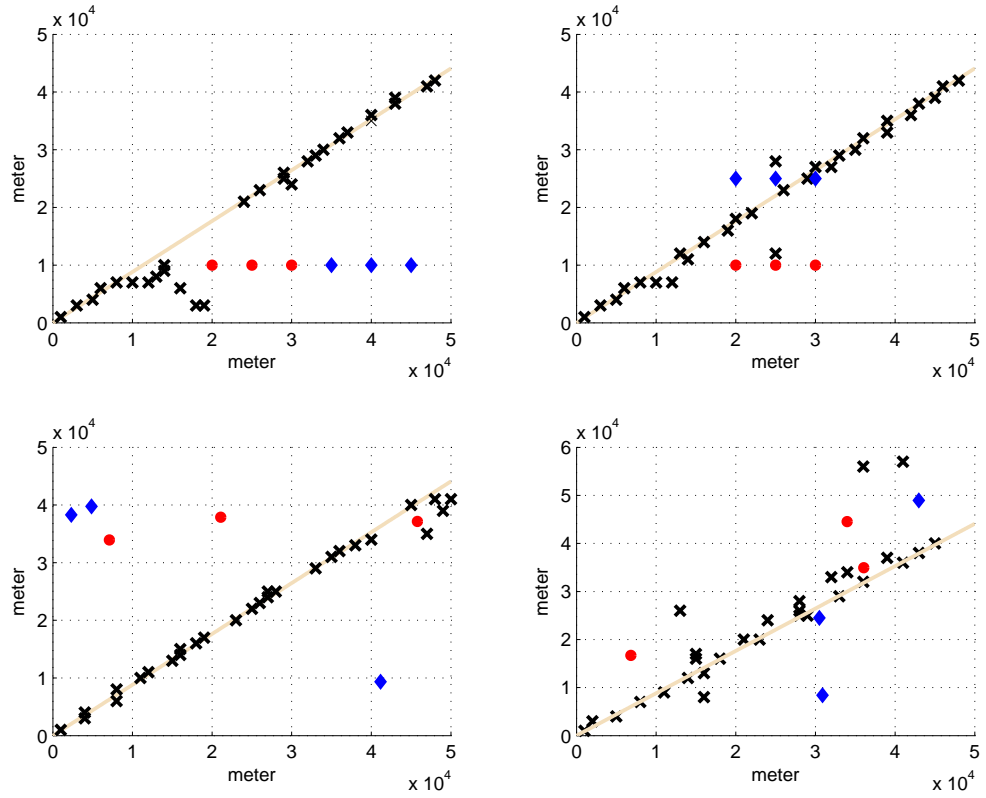


Figure 4.12: Target localization for different 3x3 MIMO radar geometries.

full work with the simulation results can be found in [54].

4.2.2 Second Method : Sub-ML Estimator - TLD&V-subML

In statistics, maximum-likelihood estimation (MLE) is a method of estimating the parameters of a statistical model. When applied to a data set and given a statistical model, maximum-likelihood estimation provides the estimates for the model's parameters [55].

In general, for a fixed set of data and underlying statistical model, the method of maximum likelihood selects values of the model parameters that produce a distribution that gives the observed data the greatest probability (i.e., parameters that maximize the likelihood function). Maximum-likelihood estimation gives a unified approach to estimation, which is well-defined in the case of the normal distribution and many other problems [55].

To apply this method for the problem given here, assume the observations at each receiver is received frequencies

$$r_{j,i} = f_{j,i} + n_{j,i} \quad ; \quad i = 1, \dots, N_R \quad ; \quad j = 1, \dots, N_T \quad (4.39)$$

where $r_{j,i}$'s are the frequencies of the received signals radiated from the j^{th} transmitter and received by the i^{th} receiver, $f_{j,i}$'s are the actual noiseless frequencies of the transmitted signal from the j^{th} transmitter at the i^{th} receiver and $n_{j,i}$'s are measurement errors which are modelled as the spatially white, i.i.d., gaussian random processes with $N(0, \sigma^2)$ [24, 56].

This models assumes that the frequencies are estimated using a frequency estimator and the error on the frequency estimate is a Gaussian distributed random variable. A maximum likelihood estimator can be defined to estimate the frequencies in Gaussian noise. For the observations given in equation (4.39), the probabilities can be written as

$$p(r_{j,i}|f_{j,i}) = \frac{1}{\sqrt{2\pi\sigma^2}} \exp\left(-\frac{(r_{j,i} - f_{j,i})^2}{2\sigma^2}\right) \quad (4.40)$$

As $n_{j,i}$'s are independent, it can be written as

$$\begin{aligned} p(\mathbf{r}|\mathbf{f}) &= \prod_{i=1}^{N_R} \prod_{j=1}^{N_T} p(r_{j,i}|f_{j,i}) \\ &= \prod_{i=1}^{N_R} \prod_{j=1}^{N_T} \frac{1}{\sqrt{2\pi\sigma^2}} \exp\left(-\frac{(r_{j,i} - f_{j,i})^2}{2\sigma^2}\right) \end{aligned} \quad (4.41)$$

where $\mathbf{r} = [r_{1,1}, r_{1,2}, \dots, r_{N_T, N_R}]^T$ and $\mathbf{f} = [f_{1,1}, f_{1,2}, \dots, f_{N_T, N_R}]^T$

As the received frequencies can be written depending on target coordinates (x, y) , the ML estimator for target localization can be defined as [57]

$$x_{ML} = \arg \max_x p(\mathbf{r}|\mathbf{f}) \quad ; \quad y_{ML} = \arg \max_y p(\mathbf{r}|\mathbf{f}) \quad (4.42)$$

or equivalently

$$x_{ML} = \arg \max_x \ln p(\mathbf{r}|\mathbf{f}) \quad ; \quad y_{ML} = \arg \max_y \ln p(\mathbf{r}|\mathbf{f}) \quad (4.43)$$

Then, the final ML equation becomes

$$\frac{d}{dx} p(\mathbf{r}|\mathbf{f}) = \frac{d}{dx} \ln p(\mathbf{r}|\mathbf{f}) = 0 \quad \text{when} \quad x = x_{ML} \quad (4.44)$$

$$\frac{d}{dy} p(\mathbf{r}|\mathbf{f}) = \frac{d}{dy} \ln p(\mathbf{r}|\mathbf{f}) = 0 \quad \text{when} \quad y = y_{ML} \quad (4.45)$$

Taking the natural logarithm of equation (4.41)

$$\ln p(\mathbf{r}|\mathbf{f}) = -\frac{N}{2} \ln(2\pi\sigma^2) - \frac{1}{2\sigma^2} \sum_{i=1}^{N_R} \sum_{j=1}^{N_T} (r_{j,i} - f_{j,i})^2 \quad (4.46)$$

where, $N = N_T \times N_R$ is the total number of the radar units. Let's differentiate equation (4.46) with respect to the x and y to get the maximum likelihood solutions, (x_{ML}, y_{ML})

$$\frac{d}{dx} \ln p(\mathbf{r}|\mathbf{f}) = \frac{1}{\sigma^2} \sum_{i=1}^{N_R} \sum_{j=1}^{N_T} (r_{j,i} - f_{j,i}) \frac{d}{dx} (f_{j,i}) \quad (4.47)$$

$$\frac{d}{dy} \ln p(\mathbf{r}|\mathbf{f}) = \frac{1}{\sigma^2} \sum_{i=1}^{N_R} \sum_{j=1}^{N_T} (r_{j,i} - f_{j,i}) \frac{d}{dy} (f_{j,i}) \quad (4.48)$$

By using equation (4.7), these differentials can be calculated as

$$\begin{aligned} \frac{d}{dx} \ln p(\mathbf{r}|\mathbf{f}) &= \sum_{i=1}^{N_R} \sum_{j=1}^{N_T} \left(r_{j,i} - f_j + \frac{f_j}{C} \left(\frac{K_{Tj}}{L_{Tj}} + \frac{K_{Ri}}{L_{Ri}} \right) \right) \\ &\times \left(\frac{(x - x_{Tj})K_{Tj}}{L_{Tj}^3} + \frac{(x - x_{Ri})K_{Ri}}{L_{Ri}^3} - V_x \left(\frac{1}{L_{Tj}} + \frac{1}{L_{Ri}} \right) \frac{f_j}{C} \right) \end{aligned} \quad (4.49)$$

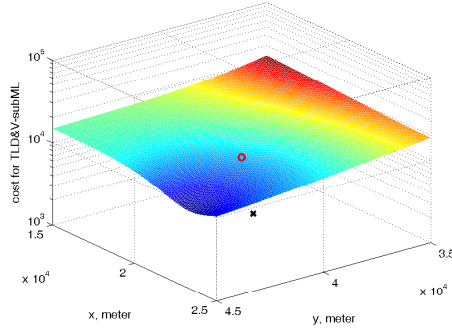
$$\begin{aligned} \frac{d}{dy} \ln p(\mathbf{r}|\mathbf{f}) &= \sum_{i=1}^{N_R} \sum_{j=1}^{N_T} \left(r_{j,i} - f_j + \frac{f_j}{C} \left(\frac{K_{Tj}}{L_{Tj}} + \frac{K_{Ri}}{L_{Ri}} \right) \right) \\ &\times \left(\frac{(y - y_{Tj})K_{Tj}}{L_{Tj}^3} + \frac{(y - y_{Ri})K_{Ri}}{L_{Ri}^3} - V_y \left(\frac{1}{L_{Tj}} + \frac{1}{L_{Ri}} \right) \frac{f_j}{C} \right) \end{aligned} \quad (4.50)$$

Actual x_{ML} and y_{ML} solutions are the values which makes zero the equations (4.49) and (4.50) respectively. But, for the case given here, only the received frequencies are used. Hence, instead of making these equations zero, grid search can be used to find the x and y coordinates which minimize these equations. Therefore, the solution becomes the sub-ML (ML with grid search) solution not the exact ML solution.

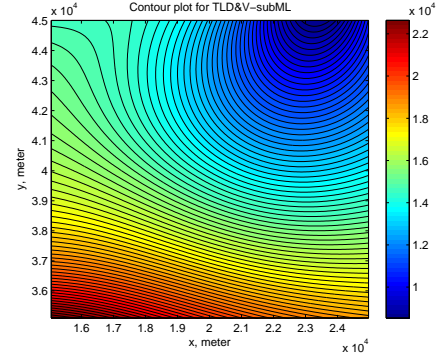
The third estimator (sub-ML method) uses equations (4.49) and (4.50) as cost functions in the grid search and tries to find the target position (x, y) separately.

This cost function can be seen in the following pages for different geometries and target positions which are given in Figure 4.2.

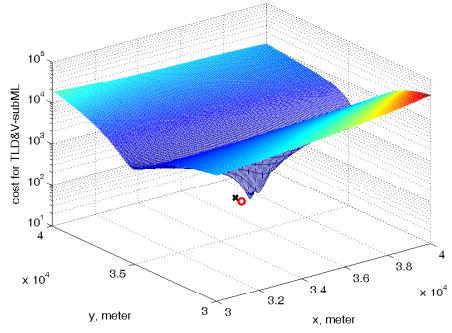
This method is presented in "IEEE Radar Conference, 2011 - RadarCon2011". The comparison of this method with other two estimator can be found in [58].



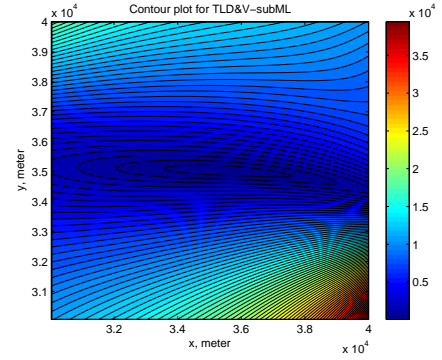
(a) Target at Case 1, Position 1



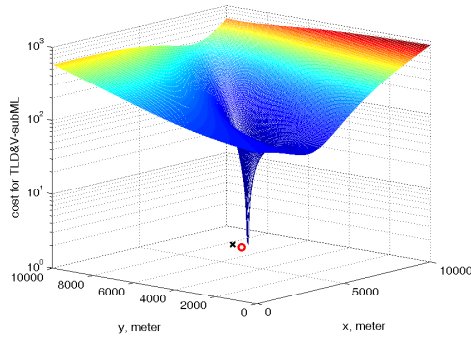
(b) Target at Case 1, Position 1



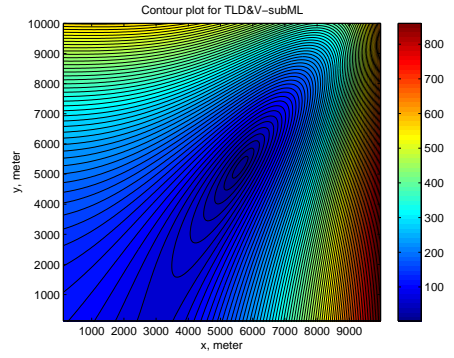
(c) Target at Case 1, Position 2



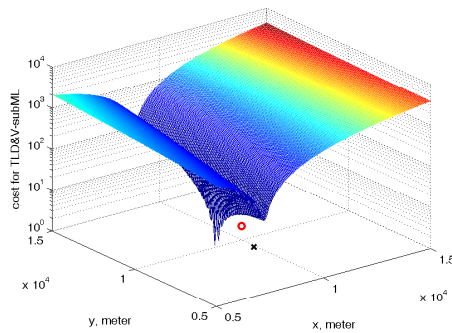
(d) Target at Case 1, Position 2



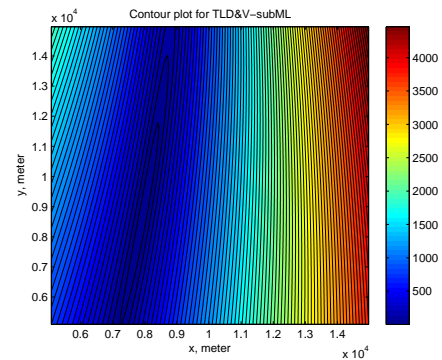
(e) Target at Case 2



(f) Target at Case 2

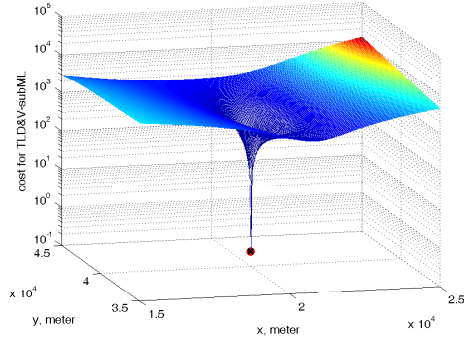


(g) Target at Case 3

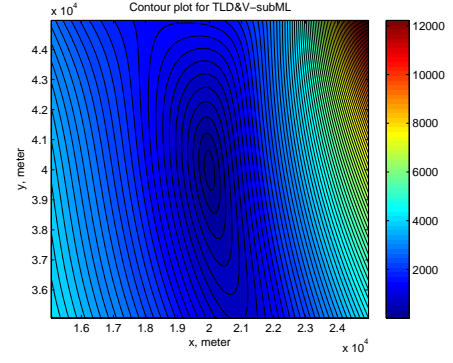


(h) Target at Case 3

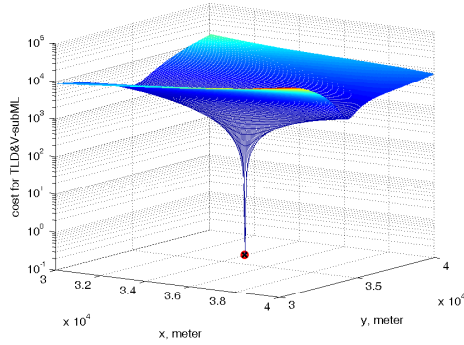
Figure 4.13: Cost functions and contour plots for the TLD&V-subML method at low SNR (SNR = -10 dB) for different geometries.



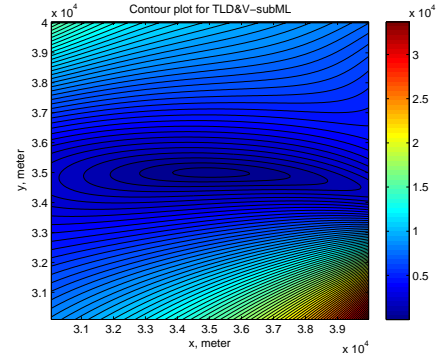
(a) Target at Case 1, Position 1



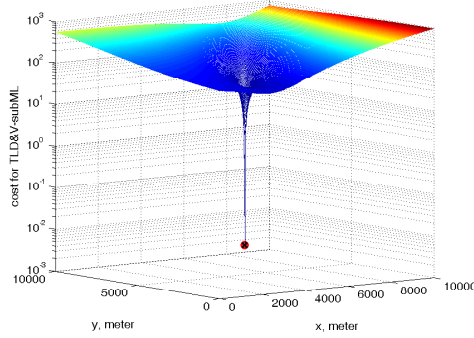
(b) Target at Case 1, Position 1



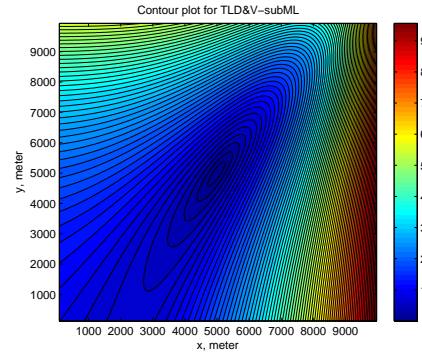
(c) Target at Case 1, Position 2



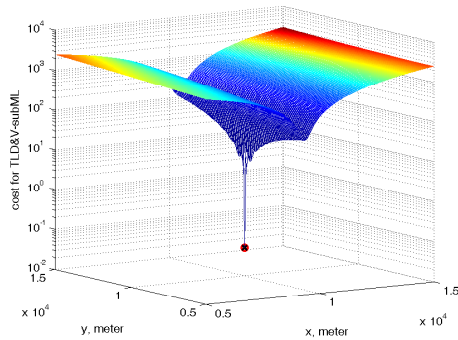
(d) Target at Case 1, Position 2



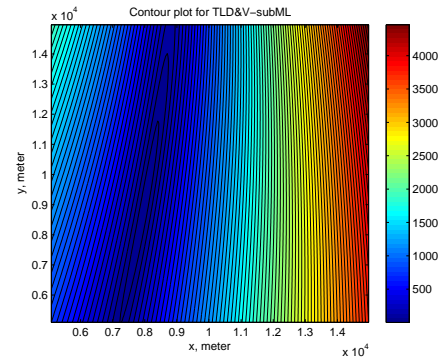
(e) Target at Case 2



(f) Target at Case 2



(g) Target at Case 3



(h) Target at Case 3

Figure 4.14: Cost functions and contour plots for the TLD&V-subML method at high SNR (SNR = 30 dB) for different geometries.

CHAPTER 5

SIMULATION RESULTS

In the previous chapters, new target localization and the target velocity estimation methods for the frequency-only MIMO radar are proposed. Then, the target and the signal models for the frequency-only MIMO radar are given and finally, the Cramer Rao Bounds (CRB) for the target localization and the target velocity estimation problems are investigated using defined signal and target models.

In this chapter, the performances of the proposed estimators are investigated via simulations. Moreover, the performances of three estimators are compared with the traditional isodoppler curves based FOA method according to the defined signal and the target model. And the performances of the estimators are compared with the CRBs for the target localization and the target velocity estimation cases.

Four methods (TLDF, TLD&V-DD, TLD&V-subML and the isodoppler based traditional FOA methods) are compared with respect to the performances of the target localization. For the velocity estimation case, the TLDF method is used only because the other methods can not estimate the target velocity.

In simulations, target is assumed at five different positions with $V = 800$ kmph velocity. Only 3×3 MIMO radar case is simulated, and the transmit frequencies are $f_1 = 10$ GHz, $f_2 = 10.3$ GHz and $f_3 = 10.5$ GHz. The simulation geometries can be seen in Figure 4.2.

The observation time is choosen as $T_{obs} = 10$ msec, and by dividing this observation time 200 sub-blocks (which are 50μ seconds), the pulse-to-pulse decorrelation between the radar cross section (RCS) coefficients are defined and this is known as Swerling-2 and Swerling-4 [44] type target fluctuations. As the target is a large aircraft, Swerling-4 type target fluctuations

are more suitable but the target localization performances are investigated for both Swerling-2 and Swerling-4 cases besides the non-fluctuating (Swerling-0) case.

For the estimation of the Doppler frequencies from the received signals, the periodogram spectral estimator is used as defined in [49]. This estimator is explained in the following section.

5.1 Frequency Estimation

In literature, there are many methods for frequency estimation. In this thesis, the periodogram spectral estimator is used to estimate the frequencies of the received unmodulated CW signals.

The periodogram spectral estimator relies on the definition of the PSD given by [49]

$$P_{xx}(f) = \lim_{M \rightarrow \infty} E \left[\frac{1}{2M+1} \left| \sum_{n=-M}^M x[n] \exp(-j2\pi fn) \right|^2 \right] \quad (5.1)$$

By neglecting the expectation operator and using the available data $(x[0], x[1], \dots, x[N-1])$, the periodogram spectral estimator is defined as

$$\hat{P}_{PER}(f) = \frac{1}{N} \left| \sum_{n=0}^{N-1} x[n] \exp(-j2\pi fn) \right|^2 \quad (5.2)$$

Then, the maximum likelihood frequency estimate is equivalent to setting

$$\hat{f} = \arg \max_f \left| \sum_{n=0}^{N-1} x[n] \exp(-j2\pi fn) \right|^2 \quad (5.3)$$

As already seen from equation (5.3), it is nothing but the Discrete Fourier Transform (DFT) of $x[n]; n = 1, 2, \dots, N$. Hence, the periodogram spectral estimator can be seen as taking the DFT of a sequence $x[n]$ and finding the location of the maximum DFT sample.

Continuous wave, unmodulated tone signals are used and the frequencies are 10, 10.3 and 10.5 GHz. The maximum target velocity is predefined as 900 kmph. This model gives the maximum Doppler frequency as 17.5 KHz. To estimate the Doppler frequencies, the received signals are sampled using the Nyquist sampling frequency which is $f_s = 35$ KHz.

The frequency estimation performance depends on the DFT size. In the following figures the effect of the DFT size on the frequency estimation can be seen for different target geometries

and for different target fluctuations. The frequency estimator performances are compared with the CRB given in [49]. In Figure 5.1, all 9 frequencies for 3×3 MIMO radar and for the target at case1, position 2 are plotted using non-fluctuating target model. In Figure 5.2, only $f_{d_{11}}$ is plotted for the target at case2 using different type of target fluctuations and using different DFT sizes. Similarly, in Figure 5.3, only $f_{d_{11}}$ is plotted again for the target at case3 using Swerling-0 type of target fluctuations and using different DFT sizes.

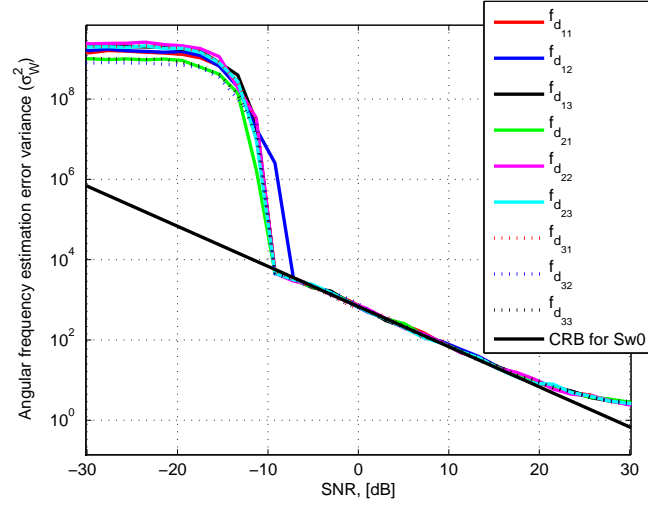


Figure 5.1: Frequency estimations for a target at case1, position2. No target fluctuation and the DFT size is 2^{16} .

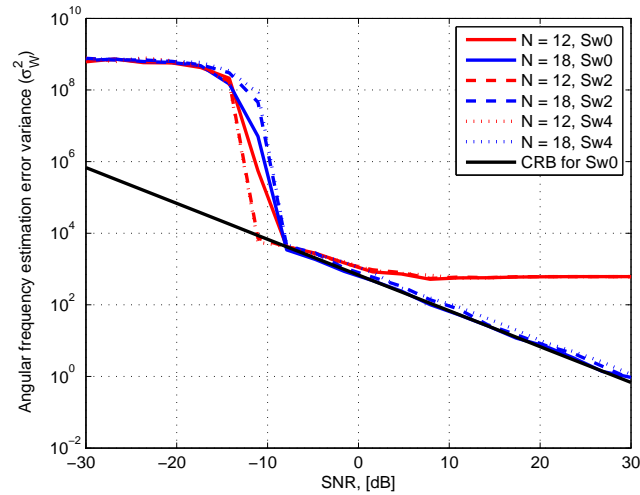


Figure 5.2: Frequency estimations for a target at case2 and for different target fluctuations. The DFT size is 2^N .

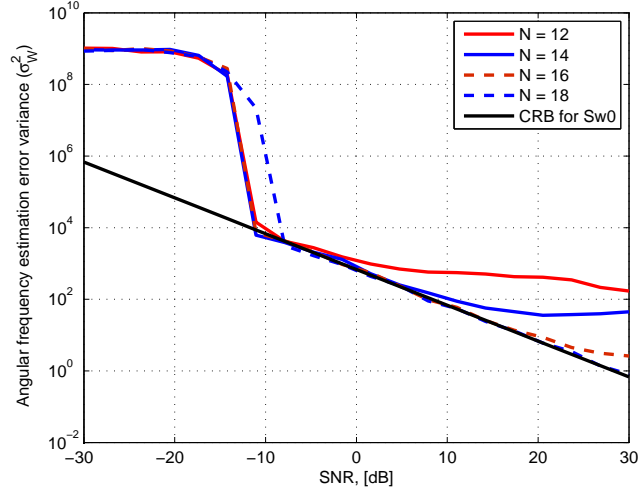


Figure 5.3: Frequency estimations for a target at case3 with Swerling-0 type target fluctuations. The DFT size is 2^N .

As it can be seen in figures above, the Doppler frequencies can be estimated accurately at high SNRs using the larger DFT sizes. The frequency estimation performances are similar for different target geometries. Moreover, the frequency estimation performances are irrespective of the target fluctuations. On the other hand, the DFT size is too large with respect to the sample size of the received signal. Hence, instead of the DFT, the DTFT (Discrete Time Fourier Transform) is applied to the received signal and then the DTFT is sampled by N sample to get N -point DFT.

In these simulations, the target is assumed as stationary on the observation time. Moreover, actually the target is moving and its position and hence the received Doppler frequencies are changing with time. To analyze this effect, the observation time, which is 10 msec, is divided by 100 subblocks, and for each block the target position, time delays and the Doppler frequencies are used to obtain more realistic received signal model. In this case, the Doppler frequencies shift a bit with respect to the stationary case, and hence the frequency estimation error increases. For this more realistic model, the frequency estimation performances can be seen in the following figures. These figures include all 9 frequency estimates for 3×3 MIMO radar for different target positions.

In Figure 5.4 and Figure 5.5, the target motion is inserted to the model as explained and the estimated Doppler frequencies are plotted for different target geometries for non-fluctuating

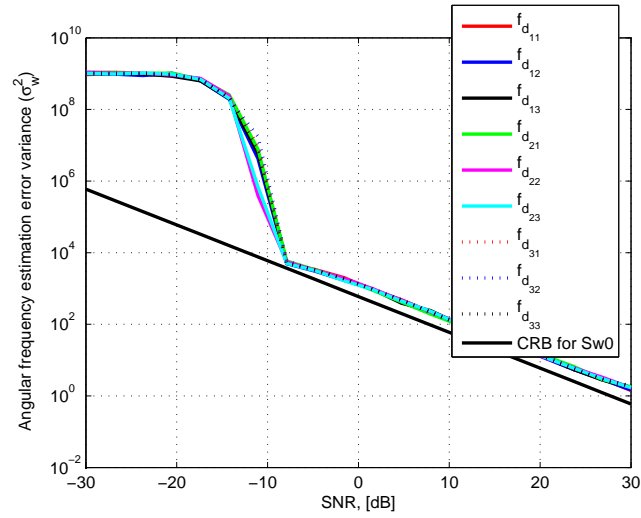


Figure 5.4: Frequency estimations for a target at case2. No target fluctuations exist and the DFT size is 2^{18} . Target is moving.

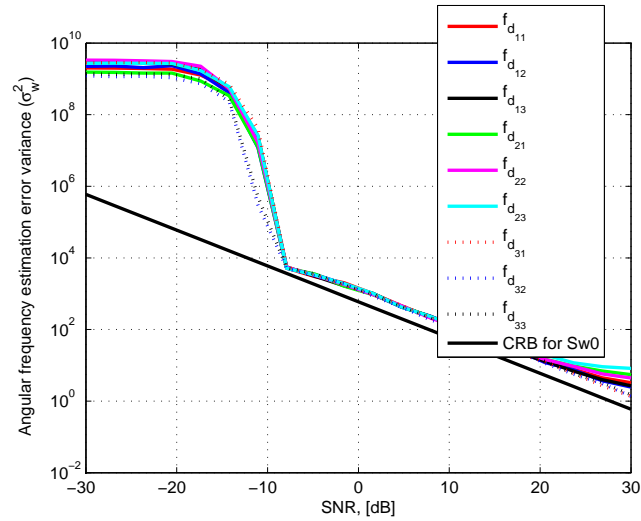


Figure 5.5: Frequency estimations for a target at case1, position2. No target fluctuations exist and the DFT size is 2^{18} . Target is moving.

target. As can be seen from Figure 5.4 and Figure 5.5, the frequency estimation error increases as expected because of the target motion which is included in the model. Although, the average Doppler frequency in the observation time and the Doppler frequency at the beginning of the observation time is different (nearly 1 – 2 Hz for given simulation parameters), the CRB is again plotted for the stationary target case.

5.2 Grid Search

In the Figure 5.6, the grid search methodology can be seen. The search area is divided by grids in two dimensions (x, y), and then each intersection points become grid points which are searched for the target localization.

For each grid points, costs are calculated by using the pre-defined cost functions for each estimator. Then, the grid point which has the minimum cost, gives the target coordinates in (x, y) plane. As space is searched in two dimension, the variation on search time is proportional with the square of the inverse of the change in grid size. For example, when the grid size is decreased to the half, search time is increased four times.

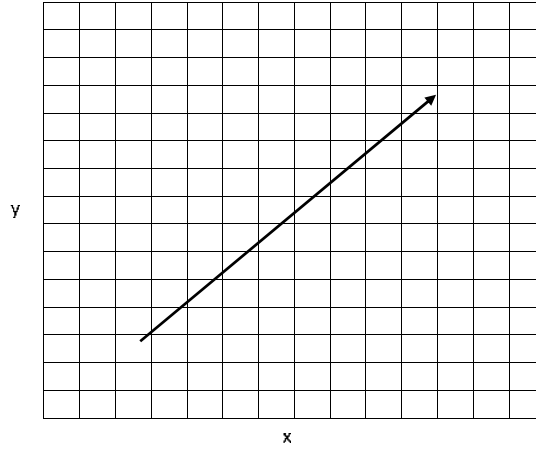


Figure 5.6: Grid search in (x, y) coordinates.

For searching a wide region, the search time can be very high, hence variable grid-size can be used as well. For this case, the $30 \times 30 \text{ km}^2$ search area is divided by 4 parts, then grid points chosen as the center of the each part. Using these 4 grid points and cost functions, one part is selected and the same operation is repeated for that chosen division. This operation is repeated as 16 times, and the final grid size becomes $30 \text{ km} / 2^{16} = 0.45 \text{ m}$. This method is decreased the search time efficiently, and the grid size or division number can be changed. If the all area is searched using 10 m constant grid size, the total search point number is: $30000/10 \times 30000/10 = 9 \times 10^6$. On the other hand, using variable grid search, the required number of grid points is only $4 \times 16 = 64$.

Advantage of using the variable grid size is the short search time. On the other hand, if a wrong part is chosen at any mid-step, then the error can be large with compared to the regular grid searching. Hence, the both methods can be used simultaneously. For example, the variable grid search can be used on the wide area, but when the grid size is decreased to the 500 meters, or user dependent any small values, then the regular grid search may be operated with acceptable grid sizes.

5.3 Target Localization and Velocity Estimation Simulations

The TLDF method can estimate the target velocity and the target direction directly from the estimated Doppler frequencies. Then, by using the estimated target velocity, the target position can be estimated via the TLDF method. On the other hand, the other three methods (TLD&V-DD, TLD&V-subML, and traditional FOA methods) require target velocity vector to be known besides the Doppler frequency to estimate the target position. Hence, in the first step the target velocity is estimated using the TLDF method, then using the estimated target velocity the other three methods can be simulated for the target position estimation.

The frequency estimation performances of the periodogram spectral estimator when target fluctuation exist are close to each other as can be seen in Figure 5.2. Hence, the target localization performances of all three cases are similar and irrespective of the target fluctuations. Therefore, for the clarity of the figures, the results are reported for the non-fluctuation case (Swirling-0) only. Instead of the target fluctuations, the DFT size is more important parameter, and hence it must be large enough to estimate the Doppler frequencies accurately. In these simulations given here, the DFT size is 2^{18} .

In this dissertation, the traditional FOA method is adapted to an active MIMO radar system to obtain a baseline performance in the simulations. When the received frequencies and the transmitted frequencies are known, Doppler shifts are also known and the locus of points for constant Doppler shift gives a curve referred to as isodoppler curves or isodops for a given target velocity. If more than one isodops exist, the intersection points of them give the target position. The traditional isodoppler curves based FOA method calculates isodops, then finds the target position from their intersections. However, if the target velocity is not known, the isodops should be found for each possible target velocity and hence the number of isodops

increases. Therefore, knowing the target velocity is a prerequisite for the traditional FOA method.

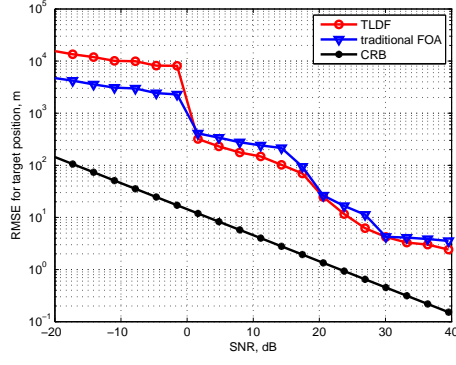
Moreover, when the variable grid size is used, wrong target position can be found. To increase the performance of the search algorithm, hybrid grid search is used. When the grid size is larger than 1000 m, variable grid size is used, and then the final 1000×1000 m region is searched by 1 m grid size. And the grid reference error is chosen randomly as maximum is being $1/2 = 0.5$ m. In the Table 5.1, the simulation parameters and assumptions are given.

Table 5.1: 3x3 MIMO Radar Simulation Parameters and Assumptions

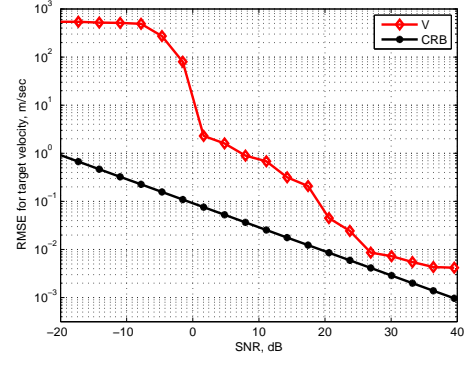
Simulation parameter	Value/Explanation
Target	1 target exists, ($P_d = 1, P_{fa}=0$), no multipath
Observation time	10 msec
Sampling frequency	35 KHz
Fluctuation type	Swerling-0 (no target fluctuation)
Frequency estimator	Periodogram spectral estimator via DFT
DFT size	2^{18}
Search area	$30 \times 30 \text{ km}^2$
Search type	Grid search, hybrid grid (variable and constant grid size)
Variable grid	Total area is divided by 4 equal size parts iteratively.
Constant grid	$(1000 \times 1000) \text{ m}^2$, 1 m grid size, gre = 0.5 m

In Figures 5.7 and 5.8, the target localization and the velocity estimation performances of the TLDF method can be seen for different target and transmitter/receiver geometries. The simulation geometries can be seen in Figure 4.2 and the other simulation parameters are as in Table 5.1. The target localization performance of the TLDF method is compared with the CRB and the traditional isodoppler curves based FOA method.

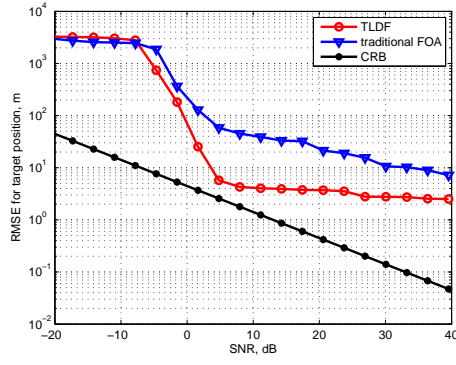
The TLDF method not only estimates the target velocity but also the direction of the target. The target movement direction estimation performances of the TLDF method can be seen in Figure 5.9 for the same target configurations.



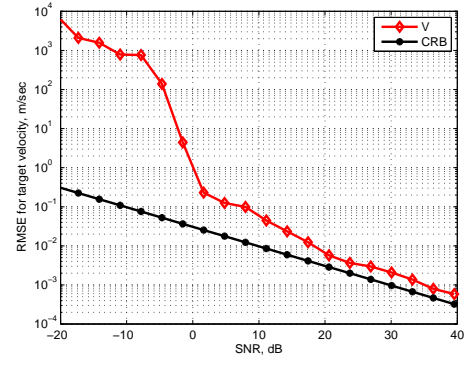
(a) The position estimation performance for the target in case1, position1.



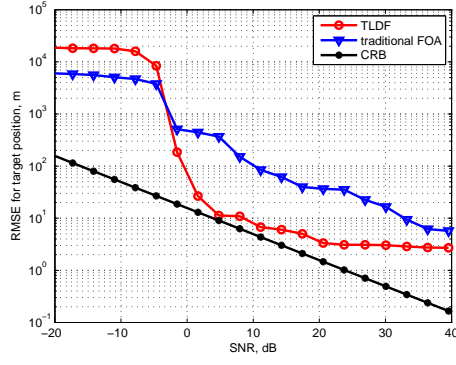
(b) The velocity estimation performance for the target in case1, position1.



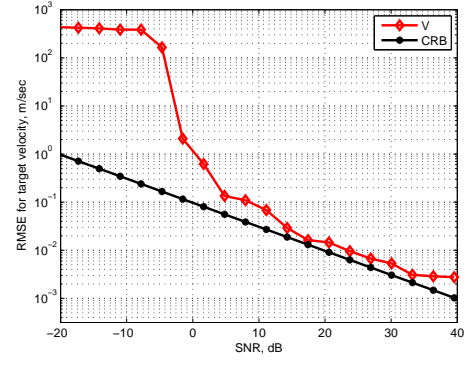
(c) The position estimation performance for the target in case2, position2.



(d) The velocity estimation performance for the target in case2, position2.

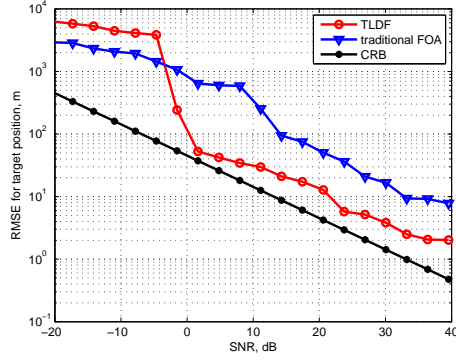


(e) The position estimation performance for the target in case3, position3.

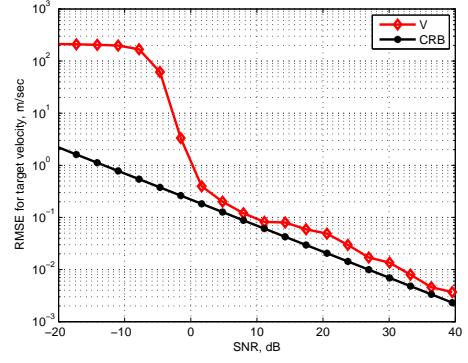


(f) The velocity estimation performance for the target in case3, position3.

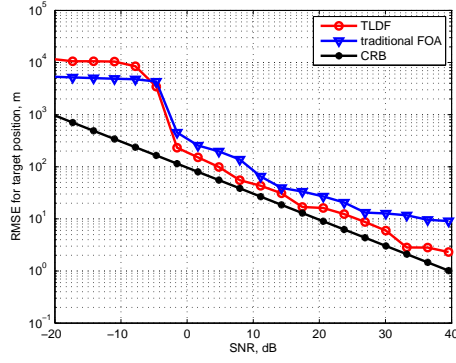
Figure 5.7: The target position and the target velocity estimation performances of the TLDF and the traditional FOA methods for a target in different positions (case 1).



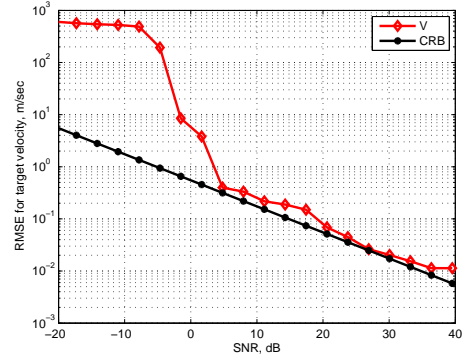
(a) The position estimation performance for the target in case2.



(b) The velocity estimation performance for the target in case2.



(c) The position estimation performance for the target in case3.



(d) The velocity estimation performance for the target in case3.

Figure 5.8: The target position and the target velocity estimation performances of the TLDF and the traditional FOA methods for a target in different positions (case 2 and case 3).

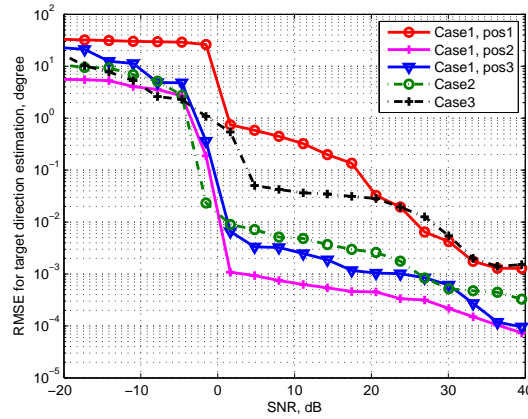
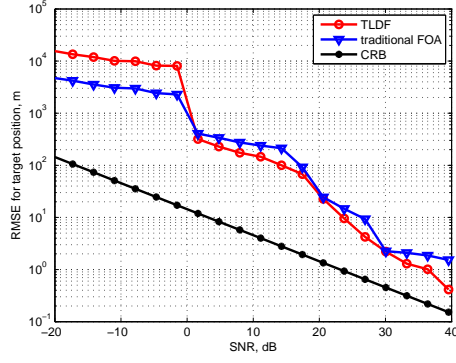


Figure 5.9: Target direction estimation performances of the TLDF method for different target cases.

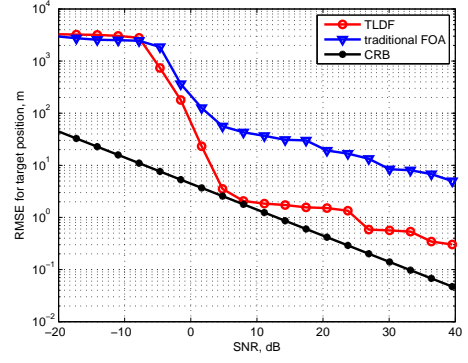
As can be seen from the simulation results, the velocity estimation performance of the TLDF method is well and close to the CRB especially for high SNRs. At low SNR values, the velocity estimation, and hence the position estimation performances are not successful. It is expected as the Doppler frequencies do not estimated accurately at low SNRs. As can be seen from the figures, not only the magnitude of the velocity, but also the direction of the target is estimated accurately.

The TLDF method shows better target position estimation performance compared to the traditional FOA method. As the target is moving on the observation time (exactly 2.2 m for these simulations), the position estimation error could not be less than nearly 2 meters. This effect can be seen in the figures.

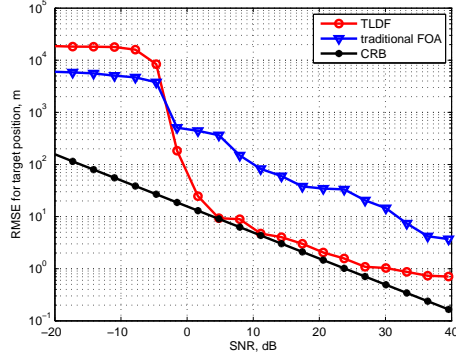
Besides the better target position estimation performance, the most important superiority of the TLDF method is, its capability of velocity estimation and this is the uniqueness of the TLDF method. These velocity estimations can be used to decrease the position estimation error because of the observation time. The target velocity is estimated using the TLDF method accurately, and the observation time is totally known. Hence, the motion of the target in the observation time frame can be calculated and then the position estimates can be updated. After this update process, the new target position estimation results can be seen in Figure 5.10.



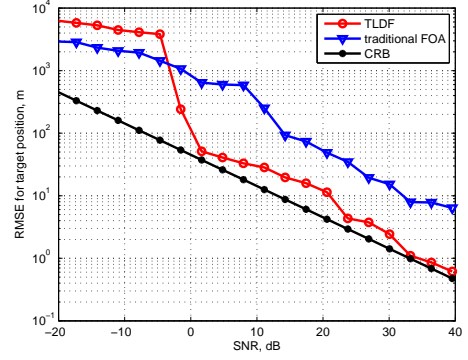
(a) For the target in case1, position1.



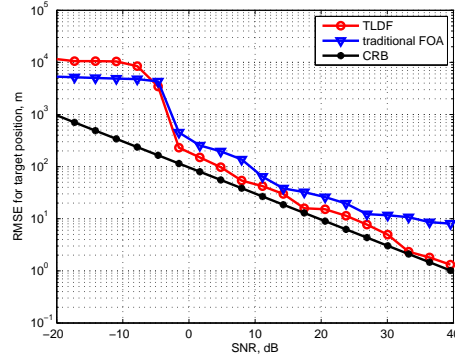
(b) For the target in case1, position2.



(c) For the target in case1, position3.



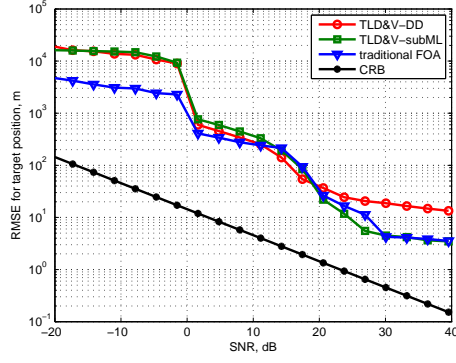
(d) For the target in case2.



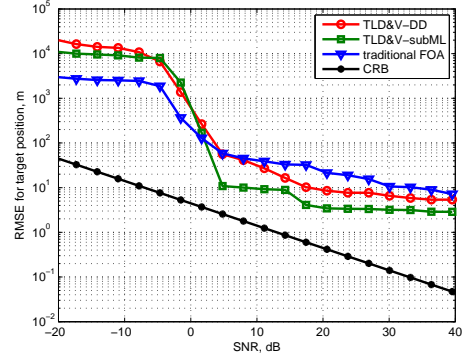
(e) For the target in case3.

Figure 5.10: The target position estimation performances of the TLDF methods for a target in different positions (after velocity updates).

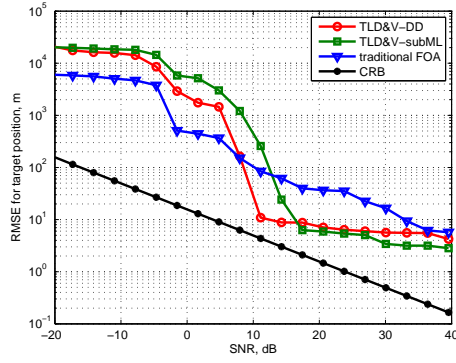
For a fair comparison of the traditional FOA method, instead of TLDF method, the TLD&V methods can be used. The target velocity vector is estimated using the TLDF method, then TLD&V-DD, TLD&V-subML and the traditional FOA methods can be applied to estimate the target position. In Figure 5.11, these three methods are compared for different target geometries given in Figure 4.2.



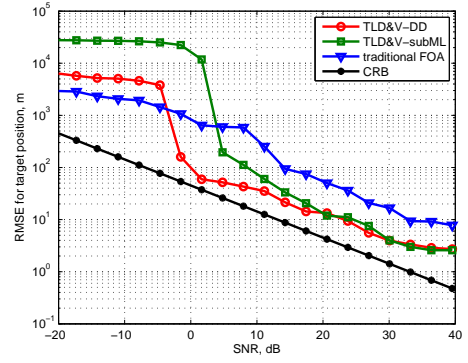
(a) For the target in case1, position1.



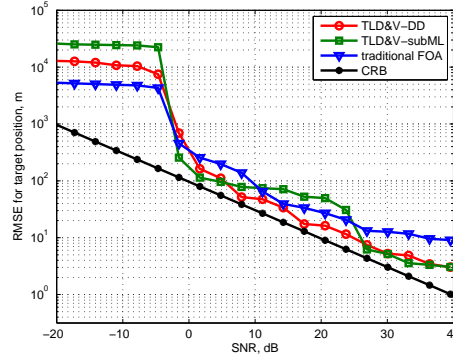
(b) For the target in case1, position2.



(c) For the target in case1, position3.



(d) For the target in case2.



(e) For the target in case3.

Figure 5.11: The target position estimation performances of the TLD&V and the traditional FOA methods for a target in different positions.

The proposed two methods (TLD&V-DD and TLD&V-subML methods) give similar performances compared to the traditional isodoppler curves based FOA method. Especially at high SNR values, their performances are better. Although, the proposed three methods have similar performances, the TLDF method is superior than the other methods because of its velocity estimation ability. The TLDF method can estimate the target velocity and the direction accu-

rately as independent from the target position estimation. But other methods require the target velocity vector to be known to estimate the position of the target.

Besides the target position estimation performances, the computational complexities of the proposed methods are important and it should be investigated. The complexity analysis is given in the next section.

5.4 Complexity Analysis

Actually the exact complexity analysis of the proposed methods are not easy because of the complex calculations. All of the proposed estimators and the traditional isodoppler based method, use the similar equations, hence the complexities are expected to be similar. The complexities of the TLDF, TLD&V-DD, TLDF&V-subML and the traditional FOA methods are almost $O(N_T N_R K^2)$. Here, N_T is the number of the transmitters, N_R is the number of the receivers and K is the number of search (grid) points in one dimension. Because of the matrix inversion involved in computations, the complexity of the TLDF method is expected as higher than the TLD&V methods. Similarly, because of the searching algorithm used for minimum value calculations, the isodoppler curves based traditional FOA has the highest computational complexity.

In the following table, the computation times for each estimator can be seen. The computation times are measured in MATLAB by using a laptop which has intel pentium M750 1.86 GHz processor and 2GB memory. These simulations are run 10 times and K is 20.

Table 5.2: Computation times for 10 trials (second)

	2 × 2 MIMO radar	2 × 3 MIMO radar	3 × 3 MIMO radar
TLD&V-DD	0.0170	0.0203	0.0265
TLD&V-subML	0.0196	0.0229	0.0295
TLDF	0.0217	0.0320	0.0404
Traditional FOA	0.0440	0.0754	0.1135

It is seen that, the traditional FOA method has the highest computational complexity and nearly requires twice time than the TLDF method in 2 × 2 MIMO radar case and requires

three times more time in the 3×3 MIMO radar case.

Actually computational time of the traditional method is more than given in the table above. Because, in these simulations, the target velocity is assumed to be known, hence for the traditional method, isodops are calculated for the given "exact" target velocity. But in real world, the target velocity is not known. Therefore, this simulations have to be repeated for different velocity values, and this increases the computation time of the traditional FOA method (similarly for TLD&V methods).

5.5 Comparison with Pulsed Radar

Pulsed radars can measure the target range by using the propagation times of the transmitted pulses. On the other hand, a simple CW radar can not measure the target range because of the continuous transmission of the wave. But, CW radar can measure the target radial velocity accurately whereas it is not possible for a simple pulsed radar. Actually, pulsed radars and CW radars can both measure the target range and the target radial velocity via some modifications.

Assume Δt represents the time delay between the transmitted and the received pulses and it takes a pulse travel to the two-way path between the radar and the target

$$R = \frac{c\Delta t}{2} \quad (5.4)$$

where c is denoted as the speed of the light. In general, a pulsed radar transmits and receives a train of pulses, as illustrated in Figure 5.12.

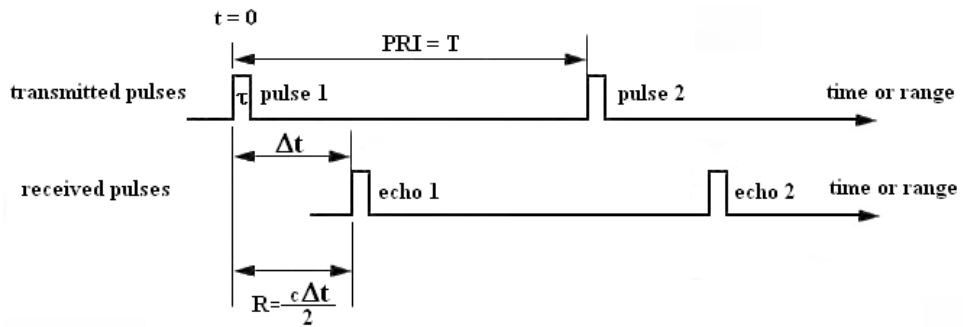


Figure 5.12: Range measurement by using pulses (from [59]).

Range resolution is defined as the ability to detect the close targets as distinct objects only by

measuring of their ranges, and it can be given as

$$\Delta R = \frac{c\tau}{2} = \frac{c}{2B} \quad (5.5)$$

where τ is the pulse width and B is the (without pulse compression) pulse bandwidth which is usually set to $B = 1/\tau$.

In general, radar users and designers alike seek to minimize ΔR in order to enhance the radar performance. As suggested by equation (5.5), in order to achieve fine range resolution one must minimize the pulse width or maximize the pulse bandwidth.

On the other hand, as represented in Figure 5.12, during each Pulse Repetition Interval (PRI) the radar radiates energy only for the pulse duration (τ seconds) and listens for target returns for the rest of PRI (T seconds). Let, P_{av} , P_t and E_p represents the average transmitted power, peak transmitted power and the pulse energy respectively. Than,

$$P_{av} = P_t \left(\frac{\tau}{T} \right) \quad (5.6)$$

$$E_p = P_t \tau = P_{av} T \quad (5.7)$$

In [60], Skolnik, showed that the theoretical rms error in measuring the two-way time delay ($\Delta t = cR/c$), taken by a radar signal in traveling at a velocity c from the radar to target at a range R and back, has been shown to be,

$$\delta_t = \frac{1}{\beta(2E/N_0)^{1/2}} \quad (5.8)$$

where E is the energy contained in the echo signal at the radar, N_0 is the noise power per cycle of the receiver bandwidth with which the signal must compete, and β is defined by the following

$$\beta^2 = \frac{(2\pi)^2 \int_{-\infty}^{\infty} f^2 |S(f)|^2 df}{\int_{-\infty}^{\infty} |S(f)|^2 df} \quad (5.9)$$

The parameter β is the 2π times the rms deviation of the energy spectrum with respect to zero frequency [60]. By using the equation (5.8), the rms range error, δR can be calculated as

$$\delta R = \frac{c}{2} \delta_t \quad (5.10)$$

and in the same work of Skolnik, for a rectangular pulse, δt and δR calculated as

$$\delta t = \left(\frac{\tau}{4BE/N_0} \right)^{1/2} \quad (5.11)$$

$$\delta R = \frac{c}{2} \delta t = \frac{c}{2} \left(\frac{\tau}{4BE/N_0} \right)^{1/2} \quad (5.12)$$

5.6 Why Pulse Compression?

As explained in the previous section, pulsed radar emits a wave in a short time duration, and then wait long time. Hence, for long range measurements, the peak power of the transmitter must be increased to increase average transmitted power, or pulse duration must be increased with the cost of range resolution decreases.

It seems that the only way to account for these problems and have good range resolution is increasing the peak transmitted power, whereas there are technical limitations for the maximum peak power, such as maximum high voltage or power from the output stage, or waveguide breakdown. So, the only approach for achieving fine range resolution while maintaining adequate average transmitted power is using pulse compression techniques [59]. In Figure 5.13, the pulse powers can be seen with and without pulse compression. After pulse compression, energy content of long-duration, low-power pulse will be comparable to that of the short-duration, high-power pulse.

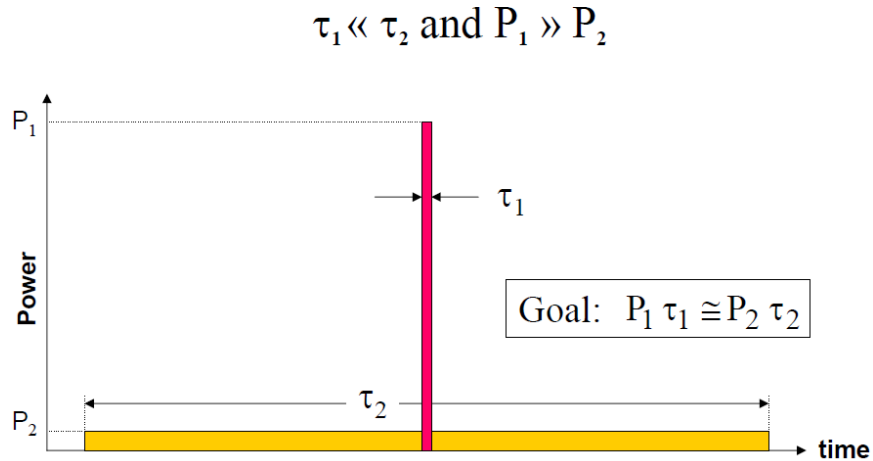


Figure 5.13: Signal powers with and without pulse compression.

5.6.1 Pulse Compression

Pulse compression allows radar to use long waveforms in order to obtain high energy and simultaneously achieve the resolution of a short pulse by internal modulation of the long pulse. This technique can increase the signal bandwidth through frequency or phase coding. Although, amplitude modulation is not forbidden but usually is not used [59]. The received echo is processed in the receiver matched filter to produce a short pulse with duration $1/B$, where B is the bandwidth of the compressed pulse. This technique is of interest when the radar is not able to generate enough required power. So, a concise summary for pulse compression is gathering two opposite benefits "High Range Resolution" and "high detection probability" concurrently. It can be stated that "radar pulse compression" is a substitute for "short pulse radar", although, each one has its own advantages and difficulties [6]. Furthermore, pulse compression has obviated limitation in average transmitted power belonging to short pulse. In the other hand, it has two disadvantages:

- Increased complexity for generating, transmitting and processing which cause more expense.
- Appearing sidelobs in compressed pulse which result in decreased range resolution.

Good and bad effects of the pulse compression can be seen in Figure 5.14 [59].

Consider two targets which can receive and reflect radar pulse. If these two reflected pulses are narrow enough, they will be separated; **A**-pulse and **B**-pulse are indicated reflected pulse from target **A** and **B** respectively (Figure 5.14-I). But, if these pulses are wide, they may overlap and may not be separable (Figure 5.14-II). If these wide pulses are passed through compression filter, two narrow pulses will be generated which can be distinguished easily (Figure 5.14-III). This is an efficacy of pulse compression but, one must tolerate a bad effect along with this advantage which is appearing extra pulses around the main one at the output of compression filter (Figure 5.14-III). This is obvious that if these side pulses have large amplitude, the radar will mistake.

Another parameter needed to introduce is pulse compression ratio which is defined as

$$\text{Pulse compression ratio} = \frac{\text{uncompressed pulse width}}{\text{compressed pulse width}} \quad (5.13)$$

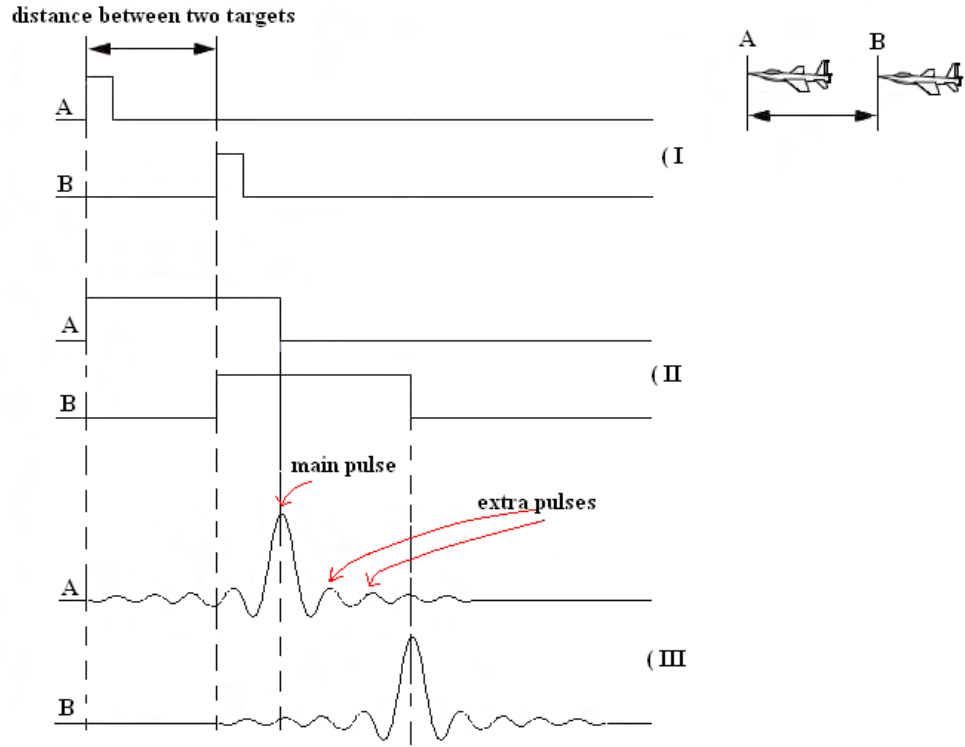


Figure 5.14: Resolving targets in range (I) two resolved targets by short-pulse (II) two unresolved targets by long-pulse (III) two resolved targets by using pulse compression with long-pulse (figure from [59])

and can be stated as follows

$$\text{Pulse compression ratio} = B\tau \quad (5.14)$$

In equation (5.14), B and τ are denoted as the pulse bandwidth and compressed pulse width and usually $B\tau \gg 1$.

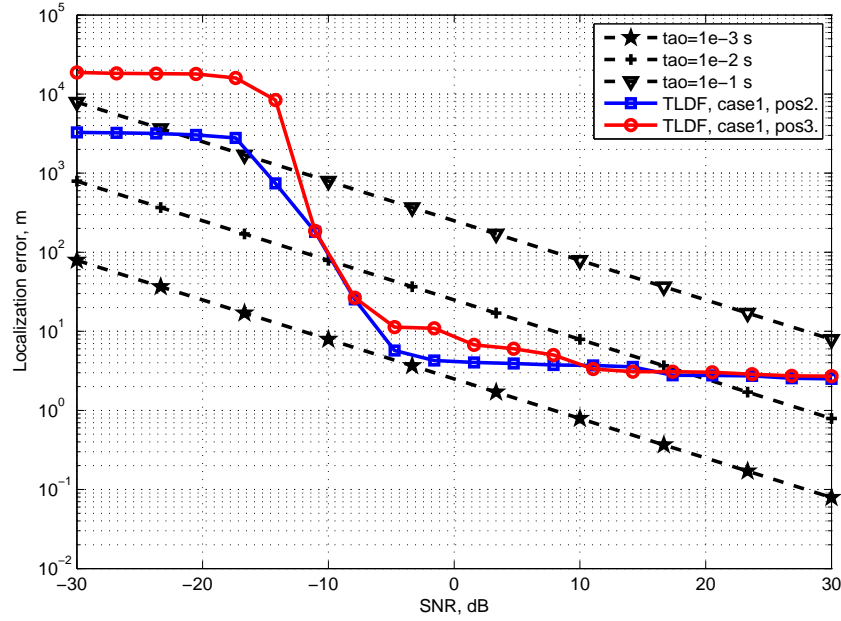


Figure 5.15: Comparison of the TLDF method localization performance with pulsed radar RMS range errors with pulse compression (pulse comparison ratio=1e+4).

In Figure 5.15, it can be observed that to obtain a similar performance to the MIMO radar the pulsed radar must be very complex with short pulse length, large pulse compression ratio, and complicated signal processing. Therefore, using the frequency-only MIMO radar, an effective performance is achievable with simpler and lower cost radar units than the monostatic pulsed radars with the same power budget.

Although the frequency-based MIMO radar and the pulsed radar have the the same average transmit power, the peak power of the frequency-based MIMO radar is less than the peak power of the pulsed radar. Therefore, simple electronics and power amplifiers can be used in the the frequency-based MIMO radar safely whereas pulsed radar requires sophisticated electronic designs.

CHAPTER 6

TARGET LOCALIZATION FOR MULTIPLE TARGETS

Previous chapters have dealt with a single target localization problem. However, when multiple targets exist the TLDF method has to be extended to localize each target. This requires a data association problem to be solved. In this chapter, the target localization problem will be investigated for the multiple targets case.

6.1 Doppler and Velocity Resolutions

Frequency-Only MIMO radar system only uses the Doppler frequencies to localize the targets. Therefore, for the multiple targets case, the Doppler resolution of the system will be an important parameter. The Doppler resolution of the system can be calculated as follows

$$\Delta_f = \frac{1}{T_{obs}} \quad (6.1)$$

where Δ_f and T_{obs} show the Doppler resolution and the observation time respectively. When two Doppler frequencies exist like f_{d1} and f_{d2} , then these Doppler frequencies can be resolved if $|f_{d1} - f_{d2}| > \Delta_f$. After two distinct Doppler frequencies are resolved, it can be used to find the positions of two different targets.

As can be seen from equation (6.1), to obtain better Doppler resolution, the observation time should be increased. On the other hand, when the observation time is increased, another important problem for the CW radars arises which can be called as position ambiguity.

Target will change its position on observation time, hence after waiting as T_{obs} , the estimated position of the target will be with some error because of the continuing target motion. This

error can be called as Position Ambiguity and it depends on the observation time and target velocity as

$$P_{amb} = V_{max} * T_{obs} \quad (6.2)$$

where V_{max} is the maximum velocity of the target and P_{amb} is the maximum position ambiguity for that system. If the $V_{max} = 900 \text{ kmph} = 250 \text{ mps}$ and $T_{obs} = 10 \text{ msec}$ then the maximum position ambiguity of this system can be calculated as $P_{amb} = 2.5 \text{ m}$.

As it can be seen from equation (6.2) $P_{amb} \sim (V_{max}, T_{obs})$. Hence, for the less Position ambiguity, short observation time should be used. But in this case, the Doppler resolution will decrease. Therefore, the observation time should be chosen carefully.

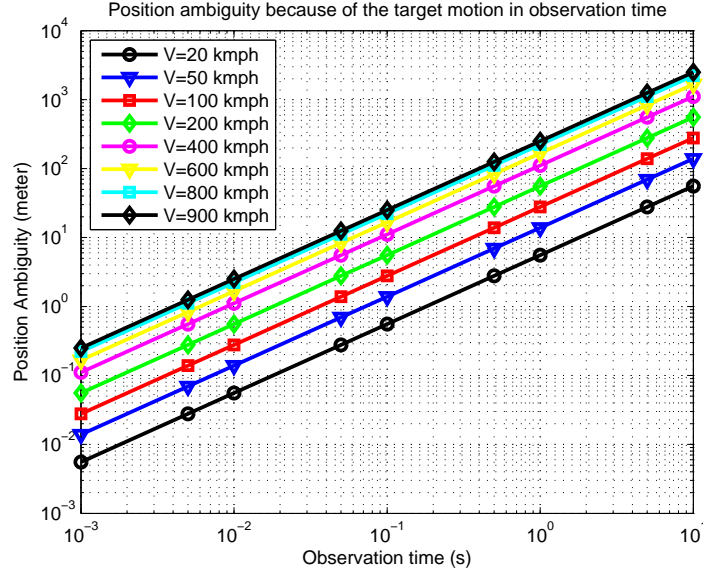


Figure 6.1: Position ambiguities in observation time for different target velocities.

The another important definition is the velocity resolution and it defines the minimum absolute difference of two target velocity to resolve both targets. It is defined as

$$\Delta_V = \frac{\Delta_f C}{2f} \quad (6.3)$$

$$= \frac{C}{2f T_{obs}} \quad (6.4)$$

$$= \frac{\lambda}{2T_{obs}} \quad (6.5)$$

where Δ_V is the velocity resolution, Δ_f is the Doppler resolution, C is the speed of light, f is the carrier frequency, λ is the wavelength and T_{obs} is the observation time. In the following figure, the Doppler and the velocity resolutions can be seen with respect to the observation time and for different carrier frequencies.

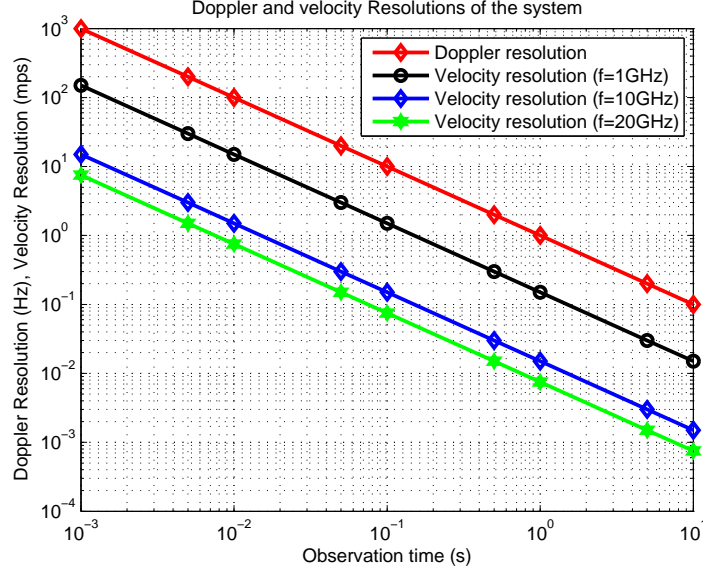


Figure 6.2: Doppler and velocity resolutions with respect to the observation time.

6.2 Data Association

For the multiple targets case, the most important problem is associating the received signals to the correct targets. This is called as "Data Association" and it is important problem especially for target tracking and for all multiple targets applications. In [61], it is defined as "Data association is the decision process of linking measurements (from successive scans) deemed to be of a common origin (i.e., a target or false alarm) such that each measurement is associated with at most one origin."

In the problem given here, only the Doppler frequencies from the moving targets exist, and these Doppler frequencies must be associated with the correct targets. Assume two targets are moving in the geometry given in Figure 6.3.

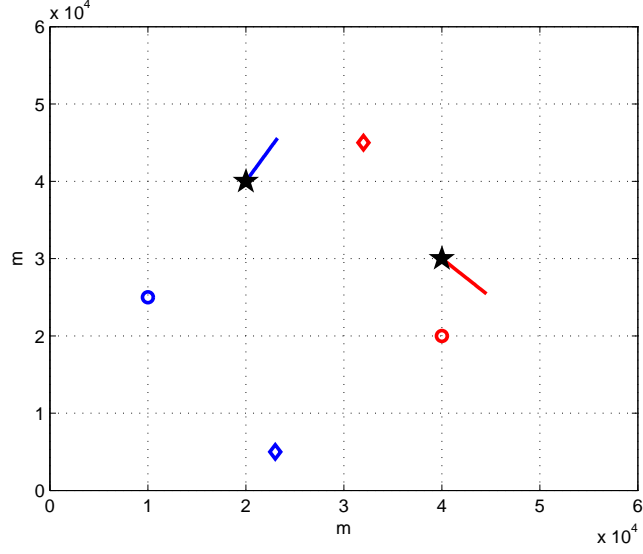


Figure 6.3: The sytem geometry for multitarget case.

In the geometry given in 6.3, there exist 2 transmitters and 2 receivers totally and 2 targets exist. The targets are located at the positions shown in the figure with the velocities of $V_1 = V_2 = 800kmph$ and with the angels of $\pi/3$ and $-\pi/4$ respectively. For this setup, the Doppler frequencies can be seen in the table 6.1.

Table 6.1: Doppler frequencies for both target

	$f_{d_{11}}$	$f_{d_{12}}$	$f_{d_{21}}$	$f_{d_{22}}$
Target1	13467.32	8232.22	1505.94	4088.002
	13475.1	8268.01	1529.7	4035.799
Target2	2919.45	6822.559	11391.9	1904.1
	2963.61	6752.582	11413.9	1951.18

In the table (6.1), $f_{d_{ij}}$'s show the Doppler frequencies with respect to the i^{th} receiver and j^{th} transmitter. For the target1 and target2, the first row shows the Doppler frequencies at that time, and the second row shows the Doppler frequencies at the previous position (0.5 seconds before).

As can be seen from the table (6.1), when data association problem is solved, the frequency tracking can be solved easily. But, first of all, the data association problem must be solved.

Four received frequencies exist for 2x2 MIMO radar case and for each of the targets. If two targets exist, then the total number of eight Doppler frequencies are obtained. These frequencies must be associated with the correct targets carefully.

Because of the frequency separation of the transmitters, the receivers know which signals radiated from which transmitters. For instance, for the configuration above, receiver 1 knows the Doppler frequencies, 13467.32 Hz and 2919.45 Hz, are result of the radiation from the transmitter 1, and similarly the Doppler frequencies, 8232.22 Hz and 6822.559 Hz, are result of the radiation from the transmitter 2. Therefore, the data association problem is reduced to the association of the Doppler frequencies from the same transmitters for each receiver.

At this point, the new advantage of the MIMO configuration appears. By using the Doppler frequencies which are arising from the same transmitter, the total number of targets can be determined easily. Some frequencies are not be able to resolved at some receivers but, because of the MIMO configuration, at some receivers all Doppler frequencies can be resolved. Hence, the total number of targets can be determined at the fusion center easily.

Let's label the estimated Doppler frequencies as f_{klm} which is the Doppler frequency of the signal which is transmitted by the m^{th} transmitter, and received by the l^{th} receiver after scattered by the k^{th} target. For two targets case, and 2x2 MIMO radar, these frequencies can be seen in the table 6.2.

Table 6.2: Possible Doppler frequencies for two targets and 2x2 MIMO radar

	Rec1, Tr1	Rec1, Tr2	Rec2, Tr1	Rec2, Tr2
Target1	f_{111}	f_{112}	f_{121}	f_{122}
Target2	f_{211}	f_{212}	f_{221}	f_{222}

As explained before, fusion center knows that we have 2 targets and because of the 2x2 structure, for each target 4 Doppler frequencies must be associated to the correct targets. By choosing randomly as f_{111} from the target 1 and f_{211} from the target 2, the all possible associated groups can be written as follows

Group 1: For target1 $\Rightarrow (f_{111}, f_{112}, f_{121}, f_{122})$ and For target2 $\Rightarrow (f_{211}, f_{212}, f_{221}, f_{222})$

Group 2: For target1 $\Rightarrow (f_{111}, f_{112}, f_{121}, f_{222})$ and For target2 $\Rightarrow (f_{211}, f_{212}, f_{221}, f_{122})$

Group 3: For target1 $\Rightarrow (f_{111}, f_{112}, f_{221}, f_{122})$ and For target2 $\Rightarrow (f_{211}, f_{212}, f_{121}, f_{222})$

Group 4: For target1 $\Rightarrow (f_{111}, f_{112}, f_{221}, f_{222})$ and For target2 $\Rightarrow (f_{211}, f_{212}, f_{121}, f_{122})$

Group 5: For target1 $\Rightarrow (f_{111}, f_{212}, f_{121}, f_{122})$ and For target2 $\Rightarrow (f_{211}, f_{112}, f_{221}, f_{222})$

Group 6: For target1 $\Rightarrow (f_{111}, f_{212}, f_{121}, f_{222})$ and For target2 $\Rightarrow (f_{211}, f_{112}, f_{221}, f_{122})$

Group 7: For target1 $\Rightarrow (f_{111}, f_{212}, f_{221}, f_{122})$ and For target2 $\Rightarrow (f_{211}, f_{112}, f_{121}, f_{222})$

Group 8: For target1 $\Rightarrow (f_{111}, f_{212}, f_{221}, f_{222})$ and For target2 $\Rightarrow (f_{211}, f_{112}, f_{121}, f_{122})$

Now, the problem is reduced to choose the correct group from the all possible groups. In the above groups, the Group 1 represents the correct association, and the other ones are associations with error.

To choose the correct association group, the target localization algorithms which are proposed in the previous sections can be used efficiently. Because of the velocity estimation ability, we will focus on the TLDF method. The procedure can be given as

- For only one radar scan, form all possible association groups,
- Choose a group by using the estimated Doppler frequencies,
- Calculate the positions and velocities of the targets for each groups by using the TLDF method (or estimate velocity by using the TLDF method, and target position with TLD&V-DD or TLD&V-subML methods),
- For next scan, by using the new estimated Doppler frequencies, calculate the new positions and the velocities of the targets for each groups,
- By using the consecutive position and velocity estimations, delete some impossible groups,
- Repeat the above steps with next scans up to one group exists.

6.2.1 Choosing Correct Association

The positions and the velocities of the targets for all possible cases can be found from the estimated frequencies as explained in the previous chapters. Then, by using these estimated target locations and the velocities, data association can be achieved. Critical step is detecting and deleting the impossible groups and decreasing the number of the living groups without deleting the correct one. For consecutive scans, by using estimated target position and the velocity estimations, the target position can be predicted for the next scan. Then, by comparing the predicted and the estimated target positions, impossible motions, and hence the impossible groups can be detected.

The procedure can be summarized as

- We have two consecutive radar scans. Target position and the velocity estimations for that scans exist for each group,
- For the analyzed group, $(\hat{\mathbf{t}}_{1p}$ and $\hat{\mathbf{v}}_{1p}$) and $(\hat{\mathbf{t}}_{2p}$ and $\hat{\mathbf{v}}_{2p}$) represent the estimations of the position and velocity vectors for target1 and target2 respectively for the previous measurement.
- Similarly $(\hat{\mathbf{t}}_1$ and $\hat{\mathbf{v}}_1)$ and $(\hat{\mathbf{t}}_2$ and $\hat{\mathbf{v}}_2)$ for the next measurement (see Figure 6.4).
- Calculate the average target velocity as;

$$\hat{\mathbf{v}}_{1avg} = \frac{\hat{\mathbf{v}}_1 + \hat{\mathbf{v}}_{1p}}{2} \text{ and } \hat{\mathbf{v}}_{2avg} = \frac{\hat{\mathbf{v}}_2 + \hat{\mathbf{v}}_{2p}}{2}$$
- Delete this group iff;

$$\frac{1}{2}|\hat{\mathbf{v}}_{1avg}|_2 > |\hat{\mathbf{t}}_1 - \hat{\mathbf{t}}_{1p}|_2 > 2|\hat{\mathbf{v}}_{1avg}|_2 \text{ and } \frac{1}{2}|\hat{\mathbf{v}}_{2avg}|_2 > |\hat{\mathbf{t}}_2 - \hat{\mathbf{t}}_{2p}|_2 > 2|\hat{\mathbf{v}}_{2avg}|_2$$
- Repeat it for each group,
- Repeat the procedure above for the next scans, upto one group exists.

Motion of the target and the position and the velocity estimations at consecutive scans can be seen in Figure 6.4 for only one target. Similar vectors can be defined for other target/targets.

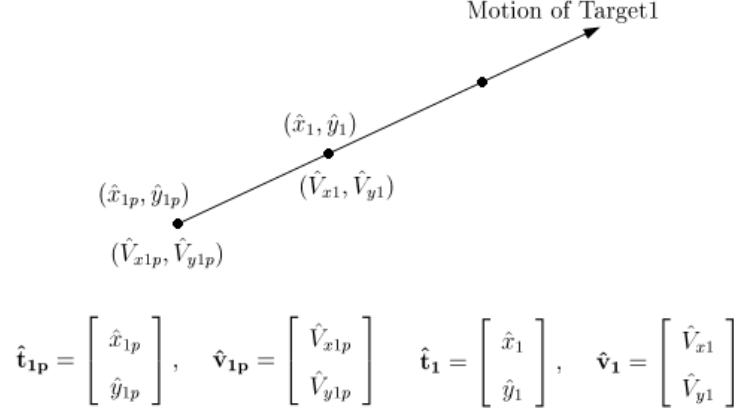


Figure 6.4: Motion of the target 1.

6.3 Simulations

Now, the data association performance is simulated using the TLDF method. Actually, the other proposed methods can be used similarly, but in that cases, the target velocity must be estimated as well. The 2x2 MIMO radar structure will be used for simulations and 2 and 3 targets with different locations and directions will be simulated. For the 2 targets case, the first target is assumed at (20km,40km) position with $V = 800$ kmph and $\theta = \pi/3$ and the second target is investigated at 4 different locations and directions which are

Case1 : [(40km, 30km), $\theta = -\pi/4$, $V = 800$ kmph]

Case2 : [(10km, 50km), $\theta = \pi/3$, $V = 800$ kmph]

Case3 : [(20km, 39.5km), $\theta = -\pi/4$, $V = 800$ kmph]

Case4 : [(20km, 39.5km), $\theta = \pi/3$, $V = 800$ kmph]

For all cases, both targets are moving linearly and the targets are illuminated every second by radars. As we have 2x2 MIMO radar and 2 targets, for each case total of 8 possible association exists. These possible associations can be seen in the following figures for each cases. In these simulations the exact Doppler frequencies are used.

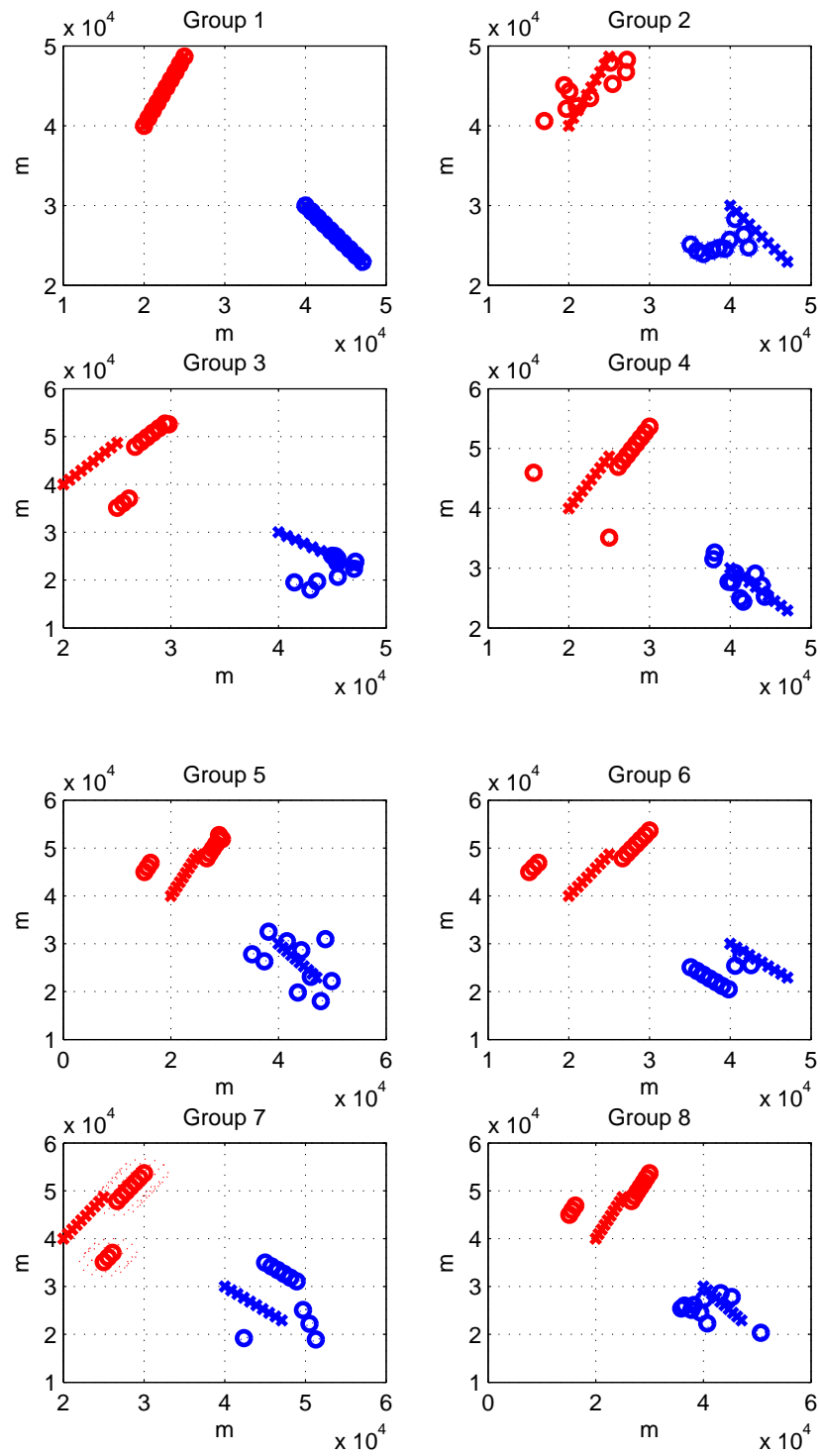


Figure 6.5: All possible groups for data association problem, 2 targets, Case1.

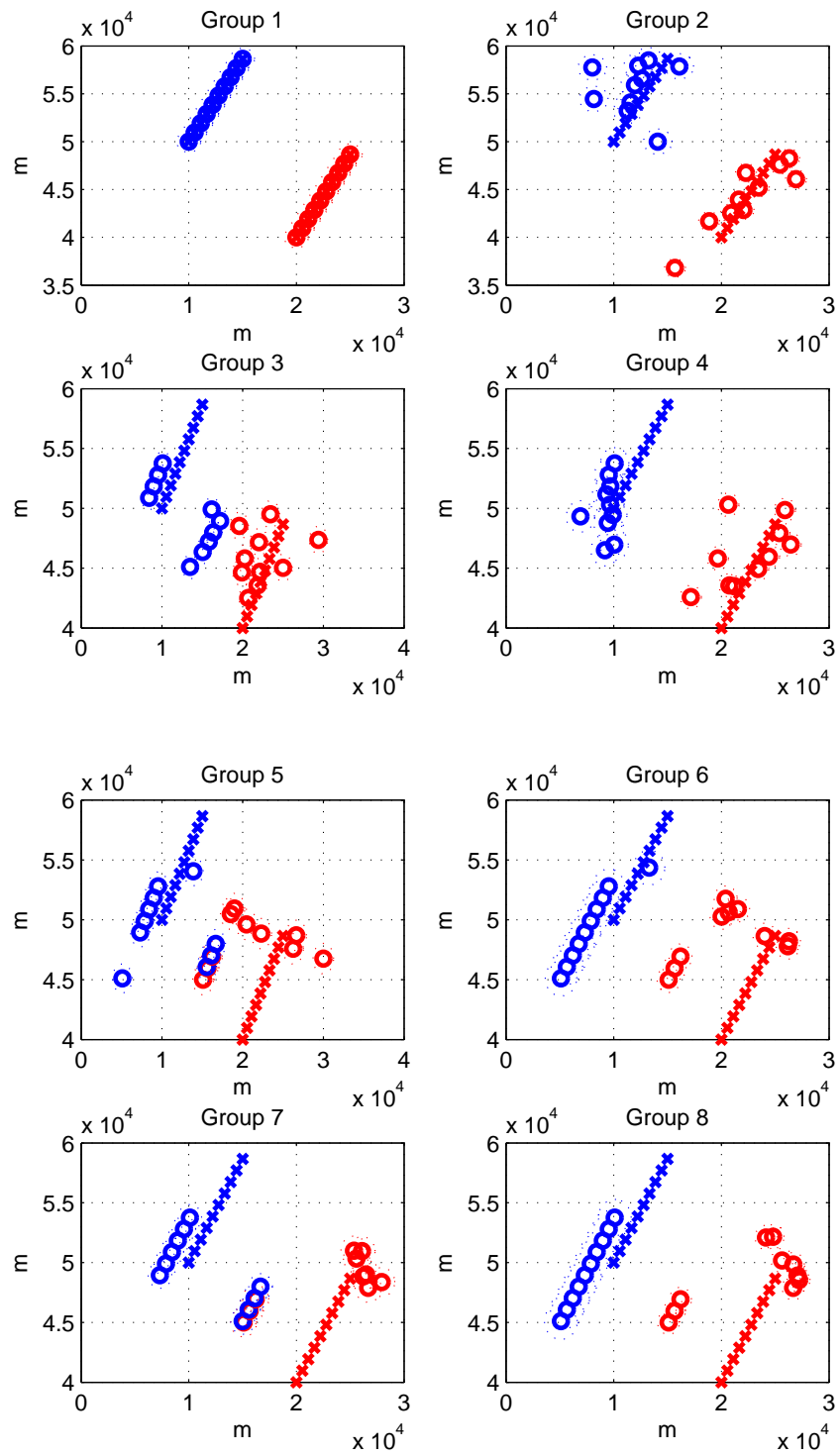


Figure 6.6: All possible groups for data association problem, 2 targets, Case2.

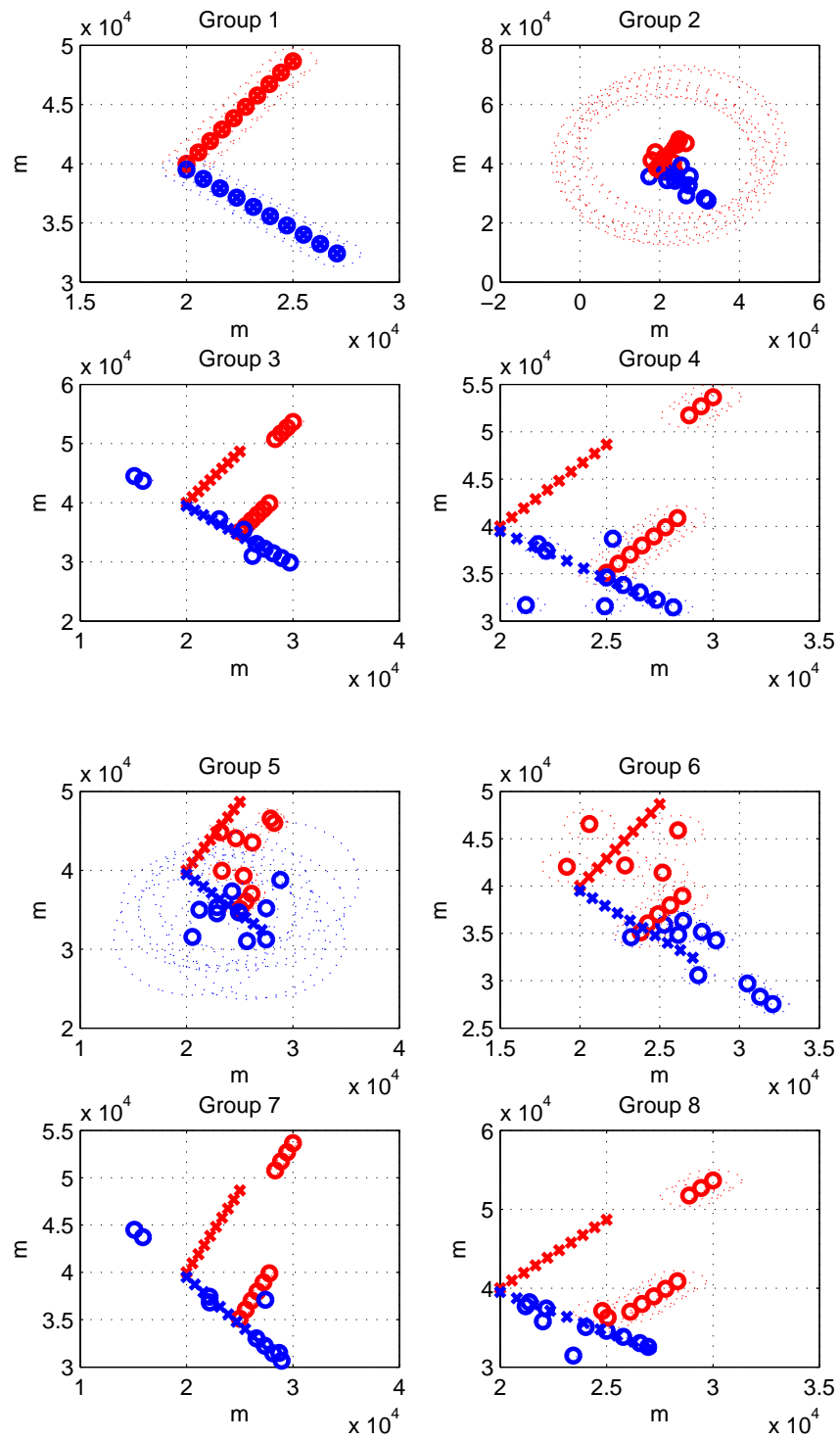


Figure 6.7: All possible groups for data association problem, 2 targets, Case3.

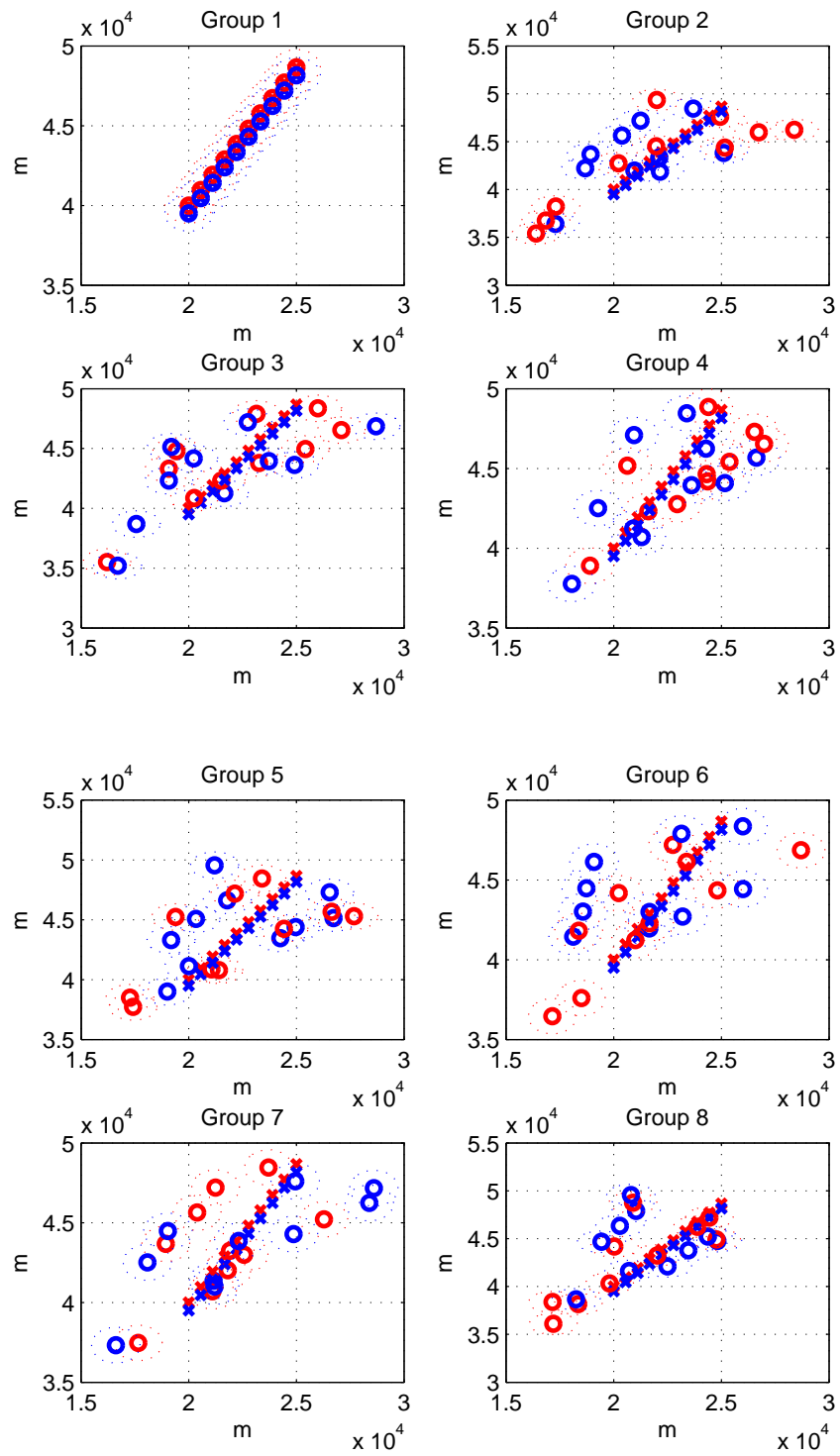


Figure 6.8: All possible groups for data association problem, 2 targets, Case4.

As can be seen from the results of 2 targets case, only for the correct association case is valid and the other association groups can be eliminated easily. Hence, the data association is achieved perfectly and both targets can be resolved using the proposed procedure.

For the 3 targets case, the targets are assumed as maneuvering. The 6 different motion models for three targets can be seen in the following figures.

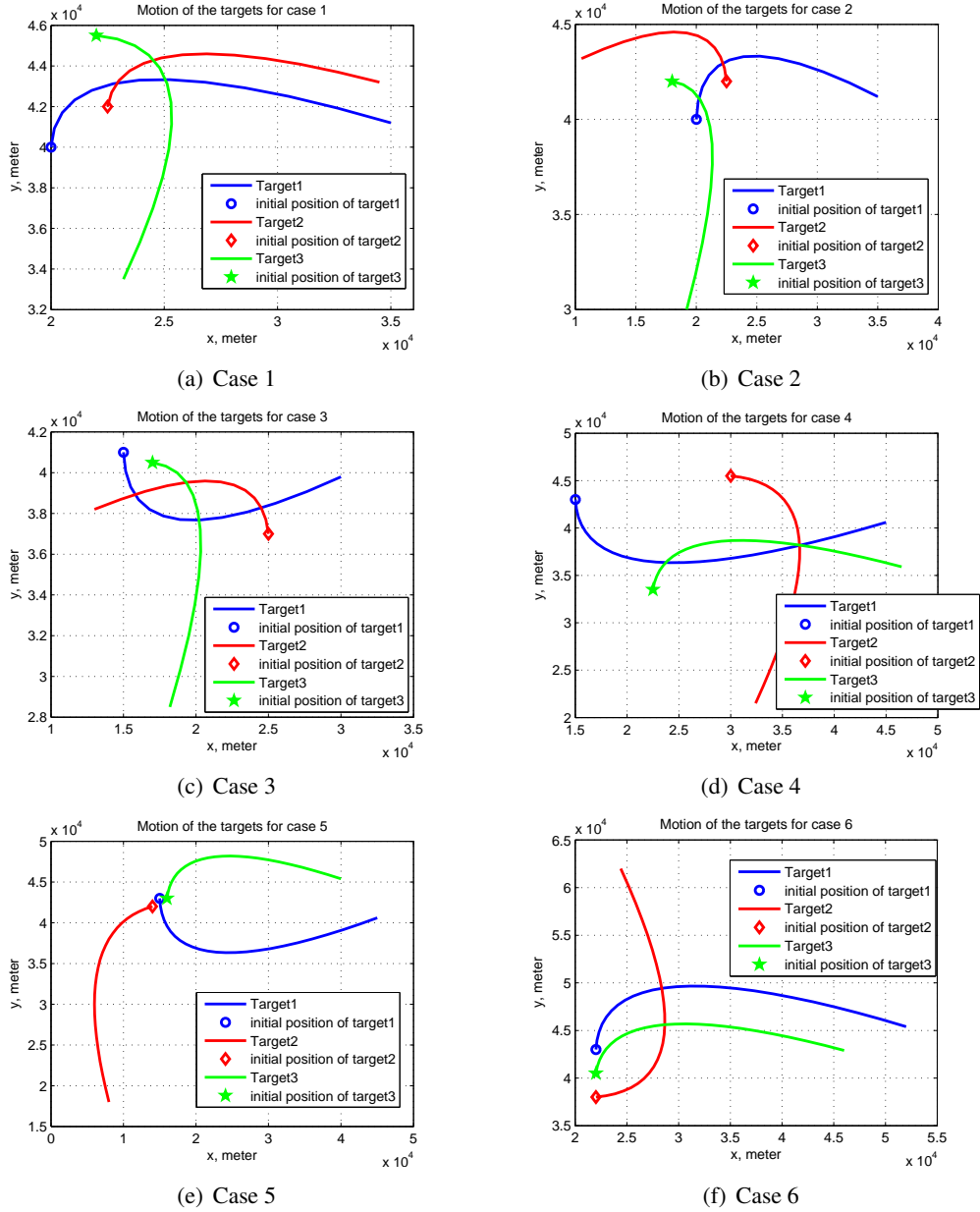


Figure 6.9: Target motion scenarios for data association problem for 3 targets.

For these cases the results are summarized in the following table.

Table 6.3: Data association results for 3 targets and for different cases.

		Case1	Case2	Case3	Case4	Case5	Case6
Target 1	OK	✓	✓	✓	✓	✓	✓
	η	11	9	11	6	13	6
	lp	1	1	1	1	1	1
Target 2	OK	✓	✓	✓	✓	×	✓
	η	8	12	13	13	—	8
	lp	1	1	1	1	4	1
Target 3	OK	✓	✓	✓	✓	✓	✓
	η	7	8	13	5	10	9
	lp	1	1	1	1	1	1

In the Table 6.3, the correctly associated frequencies for the targets are shown by using ✓ symbol. Similarly the iteration (or scan) number is represented by " η " symbol, and finally the number of live paths after each iteration is represented by 'lp' notation. For these simulations the targets are tracked for only 13 illuminations which are 3 seconds apart.

As can be seen from Table 6.3, for five cases, the Doppler frequencies can be associated with the three targets correctly. Only for the fifth case, the data association procedure can not be ended up in 13 iterations. To end up the data association, the next scans can be waited. Or as in this case, if other 2 targets is associated correctly, then the leaving frequencies can be associated directly with the second target.

As a result, the proposed data association algorithm can be used efficiently by using the TLDF method. As it is shown in the simulations, the proposed method works not only for the linearly moving targets but also for the maneuvering targets. Hence, it is independent from the target motion kinematics, hence it can be used for target tracking easily.

The proposed data association algorithm requires the estimations of the target position and the target velocity. Data association directly from the Doppler frequencies is a complex problem and it is the future work for this dissertation.

When false detection exist then the proposed data association method should be modified. Actually, because of the location diversity in MIMO configurations, the detection of the false alarms are simple. Using the estimated target direction, velocity and the position the false

detections can be detected because the false detections will give different Doppler frequencies for each scan and for each receiver. Moreover, using the received power of the each received signal a threshold can be defined to eliminate the false detections. As a result, a control structure have to be added to check all localized targets whether they exist or not.

CHAPTER 7

CONCLUSION

In this dissertation, new target localization and the target velocity estimation methods are proposed for the frequency-only MIMO radars with widely separated antennas. These methods all depend on the estimated frequencies of the received signals. The proposed three methods can be divided two with respect to the used informations to localize the target. The first method uses only the Doppler frequencies and hence it is called as "Target Localization via Doppler Frequencies - **TLDF**". The other estimators use the target velocity besides the Doppler frequencies, hence this group is called as "Target Localization via Doppler Frequencies and Target Velocity - **TLD&V**".

The TLDF method is purely new method for target localization for the frequency-only MIMO radars. The TLDF method does not require extra information besides the received frequencies and the Doppler frequencies. This method can estimate the target velocity with the target position. Target velocity can be estimated via TLDF successfully. Not only the magnitude of the velocity vector, but also the direction of the target in two dimensional space can be estimated with TLDF method.

As the frequency based methods includes highly nonlinear equations, these methods are not preferable to the traditional time based methods for the target localization. However, by combining the TLDF method with grid search, such cost functions can be solved easily and with low complexity.

TLD&V methods can be divided two. The first TLD&V method is an expansion of a passive localization method proposed for the passive sonar applications. This idea is applied to the active MIMO radar case for target localization. The method is based on the derivatives of the

received frequencies, and hence it is called as "Derivated Doppler, **TLD&V-DD**" method for target localization. It is shown that, this method can also find the target position by using the Doppler frequencies and the target velocity. The Derivated Doppler method requires angle-of-arrival information (or target velocity) besides the frequency-of-arrival information and this is the main disadvantage of this method.

The second TLD&V method is called as **TLD&V-subML** method. This method uses the Maximum Likelihood (ML) principle for the target localization. The obtained ML equation is solved in a sub-optimum manner, hence the method becomes sub-ML solution of the problem (or ML with grid search). The target localization performance of the TLD&V-subML method is close to the TLDF method.

Actually, the TLDF method is superior than the TLD&V methods. Hence, one can ask "Why should the TLD&V methods be used instead of the TLDF method or Why are they proposed?". The answer is simple: We follow the evolution order in thesis. Firstly, the TLD&V methods have appeared, and then disadvantages of them are removed by developing the TLDF method. Hence, all methods are included in this dissertation to show the evolution process. On the other hand, if the target velocity exist, then the TLD&V methods can be preferable because of their lower computation time than the TLDF method.

For all three methods, after defining the cost functions, grid search is used for target localization. Hence, the target localization performance and the search time depend upon the grid size. As expected, reducing the grid size increases the search time whereas decreases the target localization errors. By using clever grid search strategies or another cost minimizing algorithms like steepest descent, system performance can be increased. But in this case, the selection of the initial position will be another problem. In this thesis, regular grid search with constant grid size and variable grid search is used together to reduce the search time and to increase the target localization performance.

For different MIMO radar structures, which are 2x2, 2x3 and 3x3 MIMO, the target localization performances of the proposed methods are compared. As it can be seen from the simulation results, increasing the number of the transmitters and/or the receivers increases the target localization performance as expected. The TLDF, TLD&V-DD and the TLD&V-subML methods can localize the target when the SNR is high. Their performances are similar, and especially the TLD&V-subML and the TLDF have superior target localization performances

compared to the traditional isodoppler curves based target localization method.

Although, the target position estimation performances of the proposed three methods are similar, the TLDF method is superior because of its target velocity estimation capability. By using the same cost function, the TLDF method can estimate the target velocity, as well. Moreover, this velocity estimation includes the target direction information besides the magnitude of the velocity in two dimensional space. The target velocity estimation performance of the TLDF method is good and both the speed and the direction of the target can be estimated accurately at high SNR levels.

Another contribution of this thesis is that, MIMO radar signal model is expanded as including the Doppler frequency shift and the target fluctuations. Swerling target fluctuation models are used to model these target fluctuations. Moreover, the CRB for the frequency-only MIMO radar is derived for both the target localization and the velocity estimation problems. It is shown that, when the time resolution of the arrival signals are not good or not enough, only frequency information of the received signals can be used for the target localization and for the target velocity estimation.

As can be seen from the simulation results, the CRB depends on the position of the target (and also the positions of the transmit and the receive sites), the observation interval (T_{obs}), and the number of the receive and the transmit sites. When the number of the radars is increased, bound decreases as expected. Similarly, when the observation interval is increased, the CRB decreases. It is also another expected result because, if we have more information about signals, the performances of the estimators can be improved. On the other hand, the computational complexity increases as dealing with the longer data stream. Hence, the observation time should be chosen properly. Very long observation time gives better result but computational load shouldn't be forgotten. If the observation time is chosen very small, then one period of the baseband signal couldn't be covered and the correct position of the target can not be estimated.

Therefore, while choosing the proper observation interval, T_{obs} , the possible target and the frequency informations can be used to restrict T_{obs} . This helps to choose proper observation time for localization process with minimum computational load. The Doppler resolutions and the position ambiguity are other restrictions on the selection of the observation time and can not be ignored for CW radars.

As can be shown via simulations, the target localization performances of the proposed methods do not effected from the target fluctuations because of the frequency-based nature. This is another advantage of the frequency based methods. As the target amplitude fluctuations do not effect the frequency estimation, the target localization estimaton performances do not effected, as well. Therefore, these methods are able to used efficiently when the target fluctuations exist.

At the last chapter, the target localalization performance of the TLDF method is investigated for the multiple targets case. A new data association method is proposed for the frequency/Doppler-only systems. It is shown that, by using the received frequencies only, moving targets can be separated and the data association can be achieved. In simulations, maneuvering targets are used and the target localization performance of the TLDF method is analyzed for both multiple targets and maneuvering targets. Hence, the proposed methods can be used efficiently for multi targets localization and not only for targets moving linearly but also for the maneuvering targets.

Performance of these localization methods depends highly on the performance of the frequency estimators. If the Doppler frequencies can be estimated accurately, the target localization error will be decreased. Therefore, the frequency estimations for MIMO radar is still an important problem, and it can be seen as a future work on the MIMO radar.

By using the continuous wave radars, many advantages of the continuous wave radars can be included to the MIMO radar system. First of all, CW radars are simpler and cheaper than the pulsed radars, hence the cost of the radar network with CW radars are less than the pulsed radars. Moreover, when the continuous signals are used, the Doppler frequency can be measured precisely and this makes the CW radars good choice for the frequency/Doppler based systems. Besides these advantages, CW radars require less transmit peak power than their pulsed radar counterparts. Because of the low peak power, CW radars have low probability of intercept (LPI) characteristic. Therefore, the positioning of the CW emitters are more difficult than the pulsed emitters and hence, CW radars can be used safely in critical locations. On the other hand, the observation time is an important parameter for CW radars. Because the target keeps going its motion on observation time, the observation time should be choosen as small as possible.

Actually, the proposed target localization and the velocity estimation methods can be applied

to the all frequency-only systems such as wireless sensor networks (WSN) or sonar. For example, these methods can be very advantageous especially for WSNs. For WSNs, size of the sensor and the power consumption are the most important problems. By using CW signals, sensor size can be reduced. Moreover, instead of transferring whole received data to the central sensor (fusion center), by using these methods, transferring only the Doppler frequencies are more efficient. Hence, this reduces the transmission load on the sensors and decreases the power consumption.

And finally, the possible research areas for the future can be summarized as following;

- Using modulated CW signals (FMCW) for target localization,
- Target tracking for frequency-only MIMO radar,
- Instead of grid searching, using clever cost minimizing algorithms,
- Application of these methods to the WSNs.
- Joint frequency estimation for frequency-only MIMO radar.
- Data association for multiple targets using only the Doppler frequencies.

REFERENCES

- [1] P. Z. Peebles, Jr., *Radar Principles*, John Wiley and Sons, 1998.
- [2] V. S. Chernyak, *Fundamentals of Multisite Radar Systems - Multistatic Radars and Multiradar Systems*, Gordon and Breach Science Publishers, 1998.
- [3] H. Godrich, A. M. Haimovich, and R. S. Blum, *Target Localization Techniques and Tools for MIMO Radar*, IET Radar, Sonar and Navigation Journal, vol.3, Issue 4, pp.314–327, August 2009.
- [4] A. M. Haimovich, R. S. Blum, and L. J. Cimini, Jr., *MIMO radar with widely separated antennas*, IEEE Signal Processing Magazine, January 2008.
- [5] J. Li, P. Stoica, *MIMO radar with collocated antennas*, IEEE Signal Processing Magazine, September 2007.
- [6] M. I. Skolnik, *Introduction to Radar Systems*, 3th ed. McGraw-Hill, 2001.
- [7] Y. T. Chan and F. L. Jardine, *Target localization and tracking from doppler-shift measurements*, IEEE Journal of Oceanic Eng., vol. 15, pp. 251–257, Jul. 1990.
- [8] Y. T. Chan and S. Rudnicki, *Bearings-only and Doppler-bearing tracking using instrumental variables*, IEEE Trans. on Aerosp. Electron. Syst., vol. 28, pp. 1076–1083, Oct. 1992.
- [9] Y. T. Chan and J. Towers, *Passive localization from Doppler shifted frequency measurements*, IEEE Trans. on Acoust., Speech, Signal Processing, vol. 2, pp. 1465–1468, Apr. 1991.
- [10] Y. T. Chan and J. Towers, *Sequential localization of a radiating source by Doppler-shifted frequency measurements*, IEEE Trans. on Aerosp. Electron. Syst., vol. 28, pp. 1084–1090, Oct. 1992.
- [11] E. Paolini, A. Giorgetti, M. Chiani, R. Minutolo and M. Montanari, *Localization Capability of Cooperative Anti-Intruder Radar Systems*, EURASIP Journal on Advances in Signal Processing, vol. 2008, Article ID 726854, 14 pages.
- [12] <http://mathworld.wolfram.com/CassiniOvals.html>
- [13] P. C. Chestnut, *Emitter Location Accuracy Using TDOA and Differential Doppler*, IEEE Trans. on Aerosp. Electron. Syst., vol. 18, pp. 214–218, March 1982.
- [14] E. Fishler, A. Haimovich, R. S. Blum, D. Chizhik, L. Cimini, , and R. Valenzuela, *MIMO Radar : An idea whose Time has come*, Proceedings of the IEEE Radar Conference, 2004., pp. 71–78.

- [15] E. Fishler, A. Haimovich, R. S. Blum, L. J. Cimini, D. Chizhik, and R. A. Valenzuela, *Spatial diversity in radars - models and detection performance*, IEEE Trans. on Signal Processing, vol. 54, pp. 823–838, Mar. 2006.
- [16] N. H. Lehmann, E. Fishler, A. Haimovich, R. S. Blum, D. Chizhik, L. J. Cimini, Jr., and R. A. Valenzuela, *Evaluation of Transmit Diversity in MIMO-radar Direction Finding*, IEEE Trans. on Signal Processing, vol. 55, pp. 2215–2225, 2007.
- [17] N. H. Lehmann, A. M. Haimovich, R. S. Blum and L. J. Cimini, *High Resolution Capabilities of MIMO Radar*, in Proc. of 40th Asilomar Conf. on Signals, systems and Computers, Nov. 2006.
- [18] I. Bekkerman and J. Tabrikian, *Target detection and localization using MIMO radars and sonars*, IEEE Trans. on Signal Processing, vol. 54, pp. 3873–3883, Oct. 2006.
- [19] L. Xu, J. Li, P. Stoica, *Target detection and parameter estimation for MIMO radar system*, IEEE Trans. on Aerosp. Electron. Syst., vol. 44, pp. 927–939, July 2008.
- [20] Q. He, and R. S. Blum, *Cramer-Rao Bound for MIMO Radar Target Localization With Phase Errors*, IEEE Signal Processing Letters, vol.17, No. 1, January 2010.
- [21] N. D. Tran, A. Renaux, R. Boyer, S. Marcos and P. Larzabal, *MIMO radar in the presence of modeling errors: A Cramer-Rao Bound investigation*, IEEE International Conference on Acoustics, Speech and Signal Processing (ICASSP), pp. 2780–2783, 2011.
- [22] H. Godrich, A. M. Haimovich, and R. S. Blum, *Target Localization Accuracy gain in MIMO radar-based systems*, IEEE Trans. on Information Theory, vol.56, no.6, pp.2783–2803, June 2010.
- [23] B. Armstrong and B. S. Holeman, *Target tracking with a network of doppler radars*, IEEE Trans. on Aerosp. Electron. Syst., vol. 34, pp. 33–47, Jan. 1998.
- [24] Y. C. Xiao, P. Wei and T. Yuan, *Doppler Frequency-Only and T^2/R Radar Based Moving Target Location*, CIE '06., International Conference on Radar, 16-19 October 2006.
- [25] S. Gogineni and A. Nehorai, *Target Tracking Using Monopulse MIMO Radar With Distributed Antennas*, 2010 IEEE Radar Conference, pp.194-199
- [26] C. Y. Chong, F. Pascal, J. P. Ovarlez and M. Lestirgue, *MIMO radar detection in non-gaussian and heterogeneous clutter*, IEEE Journal of Selected Topics in Signal Processing, vol.4, no.1, pp. 115–126, February 2010.
- [27] Y. Yang and R. S. Blum, *MIMO radar waveform design based on mutual information and minimum mean-square error estimation*, IEEE Trans. on Aerosp. Electron. Syst., vol. 43, pp. 330–343, Jan. 2007.
- [28] J. Zhang, B. Manjunath, B. Maalouli, A. P. Suppappola and D. Morrell, *Dynamic waveform design for target tracking using MIMO radar*, in Proc. of 42th Asilomar Conf. on Signals, systems and Computers, pp. 31–35, 2008.
- [29] L. Xu, J. Li, K. W. Forsythe and D. W. Bliss, *Waveform Optimization for MIMO Radar: A Cramer-Rao Bound Based Study*, IEEE International Conference on Acoustics, Speech and Signal Processing (ICASSP), vol.2 pp. II 917–II 920, 2007.

- [30] B. J. Donnet and I. D. Longstaff, *MIMO radar - Waveform and Optimization*, 4th EMRS DTC Technical Conference, Edinburgh, 2007.
- [31] G. San Antonio, D. R. Fuhrmann and F. C. Robey, *MIMO radar ambiguity functions*, IEEE Journal of Selected Topics in Signal Processing, vol.1, no.1, pp. 167–177, February 2007.
- [32] C. Chun-Yang and P. P. Vaidyanathan, *MIMO Radar Ambiguity Properties and Optimization Using Frequency-Hopping Waveforms*, IEEE Trans. on Signal Processing, vol. 56, pp. 5629–5936, Dec. 2008.
- [33] T. Strohmer and B. Friedlander, *Compressed sensing for MIMO radar - algorithms and performance*, in Proc. of 43th Asilomar Conf. on Signals, Systems and Computers, pp. 464–468, 2009.
- [34] A. Hassanien and S. A. Vorobyov, *Transmit/receive beamforming for MIMO radar with colocated antennas*, IEEE International Conference on Acoustics, Speech and Signal Processing (ICASSP), pp. 2089–2092, 2009.
- [35] L. Lo Monte, D. Erricolo, F. Soldovieri and M. C. Wicks, *Radio Frequency Tomography for Tunnel Detection*, IEEE Transactions on Geoscience and Remote Sensing, vol. 48 no.3, pp. 1128–1137, March 2010.
- [36] D. J. Sego, H. Griffiths, M. C. Wicks, *Waveform and aperture design for low-frequency RF tomography*, IET Radar Sonar and Navigation, vol. 5, pp. 686–696, March 2011.
- [37] D. Smardzija, O. Boric-Lubecke, A. Host-Madsen, V. M. Lubecke, T. Sizer, A. D. Droitcour and G. T. A. Kovacs, *Applications of MIMO techniques to sensing of cardiopulmonary activity*, IEEE/ACES International Conference on Wireless Communications and Applied Computational Electromagnetics, pp. 618–621, 2005.
- [38] A. Amar and A. J. Weiss, *Localization of Narrowband Radio Emitters Based on Doppler Frequency Shift*, IEEE Trans. on Signal Processing, vol. 56, no.11, pp. 5500–5508, Nov. 2006.
- [39] A. J. Weiss, *Direct Geolocation of Wideband Emitters Based on Delay and Doppler*, IEEE Trans. on Signal Processing, vol. 59, no.6, pp. 2513–2521, June 2011.
- [40] H. Godrich, A. M. Haimovich, and R. S. Blum, *Cramer Rao Bound on Target Localization Estimation in MIMO Radar Systems*, 42nd Annual Conference on Information Sciences and Systems, 2008. CISS 2008., pp. 134–139
- [41] L. Michael and L. L. Scharf, *A new subspace identification algorithm for high-resolution DOA estimation*, IEEE Trans. on Antennas and Propagation, vol.AP-34, pp.276–280, 1986.
- [42] A. J. Barabell, *Improving the resolution performance of the eigen-structure based direction finding algorithm*, IEEE International Conference on Acoustics, Speech and Signal Processing (ICASSP), pp. 336–339, 1983.
- [43] P. Swerling, *Probability of Detection for Fluctuating Targets*, IRE Trans. IT-6, pp.269–308, April 1960.
- [44] M. A. Richards, *Fundamentals of Radar Signal Processing*, McGraw-Hill, New-York 2005. pp.134–139, March 2008.

- [45] A. Papoulis and S. U. Pillai, *Probability, Random Variables and Stochastic Processes*, 4th ed., McGraw-Hill, New-York 2002
- [46] J. E. Gentle, *Random Number Generation and Monte Carlo Methods*, 2nd ed., Springer, New-York 2003.
- [47] <http://en.wikipedia.org/wiki/X-band>
- [48] *Northrop Grumman Radar Notes*, prepared by Northrop Grumman Electronic Systems Baltimore, Maryland, 2nd ed., May. 2011.
- [49] S. M. Kay, *Fundamentals of Statistical Signal Processing: Estimation Theory*, vol. 1, New Jersey : Prentice Hall PTR, 1st ed., 1993.
- [50] D. J. Torrieri, *Statistical Theory of Passive Location System*, IEEE Trans. on Aerospace and Electronic Systems, vol.AES-20, No. 2, pp. 183–198, March 1984.
- [51] S. Stein, *Differential delay/Doppler ML Estimation with Unknown Signals*, IEEE Trans. Signal Processing, vol.41, pp. 2717–2719, August 1993.
- [52] M.H. Hayes, *Statistical Digital Signal Processing and Modeling*, John Wiley and Sons, Inc., 1996.
- [53] Y. Kalkan, B. Baykal, *Target Localization Methods for Frequency-Only MIMO Radar*, European Radar Conference, 2010. EURAD2010, pp.396–399, 30 Sept.-1 Oct. 2010, Paris, France.
- [54] Y. Kalkan, B. Baykal, *MIMO Radar Target Localization by Using Doppler Shift Measurements*, European Radar Conference, 2009. EURAD2009, pp.489–492, Sept. 2009, Rome, Italy.
- [55] <http://en.wikipedia.org/wiki/Maximumlikelihood>
- [56] L. Yang, M. Sun, and K. C. Ho, *Doppler-Bearing Tracking in the Presence of Observer Location Error*, IEEE Trans. on Signal Processing, vol.56, no.8, pp.4082-4086 Aug. 2008
- [57] H. V. Trees, *Detection Estimation and Modulation Theory*, John Wiley and Sons, Inc., USA, 2001.
- [58] Y. Kalkan, B. Baykal, *Target localization and velocity estimation methods for frequency-only MIMO Radars*, IEEE Radar Conference, 2011. Radarcon2011, pp.458–463, May. 2011, Kansas City, USA.
- [59] M. A. Nasrabadi and M. H. Bastani "A Survey on the Design of Binary Pulse Compression Codes with Low Autocorrelation", *Trends on Telecommunications Technologies*, In-Tech, India, 2010.
- [60] M. I. Skolnik, "Theoretical Accuracy of Radar Measurements", *IRE Transactions on Aeronautical and Navigational Electronics*, Vol:ANE-7, Issue:4, pp.123-129, 1960.
- [61] Y. Bar-Shalom and W.D. Blair, *Multitarget-Multisensor Tracking : Applications and Advances, Volume III*, Artech House, 200.

Appendix A

Radar Frequency Bands and General Usage

Table A.1: Radar Frequency Bands and General Usage

Band Designation	Operating Frequency Range	General Usage
HF	3-30 MHz	Over the Horizon surveillance
VHF	30-300 MHz	Very Long range surveillance Early warning
UHF	300-1000 MHz	Long range surveillance
L	1-2 GHz	Moderate range surveillance Terminal traffic control Long range weather
S	2-4 GHz	Moderate range surveillance Terminal traffic control Long range weather
C	4-8 GHz	Long range tracking Airborne weather detection
X	8-12 GHz	Short range tracking Missile guidance Mapping marine radar Airborne intercept
Ku	12-18 GHz	High resolution mapping Satellite altimetry
K	18-27 GHz	Automotive radar
Ka	27-40 GHz	Very high resolution mapping Airport surveillance
V	40-75 GHz	Experimental
W	75-110 GHz	Weapon guidance/fusing Automotive radar
mm	110-300 GHz	mm wave tracking

Appendix B

Derivation of the Fisher Information Matrix

The elements of the Fisher Information Matrix are

$$[J(\theta)]_{ij} = \frac{2}{\sigma^2} \text{Re} \left\{ E \left[\left[\frac{d\mathbf{s}(\theta)}{d\theta_i} \right]^H \left[\frac{d\mathbf{s}(\theta)}{d\theta_j} \right] \right] \right\} \quad (\text{B.1})$$

where $E[.]$ shows the expected value operation. Let rewrite the equation (B.1)

$$[J(\theta)]_{ij} = \frac{2}{\sigma^2} \text{Re} \{ E [\Psi] \} \quad (\text{B.2})$$

where

$$\Psi = \left[\frac{d\mathbf{s}(\theta)}{d\theta_i} \right]^H \left[\frac{d\mathbf{s}(\theta)}{d\theta_j} \right] \quad (\text{B.3})$$

From the above equations, it can be written that

$$\Psi = \left[\frac{d\mathbf{s}(\theta)}{d\theta_i} \right]^H \left[\frac{d\mathbf{s}(\theta)}{d\theta_j} \right] \quad (\text{B.4})$$

$$= \sum_{l=1}^{N_R} \left[\frac{d\mathbf{s}_l(\theta)}{d\theta_i} \right]^H \left[\frac{d\mathbf{s}_l(\theta)}{d\theta_j} \right] \quad (\text{B.5})$$

$$= \sum_{l=1}^{N_R} \sum_{n=1}^N \left[\frac{ds_l[n, \theta]}{d\theta_i} \right]^H \left[\frac{ds_l[n, \theta]}{d\theta_j} \right] \quad (\text{B.6})$$

and

$$\begin{aligned} \Psi &= \sum_{l=1}^{N_R} \sum_{n=1}^N (j2\pi T_s) \sqrt{E_e} \sum_{k=1}^{N_R} A_{lk}^*[n] s_k^*[n] \exp(j2\pi T_s \alpha_{l,k}) \left(\frac{d\alpha_{l,k}}{d\theta_i} \right) \\ &\quad \times (-j2\pi T_s) \sqrt{E_e} \sum_{m=1}^{N_T} A_{lm}[n] s_m[n] \exp(-j2\pi T_s \alpha_{l,m}) \left(\frac{d\alpha_{l,m}}{d\theta_j} \right) \\ &= 4E_e(\pi T_s)^2 \sum_{l=1}^{N_R} \sum_{n=1}^N \sum_{k=1}^{N_R} \sum_{m=1}^{N_T} A_{lk}^*[n] A_{lm}[n] s_k^*[n] s_m[n] \end{aligned} \quad (\text{B.7})$$

$$\times \exp(j2\pi T_s (\alpha_{l,m} - \alpha_{l,k})) \left(\frac{d\alpha_{l,k}}{d\theta_i} \right) \left(\frac{d\alpha_{l,m}}{d\theta_j} \right) \quad (\text{B.8})$$

From the equations above, it can be written as

$$\begin{aligned}
E[\Psi] &= 4E_e(\pi T_s)^2 \sum_{l=1}^{N_T} \sum_{n=1}^N \sum_{k=1}^{N_T} \sum_{m=1}^{N_T} E[A_{lk}^*[n]A_{lm}[n]] s_k^*[n]s_m[n] \\
&\quad \times \exp(j2\pi T_s(\alpha_{l,m} - \alpha_{l,k})) \left(\frac{d\alpha_{l,k}}{d\theta_i} \right) \left(\frac{d\alpha_{l,m}}{d\theta_j} \right) \\
&= 4E_e(\pi T_s)^2 \sum_{l=1}^{N_T} \sum_{n=1}^N \sum_{k=1}^{N_T} \sum_{m=1}^{N_T} \mu_{k,m}[n] s_k^*[n]s_m[n] \\
&\quad \times \exp(j2\pi T_s(\alpha_{l,m} - \alpha_{l,k})) \left(\frac{d\alpha_{l,k}}{d\theta_i} \right) \left(\frac{d\alpha_{l,m}}{d\theta_j} \right)
\end{aligned} \tag{B.9}$$

where $\mu_{k,m}[n] = E[A_{lk}^*[n]A_{lm}[n]]$, and

$$\mu_{k,m}[n] = E[A_{lk}^*[n]A_{lm}[n]] = \begin{cases} R_A(0) & ; \quad k = m \\ E[A_{lk}^*[n]]E[A_{lm}[n]] = 1 & ; \quad k \neq m \end{cases} \tag{B.10}$$

and, it can be written that

$$\begin{aligned}
E[\Psi] &= 4E_e(\pi T_s)^2 R_A(0) \sum_{l=1}^{N_T} \sum_{n=1}^N \sum_{k=1}^{N_T} |s_k[n]|^2 \left(\frac{d\alpha_{l,k}}{d\theta_i} \right) \left(\frac{d\alpha_{l,k}}{d\theta_j} \right) \\
&\quad + 4E_e(\pi T_s)^2 \sum_{l=1}^{N_T} \sum_{n=1}^N \sum_{k=1}^{N_T} \sum_{\substack{m=1 \\ m \neq k}}^{N_T} s_k^*[n]s_m[n] \\
&\quad \times \exp(j2\pi T_s(\alpha_{l,m} - \alpha_{l,k})) \left(\frac{d\alpha_{l,k}}{d\theta_i} \right) \left(\frac{d\alpha_{l,m}}{d\theta_j} \right)
\end{aligned} \tag{B.11}$$

and

$$\begin{aligned}
Re\{E[\Psi]\} &= 4E_e(\pi T_s)^2 R_A(0) \sum_{l=1}^{N_T} \sum_{n=1}^N \sum_{k=1}^{N_T} |s_k[n]|^2 \left(\frac{d\alpha_{l,k}}{d\theta_i} \right) \left(\frac{d\alpha_{l,k}}{d\theta_j} \right) \\
&\quad + 4E_e(\pi T_s)^2 \sum_{l=1}^{N_T} \sum_{n=1}^N \sum_{k=1}^{N_T} \sum_{\substack{m=1 \\ m \neq k}}^{N_T} s_k^*[n]s_m[n] \\
&\quad \times \cos(2\pi T_s(\alpha_{l,m} - \alpha_{l,k})) \left(\frac{d\alpha_{l,k}}{d\theta_i} \right) \left(\frac{d\alpha_{l,m}}{d\theta_j} \right)
\end{aligned} \tag{B.12}$$

Finally, the elements of the FIM can be written as

$$J_{xx} = \frac{8E_e(\pi T_s)^2 R_A(0)}{\sigma_n^2} \sum_{l=1}^{N_T} \sum_{k=1}^{N_T} \sum_{n=1}^N |s_k[n]|^2 \left(\frac{d\alpha_{l,k}}{dx} \right)^2 + \beta_{x,x} \tag{B.13}$$

$$J_{yy} = \frac{8E_e(\pi T_s)^2 R_A(0)}{\sigma_n^2} \sum_{l=1}^{N_T} \sum_{k=1}^{N_T} \sum_{n=1}^N |s_k[n]|^2 \left(\frac{d\alpha_{l,k}}{dy} \right)^2 + \beta_{y,y} \tag{B.14}$$

$$J_{V_x V_x} = \frac{8E_e(\pi T_s)^2 R_A(0)}{\sigma_n^2} \sum_{l=1}^{N_T} \sum_{k=1}^{N_T} \sum_{n=1}^N |s_k[n]|^2 \left(\frac{d\alpha_{l,k}}{dV_x} \right)^2 + \beta_{V_x, V_x} \tag{B.15}$$

$$J_{V_y V_y} = \frac{8E_e(\pi T_s)^2 R_A(0)}{\sigma_n^2} \sum_{l=1}^{N_T} \sum_{k=1}^{N_T} \sum_{n=1}^N |s_k[n]|^2 \left(\frac{d\alpha_{l,k}}{dV_y} \right)^2 + \beta_{V_y, V_y} \tag{B.16}$$

$$J_{xy} = J_{yx} = \frac{8E_e(\pi T_s)^2 R_A(0)}{\sigma_n^2} \sum_{l=1}^{N_R} \sum_{k=1}^{N_T} \sum_{n=1}^N |s_k[n]|^2 \left(\frac{d\alpha_{l,k}}{dx} \right) \left(\frac{d\alpha_{l,k}}{dy} \right) + \beta_{x,y} \quad (\text{B.17})$$

$$J_{xV_x} = J_{V_x x} = \frac{8E_e(\pi T_s)^2 R_A(0)}{\sigma_n^2} \sum_{l=1}^{N_R} \sum_{k=1}^{N_T} \sum_{n=1}^N |s_k[n]|^2 \left(\frac{d\alpha_{l,k}}{dx} \right) \left(\frac{d\alpha_{l,k}}{dV_x} \right) + \beta_{x,V_x} \quad (\text{B.18})$$

$$J_{xV_y} = J_{V_y x} = \frac{8E_e(\pi T_s)^2 R_A(0)}{\sigma_n^2} \sum_{l=1}^{N_R} \sum_{k=1}^{N_T} \sum_{n=1}^N |s_k[n]|^2 \left(\frac{d\alpha_{l,k}}{dx} \right) \left(\frac{d\alpha_{l,k}}{dV_y} \right) + \beta_{x,V_y} \quad (\text{B.19})$$

$$J_{yV_x} = J_{V_x y} = \frac{8E_e(\pi T_s)^2 R_A(0)}{\sigma_n^2} \sum_{l=1}^{N_R} \sum_{k=1}^{N_T} \sum_{n=1}^N |s_k[n]|^2 \left(\frac{d\alpha_{l,k}}{dy} \right) \left(\frac{d\alpha_{l,k}}{dV_x} \right) + \beta_{y,V_x} \quad (\text{B.20})$$

$$J_{yV_y} = J_{V_y y} = \frac{8E_e(\pi T_s)^2 R_A(0)}{\sigma_n^2} \sum_{l=1}^{N_R} \sum_{k=1}^{N_T} \sum_{n=1}^N |s_k[n]|^2 \left(\frac{d\alpha_{l,k}}{dy} \right) \left(\frac{d\alpha_{l,k}}{dV_y} \right) + \beta_{y,V_y} \quad (\text{B.21})$$

$$J_{V_x V_y} = J_{V_y V_x} = \frac{8E_e(\pi T_s)^2 R_A(0)}{\sigma_n^2} \sum_{l=1}^{N_R} \sum_{k=1}^{N_T} \sum_{n=1}^N |s_k[n]|^2 \left(\frac{d\alpha_{l,k}}{dV_x} \right) \left(\frac{d\alpha_{l,k}}{dV_y} \right) + \beta_{V_x, V_y} \quad (\text{B.22})$$

where

$$\beta_{i,j} = \frac{8E_e(\pi T_s)^2}{\sigma_n^2} \sum_{l=1}^{N_R} \sum_{n=1}^N \sum_{k=1}^{N_T} \sum_{\substack{m=1 \\ m \neq k}}^{N_T} s_k^*[n] s_m[n] \quad (\text{B.23})$$

$$\times \cos(2\pi T_s(\alpha_{l,m} - \alpha_{l,k})) \left(\frac{d\alpha_{l,k}}{d\theta_i} \right) \left(\frac{d\alpha_{l,m}}{d\theta_j} \right) \quad (\text{B.24})$$

Appendix C

Signal-to-Noise-Ratio (SNR)

The total received signal by the l^{th} receiver is

$$r_l(t) = \sqrt{E_e} \sum_{k=1}^{N_T} A_{lk}(t) s_k(t) \exp(-j2\pi(f_k + f_{d_{lk}})(t - \tau_{lk})) + w_l(t) ; \quad 0 \leq t \leq T \quad (C.1)$$

and the received signal by the l^{th} receiver from the k^{th} transmitter is

$$\begin{aligned} r_{l,k}(t) &= \sqrt{E_e} A_{lk}(t) s_k(t) \exp(-j2\pi(f_k + f_{d_{lk}})(t - \tau_{lk})) + w_{l,k}(t) ; \quad 0 \leq t \leq T \\ &= y(t) + w(t) \end{aligned} \quad (C.2)$$

where $\int_0^T |s_k(t)|^2 dt = 1$, $E_e = E/N_T$ is the normalized transmitted energy while E is the total transmitted energy, and T is the total observation time and $w_{l,k}(t)$ is the spatially and temporally white circularly symmetric zero mean gaussian noise $(0, \sigma^2)$. $A_{lk}(t)$'s are target fluctuations with $R_A(0) = 1$.

$$SNR = \frac{\text{Signal power}}{\text{Noise power}} \quad (C.3)$$

$$= \frac{\frac{E_e}{T} \int_0^T |s_k(t)|^2 dt}{\sigma^2} \quad (C.4)$$

$$= \frac{E_e}{T \cdot \sigma^2} \quad (C.5)$$

The noise variance can be calculated as

$$\sigma^2 = R_w(0) = \int_{-\infty}^{\infty} S_w(f) df \quad (C.6)$$

$$= 2 \int_0^B \frac{N_o}{2} df \quad (C.7)$$

$$= N_o B \quad (C.8)$$

Finally, the SNR becomes ($B = \frac{1}{T}$)

$$SNR = \frac{E_e}{T \cdot \sigma^2} = \frac{E_e}{TN_o B} = \frac{E_e}{N_o} \quad (C.9)$$

This is the power SNR which is the average received power to average noise power ratio within the signal bandwidth.

CURRICULUM VITAE

PERSONAL INFORMATION

Surname, Name : Kalkan, Yılmaz
Nationality : Turkish (TC)
Date and Place of Birth : 26 December 1979 , İzmir, TURKEY
email : ykalkan@metu.edu.tr, yilmaz.kalkan@gmail.com

EDUCATION

Degree	Institution	Year of Graduation
PhD	: METU, Electrical and Electronics Engineering,	2012
BS	: Kocaeli Univ., Electronics and Telecommunication Eng.,	2002
High School	: İzmir Çınarlı Teknik Lisesi, Elektronik Bölümü,	1997

WORK EXPERIENCE

Year	Place	Enrollment
2002–Present	: METU, Department of Electrical and Electronics Eng.	Research and Teaching Assistant

FOREIGN LANGUAGES

English

PUBLICATIONS

1. Y. Kalkan and B. Baykal, *Cramer Rao Bound for Target Localization with MIMO Radar*, IEEE 20th Signal Processing and Communications Applications (SIU 2012), 18-20 Nisan 2012, Muğla, Turkey.
2. Y. Kalkan and B. Baykal, *An Initial Data Association Method by Using Doppler*

Frequency for Multi Target, IEEE 20th Signal Processing and Communications Applications (SIU 2012), 18-20 Nisan 2012, Muğla, Turkey.

3. Y. Kalkan and B. Baykal, *Target Localization and Velocity Estimation Methods for Frequency-Only MIMO Radars*, 2011 IEEE Radar Conference, RADARCON11, pp.458–463, 23-26 May. 2011, Kansas City, USA.
4. Y. Kalkan and B. Baykal, *Sadece Frekans Bilgisi Kullanan MIMO Radar İçin Hız Kestirim Yöntemleri*, IEEE 19th Signal Processing and Communications Applications (SIU 2011), 20-22 Nisan 2011, Antalya.
5. Y. Kalkan and B. Baykal, *MIMO Radar İçin Frekans Temelli Hedef Konumlama Yöntemleri*, IEEE 19th Signal Processing and Communications Applications (SIU 2011), 20-22 Nisan 2011, Antalya.
6. Y. Kalkan and B. Baykal, *Target Localization Methods for frequency-only MIMO Radars*, Radar Conference, 2010. EURAD2010, pp.369–399, Sept.29-Oct.1, 2010, Paris, France.
7. Y. Kalkan and B. Baykal, *Sadece Frekans Bilgisi Kullanan MIMO Radar için Hedef Konumlama Yöntemleri*, IEEE 18th Signal Processing and Communications Applications (SIU 2010), 22-24 Nisan 2010, Diyarbakır.
8. Y. Kalkan and B. Baykal, *MIMO Radar Target Localization by Using Doppler Shift Measurements*, Radar Conference, 2009. EURAD2009, pp.489–492, Sept. 2009, Rome, Italy.
9. Y. Kalkan and B. Baykal, *MIMO Radarlarda Doppler Kayması Kullanılarak Hedef Konumunun Bulunması*, Elektrik-Elektronik-Bilgisayar ve Biyomedikal Mühendisliği 13. Ulusal Kongresi ve Fuarı, 23-26 Aralık 2009, Odtü-Ankara.